SECURITY CLASSIFICATIO

AD-A241 647

PAGE

Form Approved
OMB No. 0704-0188

1a. REPORT SECURITY CLASSIFICATION
UNCLASSIF

1b. RESTRICTIVE MARKINGS

2a. SECURITY CLASSIFICATION AUTHORITY

2b. DECLASSIFICATION / DOWNGRADING SCHEDULE

3. DISTRIBUTION / AVAILABILITY OF REPORT
Approved for public resease; distribution unlimited.

4. PERFORMING ORGANIZATION REPORT NUMBER(S)
GIT-89-008

5. MONITORING ORGANIZATION REPORT NUMBER(S)
N/A AFOSR-TR- 91 0818

6a. NAME OF PERFORMING ORGANIZATION
Georgia Institute of Technology

6b. OFFICE SYMBOL (If applicable)

7a. NAME OF MONITORING ORGANIZATION
Air Force Office of Scientific Research (AFOSR
Directorate of Physical and Geophysical Scienc

6c. ADDRESS (City, State, and ZIP Code)
School of Physics
Georgia Institute of Technology
Atlanta, Georgia 30332

7b. ADDRESS (City, State, and ZIP Code)
AFOSR/NP
Bolling Air Force Base, Bldg. 410
Washington, D. C. 20332-6448

8a. NAME OF FUNDING / SPONSORING ORGANIZATION
AFOSR

8b. OFFICE SYMBOL (If applicable)
NP

9 PROCUREMENT INSTRUMENT IDENTIFICATION NUMBER
AFOSR-89-0426

8c. ADDRESS (City, State, and ZIP Code)
Building 410
Bolling AFB, D. C. 20332-6448

10. SOURCE OF FUNDING NUMBERS

PROGRAM ELEMENT NO.	PROJECT NO	TASK NO	WORK UNIT ACCESSION NO.
61102F	2301	A4	N/A

11. TITLE (Include Security Classification)
Termolecular Association and Laser-Assisted Electron-(Excited) Atom Collisions

12. PERSONAL AUTHOR(S)
M. R. Flannery

13a. TYPE OF REPORT	13b. TIME COVERED	14. DATE OF REPORT (Year, Month, Day)	15. PAGE COUNT
Annual Technical Report	FROM 7/1/90 TO 6/30/91	8/23/91	136

16. SUPPLEMENTARY NOTATION

17. COSATI CODES		
FIELD	GROUP	SUB-GROUP

18. SUBJECT TERMS (Continue on reverse if necessary and identify by block number)
Electron Collisions, Laser Field, Dressed Atoms, Termolecular Association, Excitation

19. ABSTRACT (Continue on reverse if necessary and identify by block number)

This Second Annual Technical Report provides results of research performed during the period 7/1/90 - 6/30/91. Theoretical research was conducted on (a) laser-assisted electron-(excited) atom collisions, (b) electron-atom collisions and (c) termolecular association. Details of this research are included as Appendices (A) - (D) of this report.

91-13080

20. DISTRIBUTION / AVAILABILITY OF ABSTRACT
☒ UNCLASSIFIED/UNLIMITED ☐ SAME AS RPT ☐ DTIC USERS

21. ABSTRACT SECURITY CLASSIFICATION
UNCLASSIFIED

22a. NAME OF RESPONSIBLE INDIVIDUAL	22b. TELEPHONE (Include Area Code)	22c. OFFICE SYMBOL
Dr. Ralph E. Kelley	(202) 767-4903	NP

DD Form 1473, JUN 86 Previous editions are obsolete. SECURITY CLASSIFICATION OF THIS PAGE

91 10 16 076

UNCLASSIFIED

Abstract - Second Annual Technical Report
(7/1/90 - 6/30/91)

THIS SECOND ANNUAL TECHNICAL REPORT PROVIDES RESULTS OF RESEARCH UNDERTAKEN IN THE PERIOD 7/1/90 - 6/30/91. THEORETICAL RESEARCH WAS CONDUCTED ON :

(A) **LASER-ASSISTED ELECTRON-(EXCITED) ATOM COLLISIONS,**

$$e^- + A + N\hbar\omega \rightarrow e^- + A^* + M\hbar\omega$$

(B) **ELECTRON-EXCITED ATOM COLLISIONS,**

$$e^- + A^* \rightarrow e^- + A^{**}$$
$$\rightarrow e^- + A^+ + e^-$$

AND,

(C) **TERMOLECULAR ASSOCIATION.**

$$A + B + M \rightarrow AB + M$$

DETAILS OF THIS RESEARCH ARE INCLUDED AS APPENDICES (A)-(D) OF THIS REPORT.

TABLE OF CONTENTS

1. ACCOMPLISHMENTS DUE TO AFOSR SUPPORT :

PRINCIPAL INVESTIGATOR: M. R. Flannery
School of Physics, Georgia Institute of Technology
Grant AFOSR-89-0426, Period 7/1/90 - 6/30/91
Project Task: 2301/A4

1.1 RESEARCH OBJECTIVES AND DEVELOPMENTS

The objective of the present research program is to formulate, develop and implement new theoretical descriptions of the following atomic and molecular processes (A-C) below.

(A) **Laser-Assisted Collisions:** A new theory of laser-assisted electron-(excited) atom collisions,

$$e^- + A + nh\nu \rightarrow e^- + A^* + mh\nu \tag{1}$$

in which the dressed states of the atom A in the laser field are closely coupled and the Volkov states of the projectile electron in the laser field are included has been developed by M. R. Flannery and P. H. G. Smith. One paper has already been published, a second is in process of publication and a third has been submitted for publication. See Appendices (A)-(C).

(B) **Termolecular Recombination:** The transport-collisional set of Master equations for Termolecular Recombination,

$$A + B + M \rightarrow AB + M \tag{2}$$

as a function of gas density has been developed by M. R. Flannery. See Appendix (D).

(C) **Angular Momentum Changes in Collisions with excited atoms:** Work is progressing on the cross sections for angular momentum changes,

$$A + B(n\ell) \rightarrow A + B^+ + e^-(\epsilon, \ell')$$

in heavy-particle and electron-atom (e-B) collisions where the target atom is initially in an excited state.

The cross sections for $n\ell \rightarrow \epsilon\ell'$ collisional transitions increase as ℓ' is increased until a maximum ℓ'_{max} is attained after which the cross sections decrease preciptously. M. R. Flannery and A. Haffad have shown that this effect not only can be explained by a previous quantum description of Flannery and McCann, but also by classical scattering.

1.2 RESEARCH COMPLETED DURING CURRENT PERIOD (7/1/90 - 6/30/91)

Within this yearly period, the following projects were investigated, completed and written up for publication:

A. **Ph. D. Thesis:** 'A Semiclassical Treatment of Laser Assisted Collisions in a Soft-Photon Weak-Field Regime', by P. H. G. Smith, Georgia Institute of Technology (Ph.D. awarded 6/3/91)

B. **Papers in Press and submitted for publication:**

1. 'Electron-Atom Collisions in a Laser Field', by P. H. G. Smith and M. R. Flannery, Nucl. Instr. Meths. Phys. Res. B **56/57** (1991) 166-9. Appendix A.

2. 'ELectron-Hydrogen Collisions in a Laser Field', by P. H. G. Smith and M. R. Flannery, J. Phys. B: At. Mol. Opt. Phys. 1991 (*in press*), Appendix B.

3. 'Electron-Hydrogen Collisions with Dressed Target and Volkov Projectile States in a Laser Field', by P. H. G. Smith and M. R. Flannery, J. Phy. B: At. Mol. Opt. Phys. 1991 (*submitted for publication*), Appendix C.

4. 'Transport-Collisional Master Equations for Termolecular Recombination as a function of Gas Density', by M. R. Flannery, J. Chem. Phys. 1991 (*in press* Oct. issue), Appendix D.

1.3 RESEARCH COMPLETED DURING PREVIOUS PERIOD (7/1/89 - 6/30/90) AND WRITTEN UP AND PUBLISHED DURING CURRENT PERIOD (7/1/90 - 6/30/91).

1. 'Recombination Processes', M. R. Flannery in *Molecular Processes in Space*, 'Physics of Atoms and Molecules' series, edited by T. Watanabe , I. Shimamura, M. Shimizu and Y. Itikawa (Plenum Press, London, 1990) Chapter 7.

2. 'Electron Collision Cross Sections Involving Excited States' E. J. Mansky in *Nonequilibrium Processes in Partially Ionized Gases*, NATO ASI series B: Physics vol. 220, edited by M. Capitelli and J. N. Bardsley, Plenum Press 1990, pages 349-55.

3. 'The Issue of Basis Set Size in $e^- + H(1s \rightarrow 2s, 2p)$ Collisions', E. J. Mansky and M. R. Flannery, J. Phys. B: At. Mol. Opt. Phys. **23** L501-507 (1990).

4. 'Polarization Fractions for the $2^1P, 3^1P$ and 3^1D states of Helium' E. J. Mansky and M. R. Flannery, J. Phys. B: At. Mol. Opt. Phys. **23** 3987-92 (1990).

5. 'The Multichannel Eikonal Theory of Electron-Hydrogen Collisions I. Excitation of H(1s)' E. J. Mansky and M. R. Flannery J. Phys. B: At. Mol. Opt. Phys. **23** 4549-72 (1990).

6. 'The Multichannel Eikonal Theory of Electron-Helium Collisions I. Excitation of He(1^1S)' E. J. Mansky and M. R. Flannery, J. Phys. B: At. Mol. Opt. Phys. **23** 4573-4604 (1990).

7. 'Electron-Metastable Helium Differential and Integral Cross Sections' E. J. Mansky and M. R. Flannery, J. Phys. B: At. Mol. Opt. Phys. *in press*

8. 'Indirect Coupling Mechanisms and Stokes Parameters for Electron-Atom Scattering' E. J. Mansky and M. R. Flannery, J. Phys. B: At. Mol. Opt. Phys. *in press*

Above publications nos. 1 and 5-8 were included as Appendices B-F of the previous Annual Technical Report GIT-89-001 for the period 7/1/89 - 6/30/90 . Six (6) reprints of the first six papers (section 1.3 nos. 1-6 above) are enclosed separtely with this annual report to AFOSR under report numbers GIT-89-002, -003, -004, -005, -006 and -007, respectively. Reprints of the remaining papers nos. 7 and 8 will be sent to AFOSR when available.

1.4 SUMMARY: PAPERS PUBLISHED AND IN PRESS

A total of twelve (12) papers have either been already published (as detailed in sections 1.2 no. 1 and 1.3 nos. 1-6) or are currently in press (as in section 1.3 nos. 7,8 and in section 1.2 nos. 2,3 and 4), or have been submitted for publication (section 1.2 no. 3) during the two years (7/1/89 - 6/30/91) of the current AFOSR Grant. Reprints of all of the above papers will be sent to AFOSR.

In addition, **two Ph.D. thesis :**

1. **Termolecular Ion-Atom Association of Rare Gase Ions in Rare Gases** by M. S. Keenan (Ph.D. awarded 3/17/90)

and,

2. **A Semiclassical Treatment of Laser Assisted Collisions in a Soft-Photon Weak Field Regime** by P. H. G. Smith (Ph.D. awarded 6/3/91)

have been accomplished due to AFOSR support. Copies of these theses will also be sent to AFOSR.

2. PAPERS PRESENTED AT SCIENTIFIC MEETINGS (7/1/90 - 6/30/91)

1. 'Electron-Atom Collisions in a Laser Field', P. H. G. Smith and M. R. Flannery, Bull. Amer. Phys. Soc. **36** No. 2 (1991) 188

2. 'Angular Momentum Changes in Collisional Ionization', A. Haffad and M. R. Flannery, Bull. Amer. Phys. Soc. **36** No. 2 (1991) 188

The above two papers were presented at the 43rd Annual Gaseous Electronics Conference, 16-19 October, 1990, Champaign-Urbana, Illinois.

3. 'Functional Parallelism and Atomic Scattering Theory' E. J. Mansky, to appear in the Proceedings of the Fifth SIAM Conference on Parallel Processing for Scientific Computing (SIAM Press 1992), 25-27 March 1991, Houston Texas.

2.1 ABSTRACTS OF PAPERS PRESENTED

Abstract of Contributed Poster Paper presented at the Fifth SIAM
Conference on Parallel Processing for Scientific Computing
March 25-27, 1991, Houston , Texas

Functional Parallelism and Atomic Scattering Theory

The parallelizability of the numerical solution of systems of N coupled first-order linear partial differential equations, which arise in the solution of Schrödinger's equation in electron-atom scattering, is investigated. In particular, an optimal strategy is outlined for parallelizing the solution of systems of coupled 1^{st}-order PDE's by balancing the competing demands of scheduling (ie. load balancing), granularity and computational intensity of the algorithm. In this regard, the algorithmic phase diagram of Hockney proves instrumental in choosing which type of numerical technique (ie. rational extrapolation, Runge-Kutta, predictor-corrector) is "best" depending on the number of coupled equations N and global error tolerance chosen. Algorithmic phase diagrams and Hockney numbers $(n_{1/2}, s_{1/2}, f_{1/2})$ will be presented for the solution of N coupled PDE's ($N = 20 - 100$) which arise in the semi- classical multichannel eikonal theory of inelastic electron-atom scattering. Work supported by AFOSR under grant no. AFOSR-89-0426.

E. J. Mansky
School of Physics
Georgia Institute of Technology
Atlanta, Georgia 30332-0430.

Papers Presented at the 43rd Annual Gaseous Electronics Conference, Urbana-Champaign, Illinois, 16-19 October, 1990

D-7 **Electron-Atom Collisions in a Laser Field.*** Philip.H.G Smith and M.R.Flannery, **Georgia Institute of Technology**. A semi-classical Floquet approach is used to solve exactly, the Schrodinger equation for the laser/hydrogen interaction in a soft photon weak-field limit, to give dressed states of the atom in the laser field. Perturbative dressing is shown to provide an incomplete description, and cannot predict the distinctive features of the Floquet approach. Electron-hydrogen collisions in a laser field are then described via a multichannel eikonal treatment, in which the dressed states are closely coupled. Cross sections for 1S-2S and 1S-$2P_0$ excitations are presented as a function of field strength and impact energy, and compared with the Born-wave result.

* Research supported by AFOSR-89-0426.

D-8 Angular Momentum Changes in Collisional Ionization*, A. Haffad and M. R. Flannery, Georgia Institue of Technology - Single and Double Differential cross sections for ionization in e - H(nl) and H(1s) - H(nl) collisions are reported as a function of impact energy E, final energy ϵ and angular momentum l′ of the ejected electron. This process is assumed to occur via an energy-changing and angular momentum-changing binary collision between the Rydberg electron in state nl and the projectile e or H(1s).
The atomic projectile can also be excited. Systematic trends in the variation of the classical cross sections with final angular momentum l′ are discussed and are in accord with a previous quantal treatment[1].

*Research supported by U.S. Air Force Office of Scientific Reasearch under Grant No. AFOSR-89-0426.
[1]M. R Flannery and K. McCann, Phys. Rev. 19 (1979) 2206.

3. PERSONNEL INVOLVED

1. Professor M. R. Flannery - Principal Investigator
2. Dr. E. J. Mansky - Research Scientist II
3. Mr. P. H. G. Smith - Graduate Student (Ph.D. completed 6/3/91)
4. Mr. A. Haffad - Graduate Student (Ph.D. completed 8/16/91)
5. Mr. X. Qi - Graduate Student

4. SPECIAL HIGHLIGHT: LASER ASSISTED ELECTRON-ATOM COLLISIONS

A new theory of laser assisted electron-atom collisions has been formulated , developed and applied to,

$$e^- + H(1s) + N\hbar\omega \rightarrow e^- + H(2s, 2p_0, 2p_{\pm 1}) + N'\hbar\omega$$

The laser can perturb both the bound atomic electrons as well as the incident projectile electron. The first effect is acknowledged by a semiclassical Floquet approach used to dress the excited states of hydrogen in the laser field. This approach is compared to dressing by the traditional Perturbative approach which is then shown to provide an imcomplete description of the laser interaction and which cannot predict the distinct features provided by the Floquet approach.

The second effect of the laser interaction on the projectile electron is acknowledged via Volkov dressed states for the projectile. These states are shown to exert significant influence on the cross sections for individual state-to-state transitions which involve absorption or emission of a specified number of photons. They however have only a negligible effect on the cross sections obtained by summing over all absorptions and emissions.

APPENDIX A

Electron-Atom Collisions in a Laser Field

P. H. G. Smith and M. R. Flannery

Nuclear Instruments and Methods in Physics Research B56 57 (1991) 166–169
North-Holland

Electron–atom collisions in a laser field

Philip H.G. Smith and M.R. Flannery

School of Physics, Georgia Institute of Technology, Atlanta, GA 30332-0430, USA

Cross sections for the 1S–2S and 1S–2P$_0$ transitions in laser assisted e–H(1S) collisions are calculated in both the multichannel eikonal and the Born-wave treatments as a function of impact energy and laser field intensity and phase. The laser considered is a monotonic, plane polarized CO_2 laser (photon energy = 0.117 eV), with the polarization direction parallel to the initial projectile velocity. Floquet dressing of the hydrogen atom in the soft-photon weak-field limit reveals a concise description of the laser assisted electron–atom collision. This model also links the microscopic detail of the individual collisions with the macroscopic considerations of experimental analysis.

1. Introduction

The work reported in this paper is a study of the influence of the laser field on electron–atom collisions in the soft-photon weak-field regime. In this regime the photon energy is a lot less than the energy required to ionize the atom, and the field strengths can always be considered as a perturbation to the field of the nucleus on the bound electrons. The effect of coupling a laser field to a projectile electron in this regime during a collision with an atom has been well explained in a number of studies [1]. The effect of a laser field on the target atom, however, has met with a lot less success. This is due to the off-diagonal elements introduced into the Schrödinger equation for an atom in a laser field, which not only provide couplings between eigenstates of the isolated atom, but simultaneously involve the absorption or emission of a photon. In this model the off-diagonal elements are dealt with by creating dressed atomic states for the atom in the laser field by a semiclassical Floquet approach [2]. These dressed states are then used to solve the electron–hydrogen collision

$$e^- + H(1S) + N\hbar\omega \rightarrow e^- + H(2S, 2P_0, 2P_{\pm 1}) + N\hbar\omega. \tag{1}$$

This model can include the laser–projectile interaction by using the well-known Volkov states. As is shown in ref. [3], the Volkov states for the range of impact energies considered in this work – 50 eV, 100 eV and 200 eV – provide a wide range of high order multiphoton transitions. But as is also shown in ref. [3], when the state-to-state cross sections are summed over an increasingly wider range of projectile energies, the full treatment which includes Volkov dressing is found to converge on the treatment that neglects the laser–projectile interaction. This finding has been used to justify presenting state-to-state cross sections in this paper, calculated when neglecting the laser–projectile interaction.

2. The laser–atom coupling

The starting atomic Hamiltonian is [4]

$$H_{a,d}(r, t) = \tfrac{1}{2}P_{ra}^2 + V_a(r) + E_0 \cdot r \sin(\omega t + \delta_\omega) \tag{2}$$
$$= H_0 + V_d,$$

where H_0 is the field-free atomic Hamiltonian and E_0 is the electric field strength $= A_0\omega/c$ expressed in terms of the laser frequency ω. The phase shift is δ_ω which is explained in section 4 of this paper. This Hamiltonian can be seen to be time dependent. By expanding into Floquet states and diagonalizing a restricted version of the resultant infinite matrix [3,5], time independent dressed states can be obtained that exactly solve eq. (2). The time dependence has been removed by allowing for absorption and emission of photons of energy, so that the new dressed atomic states can be used to solve collisional problems in a time independent manner directly analogous to field-free atomic states. The cost of removing the time dependence is an infinite set of atomic states and energy levels

$$E_n = \epsilon + n\hbar\omega, \tag{3a}$$

$$|\Gamma_n\rangle = \sum_\alpha \sum_m A_{\alpha m} |\phi_\alpha, \; n+m\rangle, \tag{3b}$$

where Σ_α is a summation over field-free atomic states ϕ_α, and Σ_m is a summation over their Floquet expansion. It is emphasized that n varies across the range $-\infty$ to ∞, and so provides an infinite set of periodic dressed states.

0168-583X/91/$03.50

3. $e^- + H(1S) + N\hbar\omega$ collision

Now that dressed atomic states have been attained, they are used to solve the time dependent laser perturbed collisional Hamiltonian

$$H = \left[\tfrac{1}{2}P_R^2 + H_{a\,d}(r, t) + V(R, r)\right] \times \sum_{m=-\infty}^{\infty} J_m \exp(im\delta_-). \tag{4}$$

in a time independent manner. The summation over Bessel functions appears from the Volkov dressing of the projectile electron. As mentioned earlier, this has been well explained by others and so will not be dealt with in detail in this paper. Any experiment detects the products of the collision outside the region of the laser field where $H_{a\,d} = H_0$. To obtain results comparable with experimental observations this model calculates the state-to-state cross sections from the "measured" transition amplitude $T_{\alpha\beta}$ taken with respect to the field-free atomic states. Eq. (4) provides a solution to the "dressed" transition amplitude T_{pq} taken with respect to the Floquet dressed atomic states. By projecting the dressed states Γ_p on to the field free states ϕ_β it is possible to write the "measured" transition amplitude in terms of the "dressed" transition amplitude

$$T_{\alpha\beta} = \sum_{p}\sum_{q}\sum_{m}\left[\phi_\beta \cdot \Gamma_p\right]\left[\Gamma_p \cdot \phi_\alpha \cdot T_{pq} J_m \exp(im\delta_-)\right]. \tag{5}$$

The "measured" transition amplitude can be divided into two distinct parts (1) $(e, A, \hbar\omega)$ or $\Gamma_p J_m$ describes the collisional transition between dressed states of the atom; (2) $(A, \hbar\omega)$ or the projection $\phi_\alpha \Gamma_q$ describes the laser–atom interaction before and after the collisional event $(e, A, \hbar\omega)$. There is no analogous laser–projectile interaction $(e, \hbar\omega)$ in this model. Both these parts allow for absorption and emission of photons through interactions with the laser field. This model can be seen to give a very concise description of the laser assisted electron–atom collision, with all three interactions $(e, A, \hbar\omega)$, $(A, \hbar\omega)$ and $(e, \hbar\omega)$ as described recently [6], included exactly.

4. The dipole approximation

This model is based upon a typical crossed beam experiment, where a projectile electron beam, a target

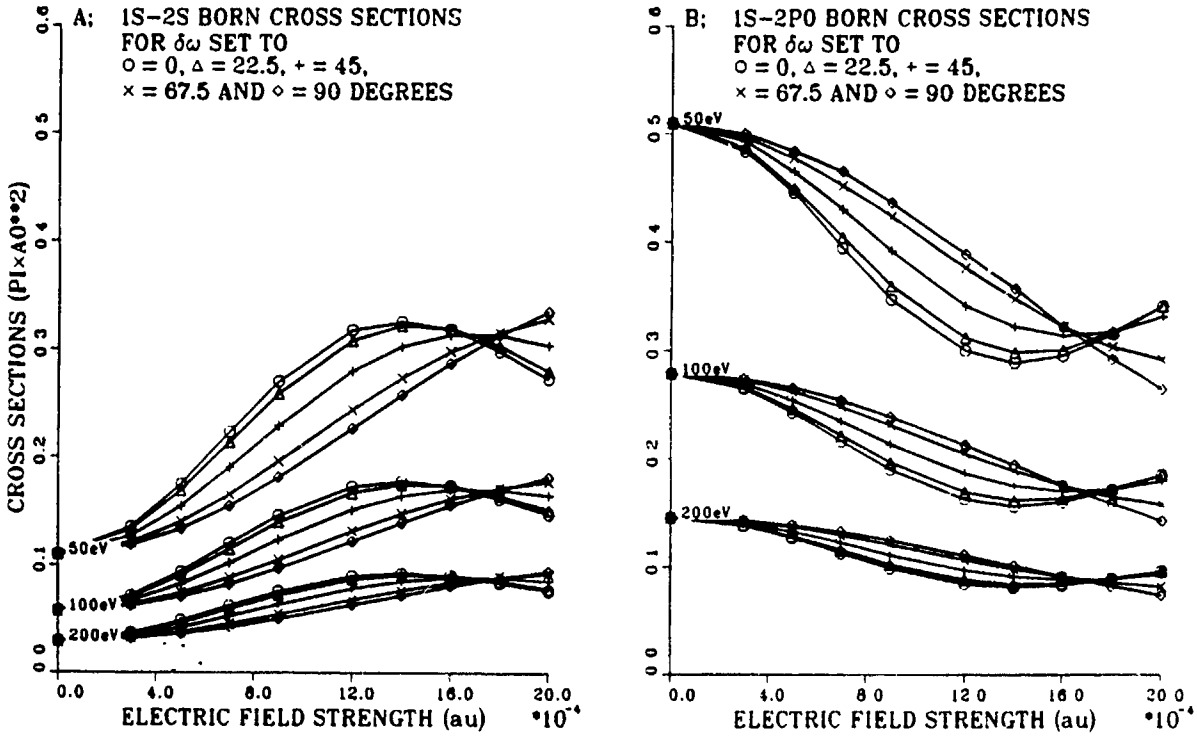

Fig. 1. Cross section vs laser field strength, for third order Floquet dressed hydrogen atoms, in laser assisted $e^- + H(1S)$ collisions, using a Born-wave treatment. (a) 1S–2S and (b) 1S–2P_0 cross sections. Cross sections are compared over a range of phases and impact energies.

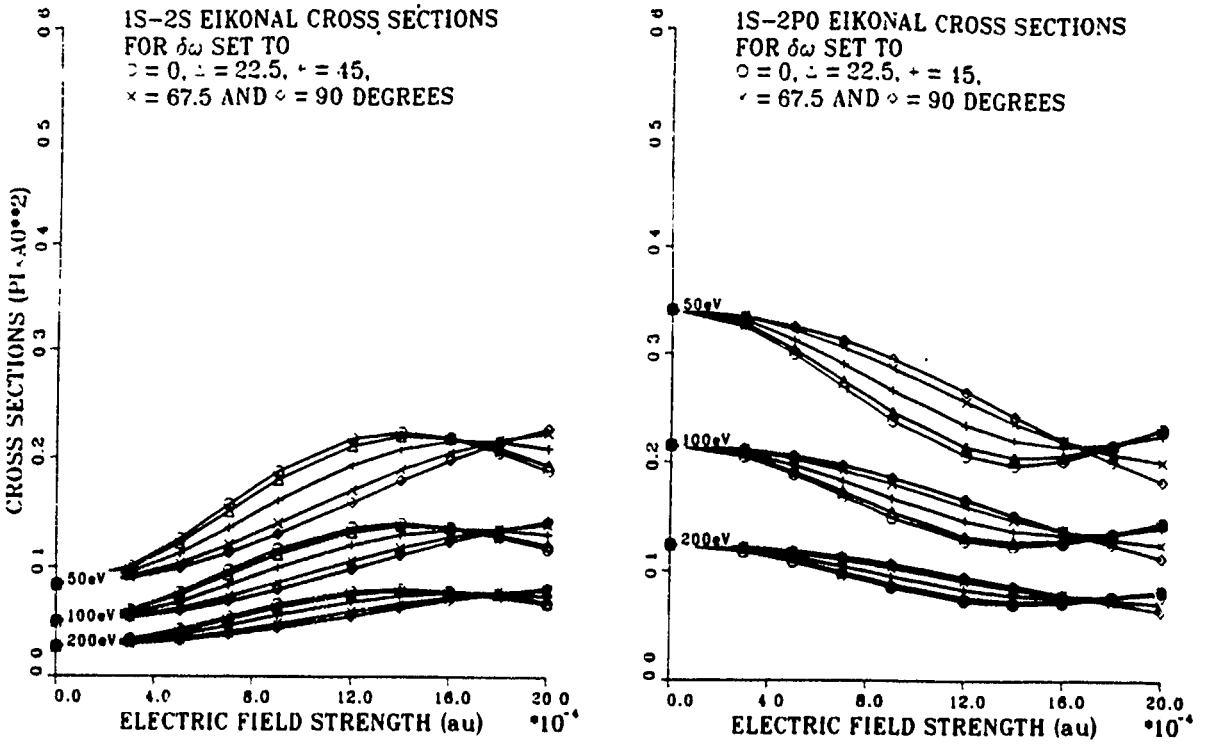

Fig. 2. Cross section vs laser field strength, for third order Floquet dressed hydrogen atoms, in laser assisted $e^- + H(1S)$ collisions, using a multichannel Eikonal treatment. (a) 1S–2S and (b) 1S–2P_0 cross sections. Cross sections are compared over a range of phases and impact energies.

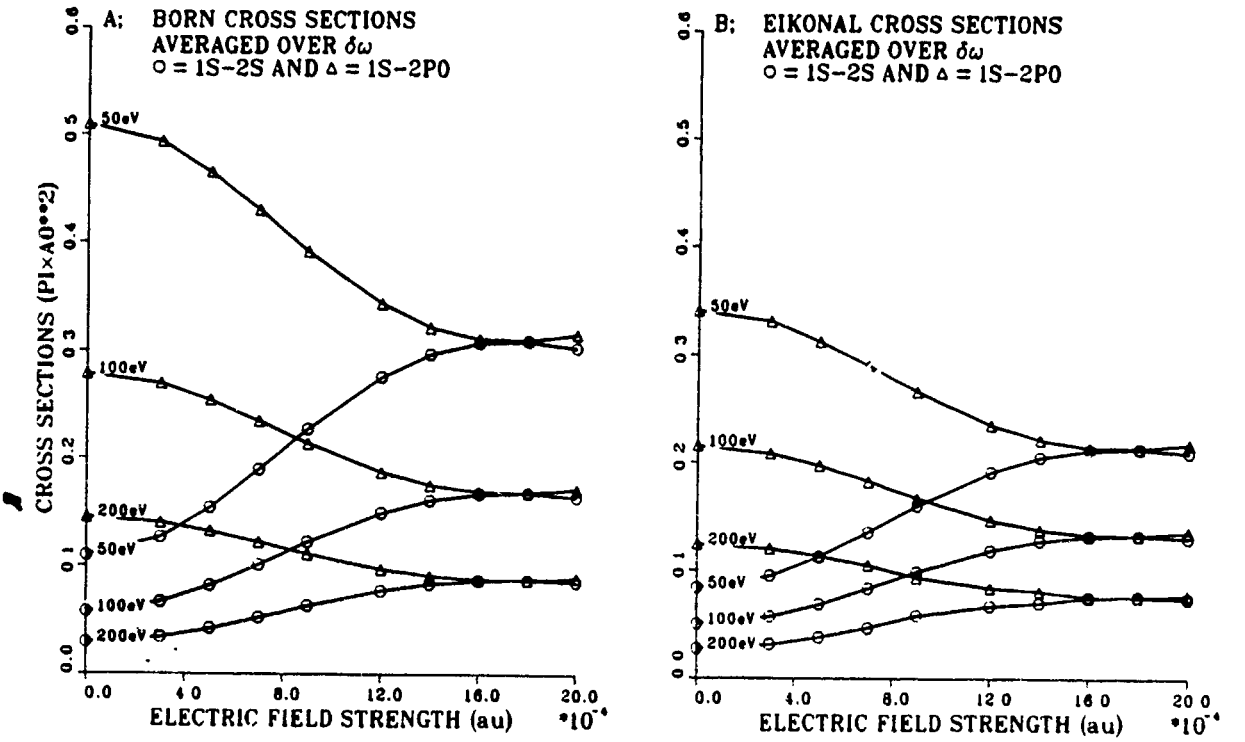

Fig. 3 1S–2S and 1S–2P_0 cross sections vs laser field strength, for third order Floquet dressed hydrogen atoms, in laser assisted $e^- + H(1S)$ collisions, using (a) Born-wave and (b) multichannel Eikonal treatments. The cross sections are averaged over δ_ω in the range 0° to 90° and compared over a range of impact energies.

atomic beam and a laser beam all cross at one point in space, with the vector potential for the laser field expressed as

$$A = \hat{\epsilon}_z A_0 \cos(k \cdot r + \omega t + \delta_\omega). \quad (6)$$

At the atomic level, a dipole approximation can be used in all calculations so that eq. (6) can be reduced to

$$A = \hat{\epsilon}_z A_0 \cos(\omega t + \delta_\omega). \quad (7)$$

However, at the macroscopic level, the dipole approximation does not hold across the full width of either the projectile or the atomic beams. This can be dealt with by varying the phase factor δ_ω in A. The wavelength for the electromagnetic radiation considered in this work is of the order of 10^{-5} m. Hence any experiment will observe a range of collisions over many wavelengths and time periods of the laser. To predict the experimental cross sections it is thus necessary to take an average over a range of δ_ω from 0° to 360°.

$$\sigma_{\text{experiment}} = \frac{1}{2\pi} \int_0^{2\pi} \sigma(\delta_\omega)\, \mathrm{d}(\delta_\omega). \quad (8)$$

5. Results

As explained in the introduction, the Volkov dressing of the projectile states provides little additional information to the summed state-to-state transitions. Hence the results presented here neglect the laser–projectile interaction, and are still considered to be a good approximation. All Floquet dressed states are taken to third order in approximation, which allows for multiphoton couplings of up to three photons in height. Third order is used since it is shown that convergence in the cross sections is reached by this time [5].

Numerical calculations of the dressed transition amplitudes of eq. (5) are based on a Born-wave treatment and a multichannel Eikonal treatment [7]. The restricted basis set – 1S, 2S, $2P_0$ and $2P_{\pm 1}$ – is used in the dressing of the atomic states, which in turn provides the basis set used in the multichannel eikonal approximation. The axis of quantization is along the direction of incidence of the projectile electron, and is also taken as the direction of polarization of the laser field.

Fig. 1 shows the 1S–2S and 1S–$2P_0$ cross sections calculated by the Born-wave treatment for a range of δ_ω from 0° to 90°. The same set of curves is repeated over the next 270°. Hence the predicted experimental cross section need be averaged only over the reduced range $\delta_\omega = 0°$ to 90°. Fig. 2 shows the same 1S–2S and 1S–$2P_0$ state-to-state cross sections calculated by the Eikonal treatment. As can be seen, the two treatments give very similar results. Fig. 3 shows the averaged 1S–2S and 1S–$2P_0$ cross sections, (a) calculated in the Born-wave approximation, and (b) calculated in the multichannel eikonal approximation.

Acknowledgement

This research is supported by AFOSR under Grant no. AFOSR-89-0426.

References

[1] D.V. Volkov, Z. Phys. 94 (1935) 250;
N.M. Kroll and K.M. Watson, Phys. Rev. A8 (1973) 804
S. Geltman and A. Macquet, J. Phys. B22 (1989) L419
[2] J.H. Shirley, Phys. Rev. B138 (1965) 979;
H. Sambe, Phys. Rev. A7 (1973) 2203;
S.I. Chu, Adv. Atom. Mol. Phys. 21 (1985) 197
[3] Philip H.G. Smith and M.R. Flannery, in preparation
[4] H.R. Reiss, Phys. Rev. A1 (1970) 803.
[5] Philip H.G. Smith and M.R. Flannery, in preparation
[6] W.R. Newell, 16th Int. Conf. on the Physics of Electronic and Atomic Collisions, New York, Abstracts of invited papers 205, eds A. Dalgarno et al. (1990) p. 122.
[7] M.R. Flannery and K.J. McCann, J. Phys. B7 (1975) L223, 2518, L522;
E.J. Mansky and M.R. Flannery, J. Phys. B23 (1990) 4549

APPENDIX B

Electron-Hydrogen Collisions in a Laser Field

P. H. G. Smith and M. R. Flannery

ELECTRON-HYDROGEN COLLISIONS IN A LASER FIELD

Philip.H.G.Smith and M.R.Flannery

School of Physics

Georgia Institute of Technology, Atlanta, GA, 30332-0430, U.S.A.

ABSTRACT: The non-perturbative Floquet method is used to provide the dressed states of a hydrogen atom in a laser field in the soft-photon weak-field regime. These dressed atomic states then provide a basis set expansion for use within a consistent semiclassical Multichannel Eikonal Treatment of laser assisted e^--H(1S) collisions. The variations with field strength of the 1S-2S and 1S-2P_0 state-to-state cross sections are presented. Special attention is employed in correlating the time frame of the laser field with the time frame of the relative orbit of the collisional species, and this is shown to require the inclusion of a phase shift δ_ω within the vector potential of the laser field. This inclusion is important when comparing with experimental results.

1.INTRODUCTION

The Floquet treatment has already been successfully employed (Chu 1985, Potvliege and Shakeshaft 1991) in calculations of laser induced multiphoton ionizations, where it provides dressed states for an atom in a laser field. That (perturbative) dressing of target states can have important consequences in laser-assisted scattering was illustrated by Byron and Joachain (1984). These dressed states are useful, not only for laser induced phenomenon, but also as a collisional basis set for laser assisted collisions. In this role they

are in fact very appealing, since the Floquet treatment naturally lends itself to a time-independent analysis, and hence are compatible with present field free scattering theories. Despite the apparent applicability of this approach, work along these lines has only just recently appeared (Sharma and Mohan 1990, Smith and Flannery 1991a, Burke et al 1991). Byron and Joachain (1984) have illustrated that perturbative dressing of the target states can have important consequences in laser-assisted scattering. Floquet dressing however provides a more complete description (Smith and Flannery 1991b).

This short paper provides an outline of the research (Smith 1991) being conducted by the authors on e^--H(1S) collisions, using a Floquet dressed basis set for a hydrogen atom in a laser field. A short paper has previously been published (Smith and Flannery 1991a) but the range of the electric field strength, over which collisional cross sections are calculated, has now been extended to provide greater insight into the role of the laser field in the collision. A more detailed account is presently under preparation. The work described here centers on the laser perturbation of the atom alone, and attempts to probe its exclusive effect by neglecting the laser perturbation of the projectile electron. In a later paper, the laser perturbation of the projectile will also be included via the use of Volkov dressed states but these will be shown to have a negligible effect on the state-to-state cross sections, within the range of electric field strengths studied in this work.

2.THEORY OF LASER ASSISTED COLLISIONS

The starting point of a discussion of laser assisted collisions is the laser perturbed

Schrödinger equation

$$i\hbar \frac{d}{dt}\psi = \left[\frac{1}{2\mu}P_R^2 + \sum_i \frac{1}{2}(p_{ri} + \mathbf{A}/c)^2 + V(\mathbf{r}) + V(\mathbf{R},\mathbf{r})\right]\psi \qquad (1)$$

The channel coordinates, $(\mathbf{P}_R, \mathbf{R})$, represent the momentum operator and the position vector for the projectile. The internal coordinates, $(\mathbf{p}, \mathbf{r})$ represent the momentum operator and the position vector for each bound electron. The electronic coordinates will be denoted collectively by $\mathbf{r}$, c is the speed of light, μ is the projectile-target reduced mass, $V(\mathbf{r})$ is the internal potential for the bound atomic electrons and $V(\mathbf{R},\mathbf{r})$ is the external projectile-target interaction potential.

After the usual dipole approximation, the vector potential for a monochromatic plane polarized laser of frequency ω is

$$\mathbf{A} = \mathbf{A}_o \cos(\omega t + \delta_\omega) \qquad (2)$$

It is customary, especially in multiphoton ionization, to omit the phase shift δ_ω and to just write the vector potential in the form $\mathbf{A}_o \cos\omega t$ or $\mathbf{A}_o \sin\omega t$. However for semiclassical collision theory there is already a time frame of reference imposed upon the collision, namely the time along the relative trajectory of the collisional species. The time $t = 0$ is usually defined at the point of closest approach between the projectile and the target, ie the orbit's passage through the periapsis. Thus, if the vector potential were used in the form $\mathbf{A}_o \cos\omega t$, it would indicate for *each* e-atom collision that the laser field was at a maxima of its cycle at the point of closest approach, as indicated by the dotted curve in the diagram of Fig.1. This is in general not true, so that it is necessary to adopt the phase shift δ_ω in order to synchronize the time-zero of the laser field with the time-zero of

the collisional e-atom orbit. The vector potential of eq.(2), used in these calculations, is therefore shifted in phase by δ_ω, from $\mathbf{A}_o \cos\omega t$, as shown by the solid line in the diagram of Fig.1. The phase shift δ_ω varies between 0 and 2π. Bachau and Shakeshaft (1984) have explicitly acknowledged the effect of the phase shift for excitation in $H^+ - H(1s)$ scattering in a nearly resonant laser field.

On omitting the projectile dependent terms from the laser perturbed Schrödinger equation eq.(1), the time-independent Floquet prescription (Shirley 1965, Sambe 1973, Chu 1985) yields the matrix equation.

$$\sum_n \Big[(\epsilon_\alpha + n\hbar\omega)\delta_{\beta\alpha}\delta_{n=m} + \mu^+_{\beta\alpha}\delta_{n=m-1} - \mu^-_{\beta\alpha}\delta_{n=m+1} \Big] A^n_{q\alpha} = Q_q A^m_{q\beta} \qquad (3)$$

The field free atomic energy levels ϵ_α and the laser induced off-diagonal couplings $\mu^\pm_{\beta\alpha} = -i\frac{1}{2}\langle\phi_\beta|\epsilon_o \cdot \mathbf{r}|\phi_\alpha\rangle$, between field free atomic states, are known so that the matrix can be diagonalized to obtain the new dressed basis set. This involves determining the "Quasi" energies Q_q and the dressed atomic states

$$\psi_q = \sum_n \sum_\alpha A^n_{q\alpha} \, |\phi_\alpha\rangle \, |n\rangle \qquad (4)$$

which are written in terms of the above combination of field free atomic states $|\phi_\alpha\rangle$ and periodic states $|n\rangle = \epsilon^{in\omega t}$. These new dressed atomic states form an orthogonal, time-independent basis set, which provides a medium in which any time-independent field free scattering theory may be applied to laser assisted collisions. However the price paid for this formal simplification is the introduction of an infinite set of periodic solutions, demanded by the Floquet prescription.

Using the Lippman Schwinger equation, it is relatively straightforward (Smith 1991)

to obtain the "dressed" transition amplitude

$$T_{pq} = \langle \psi_p | V(\mathbf{R}, \mathbf{r}) | \psi_q \rangle \ \exp(i(\mathbf{k}_i - \mathbf{k}_f) \cdot \mathbf{R}) \ \delta(Q_p + \tfrac{1}{2\mu} k_f^2 + (n-m)\hbar\omega - Q_q - \tfrac{1}{2\mu} k_i^2) \quad (5)$$

taken with respect to the dressed atomic states ψ_q. This "dressed" transition amplitude describes collisional transitions between the dressed atomic states, and includes all of the possible photon absorptions and emissions that can occur during such transitions. However the "dressed" transition amplitude, eq.(5), pertains to the wrong physical basis set for comparison with field free collisions and experimental results. Rather a transition amplitude taken with respect to the field free atomic states, ϕ_α, is required. Since the set of dressed atomic states, obtained via the Floquet prescription, is assumed to be a complete and normalized set it is possible to form the projection operator $\sum_q \ |\psi_q\rangle\langle\psi_q| = 1$. On using this projection operator, the "measured" transition amplitude

$$T_{\beta\alpha} = \langle \Phi_\beta | V(\mathbf{R}, \mathbf{r}) | \Phi_\alpha \rangle = \sum_q \sum_q \langle \phi_\beta, 0 | \psi_p \rangle \ T_{pq} \ \langle \psi_q | \phi_\alpha, 0 \rangle \quad (6)$$

taken with respect to the field free atomic states, may be written in terms of the "dressed" transition amplitude T_{pq}, taken with respect to the dressed atomic states. Writing the "measured" transition amplitude, $T_{\beta\alpha}$, in terms of the "dressed" transition amplitude, T_{pq}, in this manner effectively allows for a transition between the dressed and the field free basis sets. Hence semiclassical scattering theories can be applied in a time-independent manner and the calculated transition amplitudes then transformed to the field free "measured" basis set in order to yield the state-to-state transition cross sections. It can be shown that the calculated cross sections allow for laser photon absorption and emission and also Raman photon emission (Smith and Flannery 1991b). Both the probability amplitudes

and the photon absorption and emission locations during the collisional sequence of events are tracked by eq.(6).

Since the vector potential (2) can only be defined to within a phase shift δ_ω, as in Fig.1, it is therefore necessary to take the following average

$$\sigma_{\text{experiment}} = \frac{1}{2\pi}\int_0^{2\pi} \sigma(\delta_\omega) d(\delta_\omega) \tag{7}$$

by σ over the range of δ_ω from 0° to 360°. This proves to be an important consideration.

RESULTS: $e^- + H(1S) + N\hbar\omega \longrightarrow e^- + H(2S, 2P_0) + M\hbar\omega$

State-to-state cross sections for the 1S-2S and 1S-$2P_0$ transitions, in laser assisted e^--H(1S) collisions, are calculated by the Multichannel Eikonal Treatment as a function of impact energy and laser field intensity. All cross sections reflect a summation over the state-to-state cross sections, for all possible final projectile energies, consistent with a specified initial relative energy. Changes in the final projectile energy arise from photon absorption and emission. The laser considered is a monotonic, plane polarized CO_2 laser ($\hbar\omega = 0.117$eV), with the polarization direction parallel to the initial projectile velocity. The restricted basis set - 1S, 2S, $2P_0$ and $2P_{\pm 1}$ - is used in dressing the states, which in turn provide the basis set used within the Multichannel Eikonal Treatment. The axis of quantization is along the direction of incidence of the projectile electron and is also taken as the direction of polarization of the laser field. Convergence in the cross sections is reached (Smith and Flannery 1991b) by a third order approximation to the dressed atomic states and justifies the use of a third order approximation here.

Cross sections versus field strength for 1S-2S and 1S-$2P_0$ transitions are presented in

Fig.2, (a) and (b) respectively, for Floquet dressed hydrogen atoms. These cross sections are compared over a range of phase shifts from $\delta_\omega = 0°$ to 90°, since cross sections for δ_ω between 90° and 360° are found to be a repeat of the curves shown. It can be seen that the cross sections exhibit a very dramatic phase dependence over the field strength shown. The $\delta_\omega = 0°$ curve exhibits two stationary points, while the $\delta_\omega = 90°$ curve exhibits only one stationary point. A model purporting predictions of experimental results must take, as explained earlier, an average of the cross sections over the range of phases from $\delta_\omega = 0°$ to 360°, or the reduced range of $\delta_\omega = 0°$ to 90°. Cross sections after such averaging are presented in Fig.3a where it is immediately apparent that the 1S-2S cross section never crosses the 1S-$2P_0$ cross section. This non-crossing is very striking when compared to the percentage $2P_0$ component of the dressed state S (dressed 2S state) and the dressed state P (dressed $2P_0$ state) presented in Fig.3b. It is evident that the dressed 2S state is gaining an increasingly $2P_0$ character as the electric field strength increases, thereby raising the 1S-2S cross section at the expense of the 1S-$2P_0$ cross section. But because of the infinite set of periodic Floquet states the 1S to dressed 2S cross section is increasingly contributing to the "measured" 1S-$2P_0$ cross section, and hence prevents the "measured" 1S-2S cross section from exceeding the "measured" 1S-$2P_0$ cross section. The reasons behind this phenomenon are explained in greater depth in a later paper (Smith and Flannery 1991b).

4.CONCLUSION

The Floquet prescription used to obtain the dressed collisional basis set, has been found to yield a very concise description of the role of a laser field in collisional processes.

The overall semiclassical approach is consistent in that both the laser and the electron perturbations are described semiclassically. This description includes both the probability amplitudes and locations of photon absorption and emission during the collisional sequence of events, and are summarized by the descriptions (A,$\hbar\omega$) and (e,A,$\hbar\omega$) as given by Newell (1990).

This work has demonstrated the significant dependence, of the collisional cross sections, on the phase shift δ_ω included within the vector potential for the laser field. This phase has been found necessary to synchronize the time-zero of the laser field with the time-zero of the collisional orbit. It is suggested that any theoretical model which attempts to predict experimental results, must take an average of the phase dependent cross sections over a range of phases from $\delta_\omega = 0°$ to 360°. With this averaging it is shown, in Fig.3a, that the 1S-2S cross section rises up to, but does not exceed, the 1S-2P_0 cross section in laser assisted e^--H(1S) collisions. This feature should be experimentally observable with present day technologies.

Acknowledgement: This research was supported by the US Air Force Office of Scientific Research under Grant No AFOSR-89-0426. The authors thank Prof. Shakeshaft and the referee for bringing two additional references to their attention after this letter was submitted.

BIBLIOGRAPHY

Bachau H. and Shakeshaft R. (1984) Phys. Rev. A **30** 2752.

Burke P.G, Francken P and Joachain C.J (1991) J.Phys B:At Mol Opt Phys **24** 751.

Byron F. W. and Joachain C. J. (1984) J. Phys. B:At. Mol. Phys. **17** L295.

Chu S.I (1985) Recent developements in Semi-Classical Floquet theories for intense field multiphoton processes. Adv At Mol Phys **21** 197.

Newell W.R (1990) 16th Int Conf in the Phys of Electronic and Atomic Collisions. (N.Y) Abstracts of invited papers **205** (eds A.Dalgarno et al) 122.

Potvliege R.M and Shakeshaft R (1991) (Submitted).

Sambe H (1973) Phys Rev A **7** 2203.

Sharma B and Mohan M (1990) J.Phys B:At Mol Opt Phys **23** 3361.

Shirley J.H (1965) Phys Rev **138** B979.

Smith P.H.G (1991) Ph.D Thesis (Georgia Institute of Technology).

Smith P.H.G and Flannery M.R (1991a) Nuc Inst and Meth in Phys Res B**56/57** 166.

Smith P.H.G and Flannery M.R (1991b): In preparation.

FIGURE CAPTIONS

Figure (1): Vector potentials _____ $\mathbf{A}_o \cos(\omega t + \delta_\omega)$ and ..... $\mathbf{A}_o \cos \omega t$, for a monotonic plane polarized laser field of frequency ω, are shown positioned in time relative to the orbit's pericenter at time t = 0.

Figure (2): Cross sections vs field strength for 1S-2S and 1S-$2P_0$ transitions, (a) and (b) respectively, in laser assisted e^--H(1S) collisions using third order Floquet dressed hydrogen atoms and a Multichannel Eikonal Treatment. The cross sections are presented over a range of phase shifts δ_ω _____ =0°, _ _ _ _ _ =22.5°, ... =45°, ._._._. =67.5° and _ _ _ _ _ _ =90°, at a photon energy of $\hbar\omega = 0.0043$au.

Figure (3). Cross sections in e^--H(1S) collisions are compared against the percentage $2P_0$ component of the dressed atomic states, (a) and (b) respectively, over a range of electric field strengths for third order Floquet dressed hydrogen atoms in a laser field. The cross sections (_____ 1S-2S and _ _ _ _ _ 1S-$2P_0$) are an average of the phase dependent cross sections over a range of phases from $\delta_\omega = 0°$ to 90°, using a Multichannel Eikonal Treatment. For the percentage $2P_0$ component, _____ represents the dressed state S and _ _ _ _ _ represents the dressed state P.

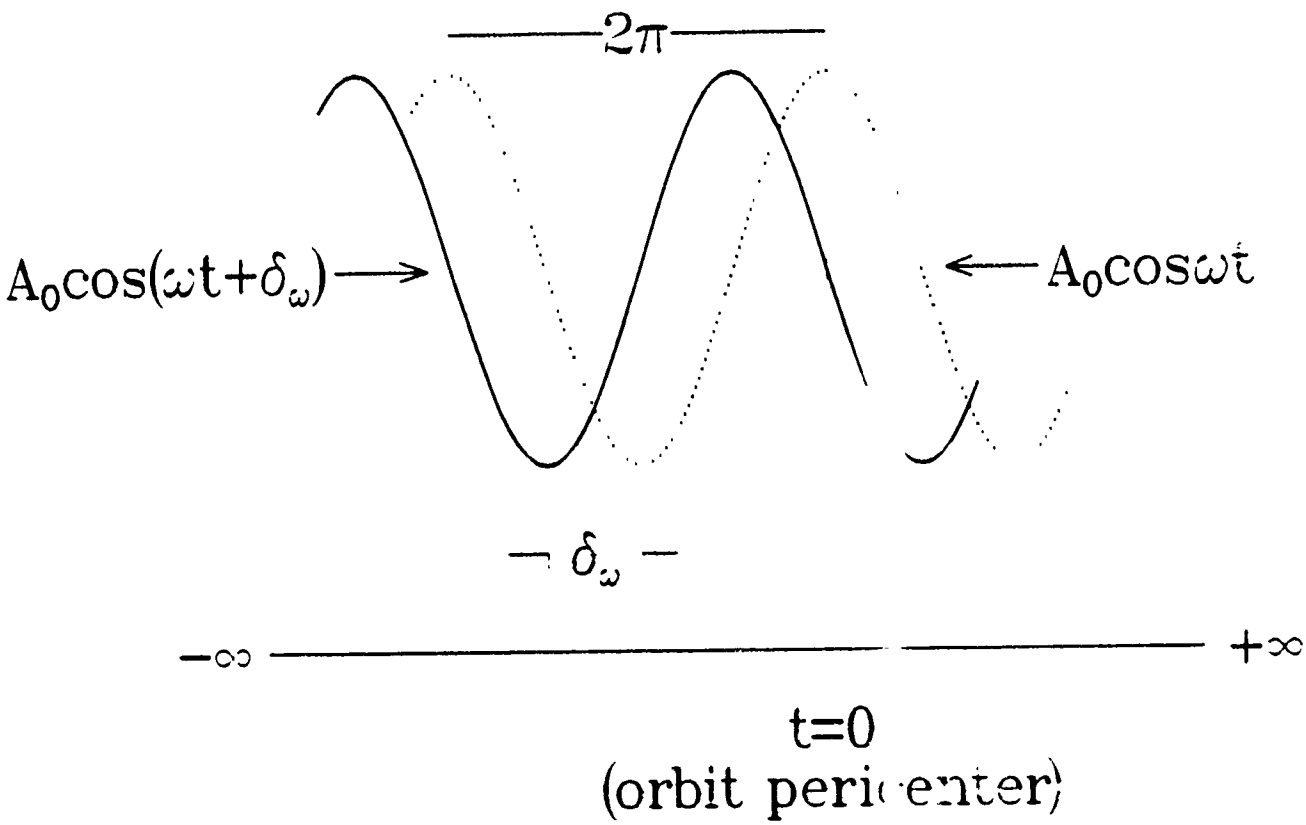

Figure (1): Vector potentials ——— $\mathbf{A}_0\cos(\omega t - \delta_\omega)$ and ..... $\mathbf{A}_0\cos\omega t$, for a monotonic plane polarized laser field of frequency ω, are shown positioned in time relative to the orbit's pericenter at time $t = 0$

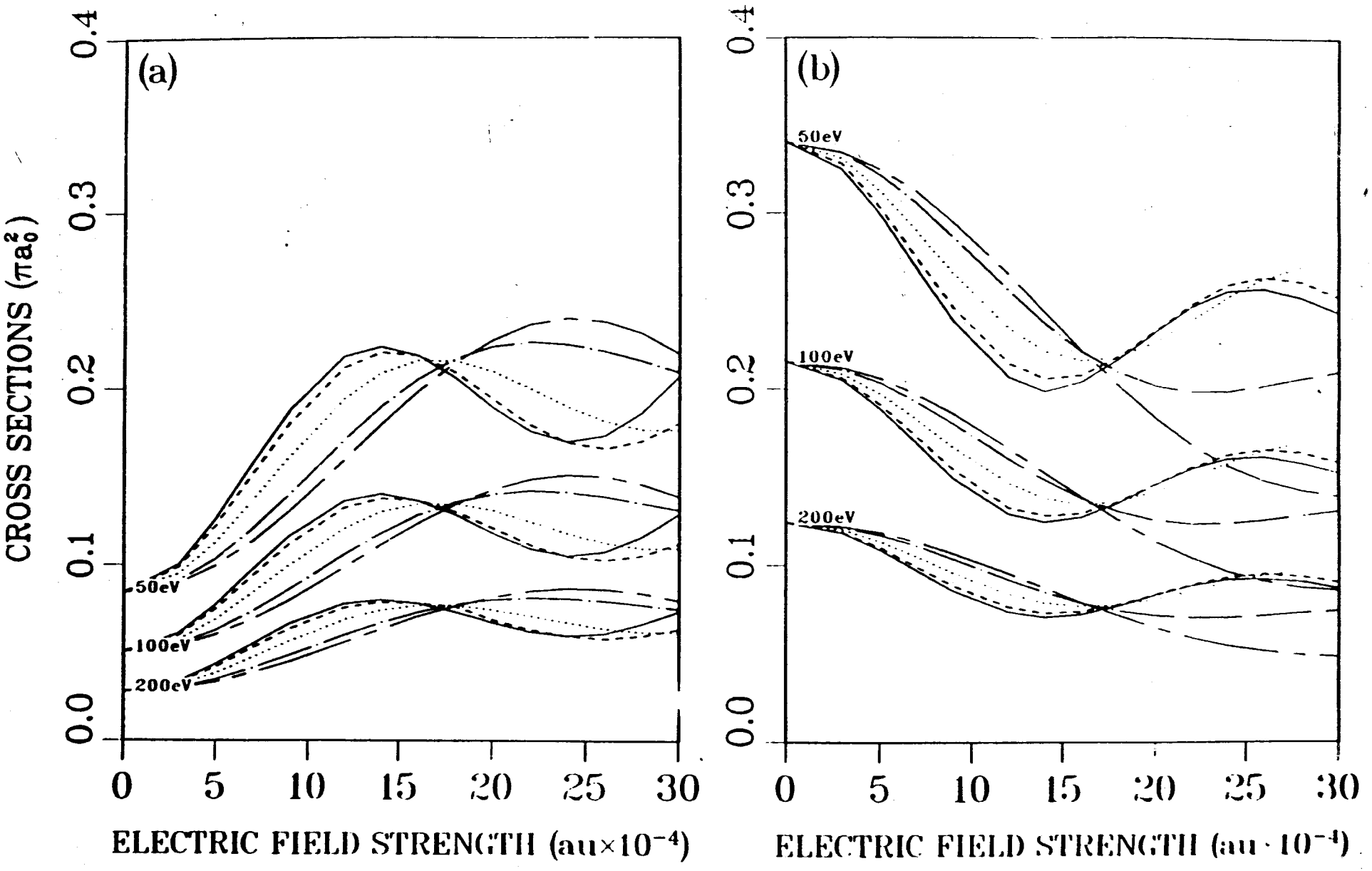

Figure (2): Cross sections vs field strength for 1S-2S and 1S-2P_0 transitions, (a) and (b) respectively, in laser assisted e$^-$-H(1S) collisions using third order Floquet dressed hydrogen atoms and a Multichannel Eikonal Treatment. The cross sections are presented over a range of phase shifts δ_s = 0°, -22.5°, -45°, -67.5° and -90° at a photon energy of $\hbar\omega$ = 0.0043au.

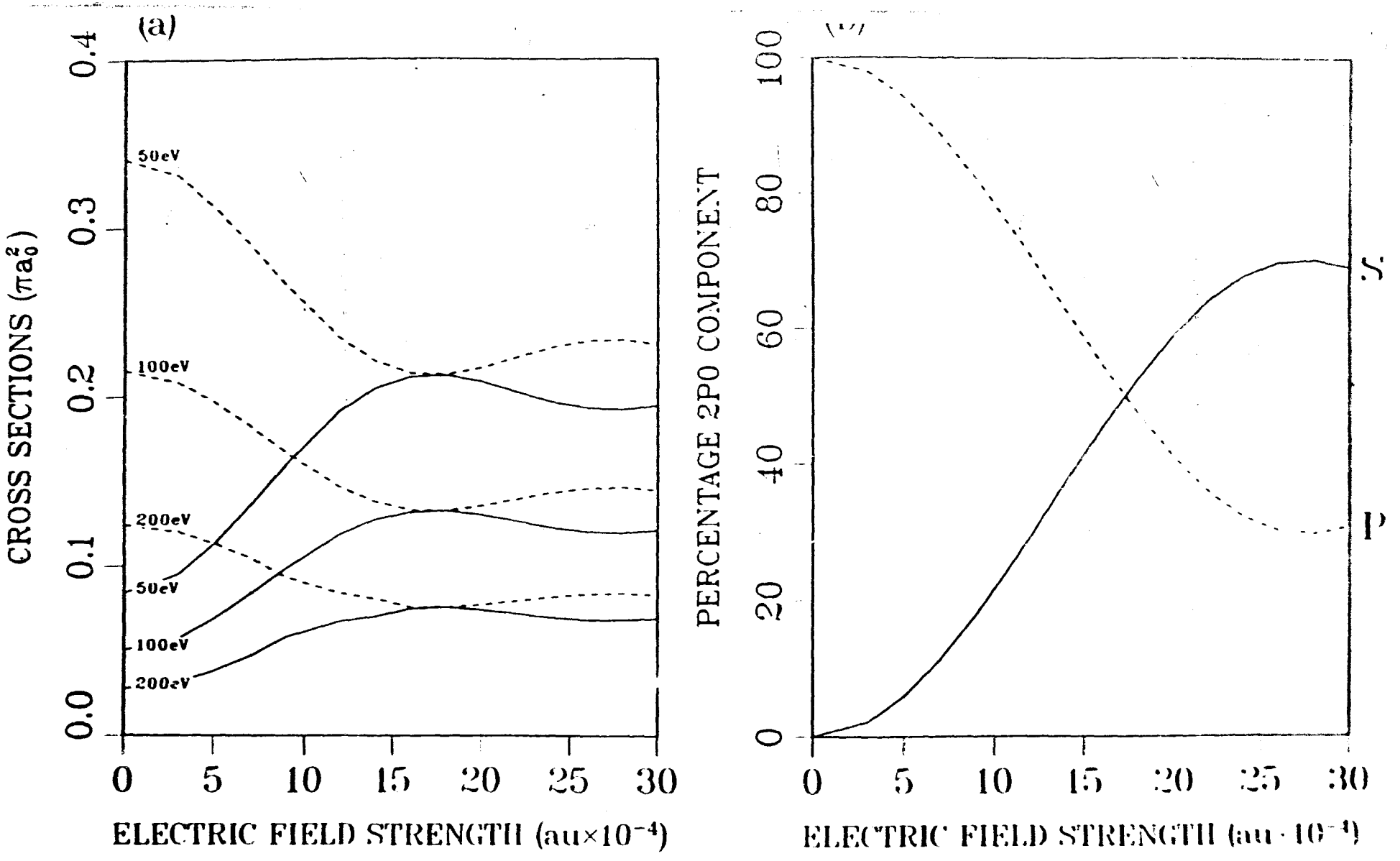

Figure (3): Cross sections in e⁻-H(1S) collisions are compared against the percentage $2P_0$ component of the dressed atomic states. (a) and (b) respectively, over a range of electric field strengths for third order Floquet dressed hydrogen atoms in a laser field. The cross sections (——— 1S-2S and - - - 1S-$2P_0$) are an average of the phase dependent cross sections over a range of phases from ϕ_L = 0° to 90°, using a Multichannel Eikonal Treatment. For the percentage $2P_0$ component, ——— represents the dressed state S and - - - represents the dressed state P.

APPENDIX C

Electron-Hydrogen Collisions with Dressed Target and Volkov Projectile States in a Laser Field

P. H. G. Smith and M. R. Flannery

ELECTRON-HYDROGEN COLLISIONS IN A LASER FIELD

Philip.H.G.Smith and M.R.Flannery

School of Physics,

Georgia Institute of Technology, Atlanta, GA, 30332-0430, USA.

Abstract: Cross sections for the 1S-2S and 1S-2P_0 transitions in laser assisted e^--H(1S) collisions are calculated in both the Multichannel Eikonal Treatment and the Born-Wave approximation, as a function of impact energy and laser field intensity. The laser considered is a monotonic, plane polarized CO_2 laser (photon energy = 0.117eV) with the polarization direction parallel to the initial projectile velocity. The first part of this paper confines the laser perturbation to the bound electrons of the atom. A semiclassical Floquet approach is used to dress the hydrogen atom in this soft-photon weak-field regime, and is shown to reveal a concise description of the laser assisted collision. The Floquet dressing is compared to dressing by the traditional time-dependent perturbation theory, showing that the Perturbative approach gives an incomplete description of the laser interaction, and cannot predict the distinct features provided by the Floquet approach. The second part of this paper extends the laser perturbation to the projectile electron, and the familiar Volkov dressed states are used. Although, in the range of impact energies and electric field strengths considered, the Volkov dressed states exert significant influence on the cross sections for individual state-to-state transitions, which involve absorption or emission of a given number of photons, they have only a negligible effect on the cross sections when

summed over all absorptions and emissions.

Special attention is employed in synchronizing the time frame of the laser field with the time frame of the trajectory of the collisional species orbit. This requires the inclusion of a phase shift δ_ω within the vector potential of the laser field. This inclusion is important when comparing theoretical cross sections with cross section measurements.

1.INTRODUCTION

The work reported in this paper studies the influence of the laser field on projectile-atom collisions, in the soft-photon weak-field regime. In this regime the photon energy is much less than the energy difference between sub-levels of the atom, and the electric field strength of the laser can always be considered as a perturbation to the electrostatic interactions between the nucleus and the bound atomic electrons. The effect of coupling a laser field to a projectile electron, in this regime, during a collision with an atom has been well explained (Volkov 1935, Kroll and Watson 1973, Geltman and Macquet 1989) via the introduction of Volkov states. Byron and Joachain (1984) have illustrated that perturbative dressing of the target states can have important consequences in laser-assisted scattering. The effect of a laser field on the target atom however involves off-diagonal elements introduced into the Schrödinger equation of the target atom by the laser field, which not only provide couplings between eigen states of the isolated atom, but simultaneously involve the absorption or emission of a photon, which in turn demands the use of a non-perturbative approach. Little work has been done on this aspect although some has recently emerged (Smith and Flannery 1991, Burke et al 1991).

This work mainly centers on the laser perturbation of the atom, and initially attempts to probe its exclusive effect by neglecting the laser perturbation of the projectile. Before the laser perturbed atomic Schrödinger equation can be used to calculate cross sections in a laser field, it is essential to remove the time-dependence and to re-instate the orthogonality of the atomic states. This is achieved using a semiclassical Floquet approach (Shirley 1965, Sambe 1973, Chu 1985) which exactly solves the laser perturbed Schrödinger equation

to produce a new set of orthogonal dressed atomic states, which can then be treated in a time-independent manner. Once these new states have been determined, they can be used within any time-independent scattering theory in a manner directly analogous to field free collisions. In this work cross sections will be presented in the Born-Wave approximation and the Multichannel Eikonal Treatment (Flannery and McCann 1975, Mansky and Flannery 1990) and are compared over a range of impact energies and electric field strengths. It will be shown that both the Born-Wave approximation and the Multichannel Eikonal Treatment produce cross sections that exhibit the same essential dependence on the electric field strength. As a comparison with the Floquet approach, cross sections will also be determined via the more traditional time-dependent Perturbation theory (Bayfield 1979). The Floquet and the Perturbative cross sections are strikingly different, and it is claimed that this difference originates from an important omission in the description of the dressed atomic states by the Perturbative approach. Floquet dressing will be shown to provide a more complete description.

Having obtained state-to-state cross sections which neglect the laser perturbation of the projectile, this perturbation will then be included within the collisional Schrödinger equation in the form of Volkov dressed states (Volkov 1935, Kroll and Watson 1973, Geltman and Macquet 1989). For a single state-to-state transition, with a specific final projectile energy, the Volkov dressed states exercise a very significant effect on the cross sections. When the state-to-state cross sections are summed over all possible final projectile energies reached through absorption and emission of photons, this work however shows that the cross sections that include the laser perturbation of the projectile, are only marginally

different from the cross sections that have neglected the perturbation of the projectile.

In order to synchronize the time frame of the relative orbit of the collisional species with the time frame of the laser field, a phase shift δ_ω must be introduced into the vector potential **A** of the laser field. Apart from Smith and Flannery (1991) this phase shift has been ignored in all the above work, and has important effects. Bachau and Shakeshaft (1984) have explicitly acknowledged the phase shift for $2p$ excitation in $H^+ - H(1s)$ inelastic scattering in a nearly resonant field.

This paper has also been able to describe in greater detail the role played by the Floquet states, so as to give a very concise description of the interaction, in terms of the probability amplitudes and the locations of photon absorption and emission during the collisional sequence of events. In section 4 the photon absorptions and emission are discussed in the form of (A,$\hbar\omega$) and (e,A,$\hbar\omega$), as recently described (Newell 1990).

2.FLOQUET DRESSED STATES OF AN ATOM IN A LASER FIELD

This theoretical model is based on a typical crossed beam experiment, in which the laser beam, projectile beam and atomic particle beam all cross at one point in space at 90° angles to each other. The collision will be considered in the center of mass frame of reference, but it should be noted that the projectile will have a much greater velocity than the target atom in the laboratory frame of reference. This is important since the atom will be inside the laser-beam for the duration of the collision, and so must be excited from one dressed atomic state to another.

When the laser perturbation of the projectile is neglected the Hamiltonian, in the center of mass frame of reference, is given by

$$H = \frac{1}{2\mu} P_R^2 + \sum_i \frac{1}{2}(\mathbf{p}_{ri} + \mathbf{A}/c)^2 + V(\mathbf{r}) + V(\mathbf{R}, \mathbf{r}) \tag{1}$$

The channel coordinates, $(\mathbf{P}_R, \mathbf{R})$, represent the momentum operator and the position vector for the projectile. The internal coordinates, $(\mathbf{p}_{ri}, \mathbf{r}_i)$, represent the momentum operator and the postion vector for each bound electron. The electronic coordinates are denoted collectively by $\mathbf{r}$, c is the speed of light, μ is the projectile-target reduced mass, V($\mathbf{r}$) is the internal potential for the bound atomic electrons and V($\mathbf{R}, \mathbf{r}$) is the external projectile-target interaction potential. Atomic units are used throughout.

The monochromatic laser, of frequency ω and phase δ_ω, should be exactly described by the vector potential

$$\mathbf{A}(\omega, \mathbf{r}_\omega, t) = \mathbf{A}_o \cos(\mathbf{k}_\omega \cdot \mathbf{r}_\omega + \omega t + \delta_\omega) \tag{2}$$

But at the atomic scale, since the reduced wavelength $\lambda_\omega = \frac{1}{k_\omega}$ is much larger than atomic

dimensions, the dipole approximation is valid so that the vector potential reduces to

$$\mathbf{A} = \mathbf{A}_o \cos(\omega t + \delta_\omega) \tag{3}$$

In semiclassical scattering theories, the point of closest approach (the periapsis), between the projectile and the target, is generally defined as occurring at time t=0. If the vector potential, under the dipole approximation, was written as $\mathbf{A} = \mathbf{A}_o \cos(\omega t)$, then this would indicate that for *each* collision the electric field strength was at a maxima of its cycle at the point of closest approach, as indicated by the dotted curve in Fig.1. Since this is not in general true, it is necessary to use the vector potential given in eq.(3), where δ_ω is the phase shift of the vector potential eq.(3), from $\mathbf{A}_o \cos(\omega t)$, at the point of closest approach as indicated by the solid curve in Fig.1.

To dress the atomic states it is necessary to consider the effect of the laser field on the isolated atomic target. This is done by removing the projectile components from the Hamiltonian eq.(1). On applying the unitary transformation $U = \exp(i \sum_i \mathbf{A} \cdot \mathbf{r}_i / c)$, (Reiss 1970), the Schrödinger equation for an atom in a laser field is then expressed as

$$i\hbar \frac{d}{dt}\psi' = \left(\sum_i \left[\tfrac{1}{2} p_{ri}^2 - i \tfrac{1}{2} \epsilon_o \cdot \mathbf{r}_i \left(\epsilon^{i(\omega t + \delta_\omega)} - \epsilon^{-i(\omega t + \delta_\omega)} \right) \right] + V(\mathbf{r}) \right) \psi' \tag{4}$$

where ϵ_o is the electric field strength $\mathbf{A}_o \omega / c$, and where it has been assumed that the periodicity is the only time-dependent part of the vector potential. The solution of eq.(4) is the dressed atomic state ψ' (at present unknown). On using the field free atomic Hamlitonian $H_o = \sum_i \frac{1}{2} p_{ri}^2 + V(\mathbf{r})$, and on setting $\mu_i^{\pm} = -i \frac{1}{2} \epsilon_o \cdot \mathbf{r}_i \epsilon^{\pm i \delta_\omega}$, the laser perturbed atomic Schrödinger equation eq.(4) is written in the more compact form

$$\left(H_o + \sum_i \mu_i^{\pm} (\epsilon^{i\omega t} - \epsilon^{-i\omega t}) - i\hbar \frac{d}{dt} \right) |\psi'\rangle = 0 \tag{5}$$

which is now suitable for application of the Floquet prescription (Shirley 1965, Sambe 1973, Chu 1985). Under this prescription, the solution to eq.(5) is of the form

$$|\psi'\rangle = |\psi'_q\rangle = e^{-iQ_q t/\hbar}|G_q\rangle \tag{6}$$

where Q_q is the energy or "quasi-energy" of the new dressed state, and G_q has a periodic time-dependence of period $\frac{2\pi}{\omega}$. Since G_q is periodic in time, it is expanded by the Fourier series

$$|G_q\rangle = \sum_n |G_q^n, n\rangle \tag{7}$$

where the Floquet notation, introduced by Shirley (1965) is used. Thus

$$|\psi, n\rangle = |\psi\rangle|n\rangle \qquad \text{with} \quad \langle t|n\rangle = e^{in\omega t} \tag{8}$$

and $|n\rangle$ will be called a "periodic" state for clarity later. Using this Fourier expansion, the Schrödinger equation eq.(5) can now be rewritten so as to explicitly include the periodic photon dependence $n\hbar\omega$ as

$$\sum_n \left(H_o + n\hbar\omega + \sum_i \mu_i^{\pm}(e^{i\omega t} - e^{-i\omega t}) \right) e^{-iQ_q t/\hbar}|G_q^n, n\rangle = \sum_n Q_q e^{-iQ_q t/\hbar}|G_q^n, n\rangle \tag{9}$$

In this weak-field regime the dressed atomic states can be approximated by a combination of field free atomic states, as

$$|\psi'_q\rangle = \sum_n A_{q\alpha}^n |\phi_q, n\rangle \tag{10}$$

where the periodic time-dependence of the coefficients has been separated by using the periodic states $|n\rangle$. On comparing this with the Floquet dressed atomic states

$$|\psi'_q\rangle = e^{-iQ_q t/\hbar} \sum_n |G_q^n, n\rangle \tag{11}$$

then the laser perturbed Schrödinger equation eq.(9) can be written in the matrix representation as

$$\sum_n \left[(\epsilon_\alpha + n\hbar\omega)\delta_{\beta\alpha}\delta_{n=m} + \mu^+_{\beta\alpha}\delta_{n=m-1} - \mu^-_{\beta\alpha}\delta_{n=m+1} \right] A^n_{q\alpha} = Q_q A^m_{q\beta} \qquad (12)$$

The field free atomic energy levels ϵ_α and the laser induced off-diagonal elements $\mu^\pm_{\beta\alpha} = -i\frac{1}{2}\langle\phi_\beta|\epsilon_o\cdot\mathbf{r}|\phi_\alpha\rangle e^{\pm i\delta_\omega}$ are known, so that the matrix defined by eq.(12) can be diagonalized to obtain the quasi energies Q_q and the dressed atomic states ψ'_q. Because the Floquet prescription allows for an infinite set of periodic states, from $n = -\infty$ to ∞, it is necessary to truncate the matrix. But as long as the off-diagonal couplings $\mu^\pm_{\beta\alpha}$ are small, this truncation can be quite severe whilst still allowing convergent dressed states to be obtained. Fig.2 shows a specific example of a Floquet matrix for a hydrogen atom in a laser field. Significant couplings only occur between field free atomic states ϕ_β and ϕ_α if the energy level separation is of the order of, or less than, the photon energy of the laser

$$|\epsilon_\alpha - \epsilon_\beta| \leq \hbar\omega \qquad (13)$$

For a collisional problem that considers excitation from the n=1 to the n=2 sub-levels, internal couplings within the n=2 manifold need only be considered at the photon energies used within this work.

To a first order approximation, which allows only single photon coupling, the matrix of Fig.2 yields the dressed atomic states

$$|S\rangle = A|2S,n\rangle + B\epsilon^{i\delta_\omega}|2P_0,n+1\rangle + B\epsilon^{-i\delta_\omega}|2P_0,n-1\rangle \qquad (14a)$$

$$|P\rangle = A|2P_0,n\rangle + B\epsilon^{i\delta_\omega}|2S,n+1\rangle + B\epsilon^{-i\delta_\omega}|2S,n-1\rangle \qquad (14b)$$

It is emphasized for these dressed atomic states, that n varies across the range from $n = -\infty$ to ∞, giving rise to an infinite set of periodic Floquet states. In higher order approximations to the dressed states, multiphoton couplings are included, so that eq.(14 a, b) include further terms for n$\pm$2, n$\pm$3 etc. Results of section 5 shows that convergence is achieved by a third order approximation, so that terms up to n$\pm$3 provide an adequate description of the dressed atomic states, over the electric field strength range considered in this work.

From the form of eq.(14 a, b), it can be seen that the fractional 2S and $2P_0$ components of both dressed states S and P change with varying electric field strength. The character of the dressed states S and P will then change with increasing ϵ_o. This changing character of the dressed states is clearly seen from the radial distribution functions, where the radial distribution functions $D_S(r)$ and $D_P(r)$ are defined by the equations

$$\langle S|S\rangle = \int_0^\infty D_S(r)dr \int_0^{2\pi} \int_0^\pi d\cos\theta d\phi \tag{15a}$$

$$\langle P|P\rangle = \int_0^\infty D_P(r)dr \int_0^{2\pi} \int_0^\pi d\cos\theta d\phi \tag{15b}$$

The radial distribution functions, for the dressed states S and P, are shown in Fig.3a - Fig.3c as the electric field strength ϵ_o increases from 0 au to 3×10^{-3} au. These radial distribution functions correspond to third order Floquet dressed hydrogen atoms. Convergence in the state-to-state cross sections of section 5, for third order Floquet dressed atomic states, is used to justify a third order approximation here. It is seen that as the field strength increases, the radial distribution function $D_S(r)$ loses its intrinsic 2S character, while gaining an increasingly $2P_0$ character. In a similar fashion the radial distribution function $D_P(r)$ is losing its intrinsic $2P_0$ character, while gaining an increasingly 2S

character. The plot in Fig.4 attempts to represent this, by looking at the percentage component of the $2P_0$ field free radial distribution function, $D_{2P_0}(r)$, in both $D_S(r)$ and $D_P(r)$. This shows very clearly the play off between the dressed states S and P indicated in the set of plots in Fig.3. As the electric field strength rises, both states S and P simultaneously give up some of their intrinsic zero field character, and assume more of each other's intrinsic zero field character. This character swapping continues past the point, where the dressed state S has more of a $2P_0$ character than the dressed state P. If the statement is made, for the collisional energies studied in this work, that the field free 1S-$2P_0$ state-to-state integral cross section is always larger than the field free 1S-2S state-to-state integral cross section, ie if

$$\sigma_{1S,2P_0} > \sigma_{1S,2S} \tag{16}$$

then from the plot of Fig.4 it might be reasonable to expect, as the electric field strength rises, that the laser assisted 1S-2S state-to-state cross section will rise, and the laser assisted 1S-$2P_0$ state-to-state cross section will fall. This rise and fall can also be expected to continue past the point where the laser assisted 1S-2S state-to-state cross section is greater than the laser assisted 1S-$2P_0$ state-to-state cross section.

3.TIME-INDEPENDENT SCATTERING CROSS SECTIONS

In section 2 the time-dependent Schrödinger equation for an atom in a laser field, was solved using the Floquet prescription to obtain new eigenstates, or dressed states for the atom in a time-independent form. The time-dependence has been removed by allowing for absorption and emission of photons. These dressed states can now be used to solve collisional problems in a manner directly analogous to field free collisions. In this work the scattering cross sections for the laser assisted collisions are derived from the Lippman Schwinger equation (Bransden 1970). This approach is valid to all orders of approximation of the dressed states, given the necessary assumption that the dressed states form a complete and normalized set. From section 2 the laser assisted collision can be described by the Hamiltonian

$$\begin{aligned} H &= \tfrac{1}{2\mu}P_R^2 + \sum_i \left[\tfrac{1}{2}p_{ri}^2 - i\tfrac{1}{2}\epsilon_o \cdot \mathbf{r}_i(e^{i\omega t} - e^{-i\omega t})\right] + V(\mathbf{r}) + V(\mathbf{R},\mathbf{r}) \\ &= H_F + V(\mathbf{R},\mathbf{r}) \end{aligned} \tag{17}$$

When the interaction potential $V(\mathbf{R},\mathbf{r})$ is removed, the remainder H_F describes the projectile far removed from the target atom, which remains in the presence of the laser field. The solution Φ of the Schrödinger equation

$$(i\tfrac{d}{dt} - H_F)\Phi = 0 \tag{18}$$

is the combination $\Phi_q = \psi'_q \exp(i\mathbf{k}_q \cdot \mathbf{R})$ of the dressed atomic states ψ'_q of section 2, with a field-free projectile plane wave. The scattered collisional wave function in the presence of V then satisfies

$$|\Psi_q^{\pm}, t\rangle = \epsilon^{-iE_q t/\hbar}|\Phi_q\rangle + \lim_{\epsilon\to 0}\frac{1}{E_q \pm i\epsilon - H_o} V\, \epsilon^{-iE_q t/\hbar \pm \epsilon t/\hbar}|\Psi_q^{\pm}\rangle \tag{19}$$

The probability of a transition between the scattered collisional wave functions Ψ_q^+ and Ψ_p^- is given by the S-matrix

$$S_{pq}(t) = \langle \Psi_p^- | \Psi_q^+ \rangle \tag{20}$$

On inserting the scattered collisional wavefunction eq.(19) into the S-matrix eq.(20), and expanding the dressed atomic states ψ' into the combination of field free atomic states ϕ of eq.(10), the S-matrix is then

$$\begin{aligned} S_{pq}(t) &= \langle \Phi_p | \Phi_q \rangle \delta_{pq} \\ &+ \sum_m \sum_\beta A_{p\beta}^m \langle \Phi_\beta | e^{i(Q_p + \frac{1}{2\mu}k_f^2 - m\hbar\omega)t/\hbar} \\ &\times \sum_n \sum_\alpha A_{q\alpha}^n \frac{1}{Q_q + \frac{1}{2\mu}k_i^2 - n\hbar\omega + i\epsilon - Q_p - \frac{1}{2\mu}k_f^2 + m\hbar\omega} \\ &\times e^{-i(Q_q + \frac{1}{2\mu}k_i^2 - n\hbar\omega + i\epsilon)t/\hbar} V | \Psi_\alpha^+ \rangle \end{aligned} \tag{21}$$

Under the following definition

$$\begin{aligned} &\lim_{\epsilon \to 0} \frac{\exp\left[i(Q_p + \frac{1}{2\mu}k_f^2 - Q_q - \frac{1}{2\mu}k_i^2 + (n-m)\hbar\omega - i\epsilon)t/\hbar\right]}{Q_q + \frac{1}{2\mu}k_i^2 - n\hbar\omega + i\epsilon - Q_p - \frac{1}{2\mu}k_f^2 + m\hbar\omega} \\ &= 2\pi\, i\delta\left(Q_p + \tfrac{1}{2\mu}k_f^2 + (n-m)\hbar\omega - Q_q - \tfrac{1}{2\mu}k_i^2\right) \end{aligned} \tag{22}$$

of the Dirac δ-function, eq.(21) becomes

$$S_{pq}(t) = \langle \Psi_p | \Psi_q \rangle \delta_{pq} + i2\pi\, T_{pq}\, \delta\left(Q_p + \tfrac{1}{2\mu}k_f^2 + (n-m)\hbar\omega - Q_q - \tfrac{1}{2\mu}k_i^2\right) \tag{23}$$

Using terminology directly analogous to field free collisions, the S-matrix eq.(23) has been written in terms of the transition amplitude

$$T_{pq} = \sum_n \sum_\alpha \sum_m \sum_\beta A_{p\beta}^m A_{q\alpha}^n \langle \Phi_\beta | V | \Psi_\alpha^+ \rangle = \langle \psi_p | V | \psi_q \rangle \exp\left(i(\mathbf{k}_i - \mathbf{k}_f) \cdot \mathbf{R}\right) \tag{24}$$

and includes all of the possible photon absorptions and emissions that can occur during collisonal transitions between the dresses states. For a field free collision, k_q and k_p would be defined as the wave numbers for the projectile, associated with the initial atomic state ψ'_q and the final atomic state ψ'_p, and the difference between k_q and k_p depends on the difference

$$Q_q - Q_p = \tfrac{1}{2\mu}k_p^2 - \tfrac{1}{2\mu}k_q^2 \tag{25}$$

between the energy levels of ψ'_q and ψ'_p. The initial asymptotic wave number for a laser assisted collision is still k_q, since the projectile has not yet interacted with the atom, but the final wave number k_f differs from k_p so as to satisfy the conservation of energy requirement

$$\tfrac{1}{2\mu}k_f^2 = Q_q + \tfrac{1}{2\mu}k_q^2 - Q_p - (n-m)\hbar\omega \tag{26}$$

Since k_p is defined by eq.(25), k_f can be defined by

$$\tfrac{1}{2\mu}k_f^2 = \tfrac{1}{2\mu}k_p^2 - (n-m)\hbar\omega \tag{27}$$

This shows that k_f can differ from k_p by the photon energy $(n-m)\hbar\omega$, which corresponds to the number of photons absorbed or emitted in the state-to-state transition.

The S-matrix obtained in this treatment describes scattering within the dressed basis set. The associated scattering amplitudes which can be derived from various theoretical techniques, only describe transitions between dressed states that are part of the new basis set. To obtain results that can be directly compared with field free collisions and experimental results, it is necessary to calculate the laser assisted scattering cross sections with respect to the field free basis set. From Bransden (1970) the cross section for a

transition from the field free atomic state ϕ_α to field free atomic state ϕ_β is

$$\sigma_{\beta\alpha} = \frac{1}{k_i(2\pi)^3} \int d\Omega \int dk_f \; k_f^2 \; W_{\beta\alpha} \tag{28}$$

where $W_{\beta\alpha}$ is the transition rate. For any given scattering angle and state-to-state transition, there can be more than one wave number for the projectile, corresponding to absorption and emission of energy from the laser field. This means that the transition rate is defined as

$$W_{\beta\alpha} = \sum_{k_f} 2\pi\mu^2 \; |T_{\beta\alpha}|^2 \; \delta(\epsilon_\beta - \epsilon_\alpha + \tfrac{1}{2\mu}k_f^2 - \tfrac{1}{2\mu}k_\alpha^2 + \delta E) \tag{29}$$

where it is written in terms of the transition amplitude T_{pq}, and includes the unknown energy change δE due to the influence of the laser. In eq.(29) the final wave number k_f must be written in terms of the wave number k_β, associated with the atomic state ϕ_β in a field free collision. Using the definition of k_β

$$\tfrac{1}{2\mu}k_\beta^2 = \epsilon_\beta + \tfrac{1}{2\mu}k_\alpha^2 - \epsilon_\alpha \tag{30}$$

in the delta function of eq.(29), the resulting equation

$$\tfrac{1}{2\mu}k_f^2 = \tfrac{1}{2\mu}k_\beta^2 - \delta E \tag{31}$$

relating k_f to k_β is very similar to eq.(27), and includes the unknown energy change δE. It is now possible to insert the transition rate eq.(29) into the integral cross section eq.(28). Using $|k_f|dk_f = d(\frac{1}{2}k_f^2)$ so that the integration over k_f can be evaluated, the integral cross section becomes

$$\sigma_{\beta\alpha} = \frac{1}{k_i(2\pi)^3} \int d\Omega \; \sum_{k_f} k_f \; 2\pi\mu^2 \; |T_{\beta\alpha}|^2 \; \delta(\tfrac{1}{2\mu}k_f^2 - \tfrac{1}{2\mu}k_\beta^2 + \delta E) \tag{32}$$

which is equivalent to the standard integral cross section in the field free basis set, except that allowance has been made for the absorption or emission of an unknown amount of energy δE from the laser field during the collision. The set of dressed atomic states obtained in section 2 are assumed to be a complete and normalized set so that $\sum_q |\psi_q\rangle\langle\psi_q| = 1$. On using this projection operator the "measured" transition amplitude, taken with respect to the field free basis set, is written in terms of the "dressed" transition amplitude, taken with respect to the dressed basis set as

$$T_{\beta\alpha} = \langle\Phi_\beta|V|\Phi_\alpha\rangle = \sum_p \sum_q \langle\phi_\beta, 0|\psi_p\rangle\, T_{pq}\, \langle\psi_q|\phi_\alpha, 0\rangle \tag{33}$$

The "dressed" transition amplitude T_{pq} of eq.(24) has been determined by the Lippman Schwinger equation, and according to eq.(26), k_f must satisfy the conservation of energy requirement

$$Q_p + \tfrac{1}{2\mu}k_f^2 - Q_q - \tfrac{1}{2\mu}k_q^2 + n\hbar\omega = 0 \tag{34}$$

where n has replaced $m - n$. As demonstrated in eq.(33) the "measured" transition amplitude, $T_{\beta\alpha}$, can be obtained from the "dressed" transition amplitude, T_{pq}, and k_f must satisfy the second conservation of energy requirement

$$\epsilon_\beta + \tfrac{1}{2\mu}k_f^2 - \epsilon_\alpha - \tfrac{1}{2\mu}k_\alpha^2 + \delta E = 0 \tag{35}$$

obtained from eq.(30). The final wave number, k_f, of the scattered projectile must be identical for both equation eq.(34) and eq.(35). This provides an opportunity to determine the total energy absorbed or provided by the laser field. It may be a natural assumption that this energy δE is an integer number of laser photon energies $n\hbar\omega$. But on diagonalizing the Floquet matrix to obtain the dressed wave function, it can be seen for some transitions

to occur, that the energy change δE cannot be an integer number of laser photon energies. In molecular spectroscopy an analogous situation occurs, where a molecule is excited to a higher energy level by a laser photon, which has more energy than is required for the transition (Weissbluth 1989). In the Raman effect, the molecule absorbs the laser photon and then emits a new Raman photon to remove the excess energy. This is the process that is assumed to be occuring whenever necessary, with no additional restrictions applied to the transition because it must proceed via the Raman effect. A discussion of this effect is given in section 4, and is shown to play a significant role in the laser dependent changes in the integral cross sections.

Since the vector potential eq.(2) can only be defined to within a phase shift δ_ω, as in Fig.1, it is therefore necessary to take the following average

$$\sigma_{\text{experiment}} = \frac{1}{2\pi} \int_0^{2\pi} \sigma(\delta_\omega)\, d(\delta_\omega) \tag{36}$$

of σ over the range of δ_ω from 0° to 360°.

4.THE ROLE OF THE FLOQUET DRESSED STATES

In discussing the use of Floquet theory in laser assisted collisions, reference will be made to a reduced Floquet system of a hydrogen atom in a laser field. An abbreviated energy level diagram is shown in Fig.5; The states shown are only a limited number of the infinite set of periodic Floquet states. In a first order approximation which allows for single photon coupling only, the system is adequately described by the following 7 states selected in the diagram of Fig.5,

$$|1\rangle = |1S,0\rangle \tag{37a}$$

$$|2\rangle = A|2S,-1\rangle + B\epsilon^{i\delta_\omega}|2P_0,0\rangle + B\epsilon^{-i\delta_\omega}|2P_0,-2\rangle \tag{37b}$$

$$|4\rangle = A|2S,0\rangle + B\epsilon^{i\delta_\omega}|2P_0,+1\rangle + B\epsilon^{-i\delta_\omega}|2P_0,-1\rangle \tag{37c}$$

$$|6\rangle = A|2S,+1\rangle + B\epsilon^{i\delta_\omega}|2P_0,+2\rangle + B\epsilon^{-i\delta_\omega}|2P_0.0\rangle \tag{37d}$$

$$|3\rangle = A|2P_0,-1\rangle + B\epsilon^{i\delta_\omega}|2S,0\rangle + B\epsilon^{-i\delta_\omega}|2S,-2\rangle \tag{37e}$$

$$|5\rangle = A|2P_0,0\rangle + B\epsilon^{i\delta_\omega}|2S,+1\rangle + B\epsilon^{-i\delta_\omega}|2S,-1\rangle \tag{37f}$$

$$|7\rangle = A|2P_0,+1\rangle + B\epsilon^{i\delta_\omega}|2S,+2\rangle + B\epsilon^{-i\delta_\omega}|2S,0\rangle \tag{37g}$$

For illustration purposes a first order approximation has been used here in the atomic dressing to reduce the number of possible transitions available; but all that is said here is valid to any order of approximation

For the purposes of numerical calculations, the energy levels 2S and $2P_0$ can be considered to be degenerate, though it must be kept in mind that this is not so. Even if the field free energy levels were degenerate, this degeneracy would be broken when in the influence of the laser field due to coupling between the 1S and $2P_0$ states.

Consider the laser perturbed Schrödinger equation eq.(4)

$$i\hbar\frac{d}{dt}\psi' = \left(\sum_i \left[\frac{1}{2}p_{r_i}^2 - i\frac{1}{2}\epsilon_o \cdot \mathbf{r}_i(\epsilon^{i(\omega t+\delta_\omega)} - \epsilon^{-i(\omega t+\delta_\omega)})\right] + V(\mathbf{r})\right)\psi' \qquad (38)$$

The laser induced perturbation $\frac{1}{2}\epsilon_o \cdot \mathbf{r}_i$, provides a dipole coupling between previously orthogonal field free atomic states, a coupling that contains a time-dependence $e^{i\omega t}$. Because of this time-dependent coupling, the field free states are no longer eigenfunctions of the Schrödinger equation, and the Schrödinger equation is then no longer time-independent. In section 2 it was shown that the Floquet prescription results in a new orthogonal basis set, composed of dressed atomic states which can be treated in a time-independent manner. These three properties (orthogonality, eigen functions and time-independence) of the Floquet dressed atomic states, allow traditional, field free, time-independent scattering theories to be applied to laser assisted collisions. However the price to be paid for these three properties is the introduction of the infinite set of periodic solutions. The transition between the finite set of field free atomic states, and the infinite set of dressed atomic states, is achieved by projection. This has been introduced in eq.(33) of section 3, where the "measured" transition amplitude, taken with respect to the field free basis set, is written in terms of the "dressed" transition amplitude, taken with respect to the dressed basis set. Because the dressed atomic states have a periodic time-dependence it is necessary, in order to achieve this projection, to write the field free atomic states as a combination of field free atomic states and periodic states. In the expansion

$$|\phi_\alpha\rangle = \sum_n A_n \epsilon^{-in\omega t}|\phi_\alpha, n\rangle \qquad (39)$$

of the field free atomic state into a field free state and periodic state combination, A_n is non-zero only when $n = 0$. Thus the field free atomic state $|\phi_\alpha\rangle$ is equivalent to the $n = 0$

Floquet state $|\phi_\alpha, 0\rangle$. Using this with the above set of dressed atomic states eq.(37), the new dressed basis set (in this first order approximation), for a hydrogen atom originally in the 2S field free state, for example, will have a non-zero population density only in the dressed atomic states labelled 3, 4 and 7. Conversely, any population density in the dressed atomic states 3, 4 and 7 of the dressed basis set, will each contribute to the population density of the 2S state of the field free basis set. In order for population densities in the dressed states 3 and 7 to contribute to the population density in the field free state 2S, the laser field is required to provide (or absorb) a *non*-integer number of laser photon energies. This is because the 2S and 2P field-free energies are, in fact, not degenerate, and because $E_3 = E_5 - \hbar\omega$ and $E_7 = E_5 + h\omega$, as asserted by Floquet theory. Although it is not immediately obvious, the same problem is associated with the dressed state 4. Due to 2S-nP (n>2) couplings, the energy of state 4 shifts with changing electric field strengths so that $E_4 \neq E_{2S}$. As mentioned in section 3, production of these non integer photons, is known as the Raman effect, and as can be seen, a Raman photon will be involved whenever the "dressed" transition amplitudes are projected on to the "measured" transition amplitudes. This is considered an atom-field effect and will not involve the projectile directly. For collisions within the dressed basis set, all energy differences for atomic transitions, are accounted for by changes in the wave number of the projectile, plus the absorption or emission of an integer number of laser photons.

To show the effect of the Floquet approach on a laser assisted collision, the 1S-2S excitation in an electron-hydrogen collision

$$H(1S) + \epsilon^- + N\hbar\omega \text{ —— } H(2S) + \epsilon^- + M\hbar\omega \tag{40}$$

will be considered for first order dressed atomic states. Table 1 shows the "dressed" transition elements and their probability amplitudes when projected onto the "measured" transition amplitude T_{1S2S}. These values can then be used in a first order Born-Wave approximation. It is interesting to note that the 3 "dressed" transition amplitude elements for T_{31} are the same as the 3 "dressed" transition amplitude elements for T_{71}, with identical changes in the projectile energy. In fact the transition amplitude elements for T_{31} are duplicated for all transitions $1 \longrightarrow$ P where P represents all states

$$|P\rangle = A|2P_0, n\rangle + B\epsilon^{i\delta_\omega}|2S, n+1\rangle + B\epsilon^{-i\delta_\omega}|2S, n-1\rangle \tag{41}$$

This feature of the Floquet dressed atomic states is very useful for the closely coupled calculations required in the Multichannel Eikonal Treatment of the collision, where the infinite set of periodic states tend to make such calculations appear at first sight prohibitive. Consider two members of the set P of states defined by eq.(41),

$$|\psi_p, 1\rangle, \quad \text{energy level} = Q_p + \hbar\omega$$

and

$$|\psi_p, 0\rangle, \quad \text{energy level} = Q_p$$

In a transition between these two states, the change in projectile energy due solely to the difference in energy levels is $\hbar\omega$, ie $\frac{1}{2\mu}k_{p1}^2 = \frac{1}{2\mu}k_{p0}^2 - \hbar\omega$. Then $\langle\psi_p, 1|\psi_p, 0\rangle = 0$, since a photon must be absorbed from the laser field in the transition, a photon which neither $|\psi_p, 1\rangle$ nor $|\psi_p, 0\rangle$ can absorb yet still preserve their energy levels. If however each state is associated with a projectile of the same energy, forming a collisional wavefunction $\Psi_p = \psi_p \, exp(i\mathbf{k} \cdot \mathbf{R})$, then, for a collisional transition from atomic state $|\psi_p, 0\rangle$ to $|\psi_p, 1\rangle$,

the projectile can absorb the laser photon as is required, and regain the energy $\hbar\omega$ which it lost in making the transition to the higher energy level. Hence the projection between the two collisional wave functions is

$$\langle \psi_p, 1| \exp(-i\mathbf{k}_f \cdot \mathbf{R}) \exp(i\mathbf{k}_i \cdot \mathbf{R}) |\psi_p, 0\rangle = 1 \tag{42}$$

ie the wave functions are no longer orthogonal when

$$\tfrac{1}{2\mu}k_f^2 = \tfrac{1}{2\mu}k_{p1}^2 - \hbar\omega = \tfrac{1}{2\mu}k_{p0}^2 = \tfrac{1}{2\mu}k_i^2 \tag{43}$$

This result can be extended to all other members of set P, with the same results for other sets of periodically repeating dressed atomic states. This feature of Floquet dressed states makes it impossible to define the probability amplitude of being in a given dressed atomic state when combined with a projectile wave function. Or described another way the system exists in a state of flux between all periodic states of the same form associated with a given projectile energy. This necessitates a summation of the probability amplitudes over what are termed "grouped" states (Smith 1991). Hence the entire infinite set of periodic Floquet states can be included exactly within the closely coupled calculation. Although essential for the Multichannel Eikonal Treatment these "grouped" states can be ignored in the first Born approximation.

Inserting the contents of Table (1) into eq.(33), which relates the "measured" transition amplitude to the "dressed" transition amplitude, T_{1S2S} becomes

$$T_{1S2S} = A^2 V_{1S2S}\, \delta(\tfrac{1}{2\mu}k_f^2 = \tfrac{1}{2\mu}k_{2S}^2)$$

$$+ ABV_{1S2P_0} e^{-i\delta_\omega}\, \delta(\tfrac{1}{2\mu}k_f^2 = \tfrac{1}{2\mu}k_{2S}^2 - \hbar\omega)$$

$$+ ABV_{1S2P_0} e^{i\delta_\omega}\ \delta(\tfrac{1}{2\mu}k_f^2 = \tfrac{1}{2\mu}k_{2S}^2 + \hbar\omega)$$

$$+ ABV_{1S2P_0}(e^{i\delta_\omega} + e^{-i\delta_\omega})\ \delta(\tfrac{1}{2\mu}k_f^2 = \tfrac{1}{2\mu}k_{2P_0}^2)$$

$$+ B^2V_{1S2S}(1 + e^{-i2\delta_\omega})\ \delta(\tfrac{1}{2\mu}k_f^2 = \tfrac{1}{2\mu}k_{2P_0}^2 - \hbar\omega)$$

$$+ B^2V_{1S2S}(e^{i2\delta_\omega} + 1)\ \delta(\tfrac{1}{2\mu}k_f^2 = \tfrac{1}{2\mu}k_{2P_0}^2 + \hbar\omega) \qquad (44)$$

In contrast the laser assisted differential cross section can be calculated using the traditional time-dependent Perturbation theory (Bayfield 1979). For an oscillatory perturbing potential

$$H(\mathbf{r},t) = -i\epsilon_o \cdot \mathbf{r}(e^{i\omega t}e^{i\delta_\omega} - e^{-i\omega t}e^{-i\delta_\omega}) \qquad (45)$$

the perturbed or dressed wave function is

$$\phi_\alpha^P = \sum_{n=0}^{\infty}\sum_{\beta} a_\beta^n(t)\ \phi_\beta\ e^{-i\epsilon_\beta t/\hbar} \qquad (46)$$

where $\sum_\beta$ is a summation over the unperturbed atomic states and ϵ_β is the energy level of state Φ_β. To a first order approximation this gives just three dressed states for the laser perturbed 1S, 2S and $2P_0$ field free states

$$\phi_{1S}^P = |\phi_{1S}\rangle e^{-i\epsilon_{1S}t/\hbar} \qquad (47a)$$

$$\phi_{2S}^P = \Big(D_1|\phi_{2S}\rangle + D_2|\phi_{2P_0}\rangle e^{i\omega t}e^{i\delta_\omega} + D_2|\phi_{2P_0}\rangle e^{-i\omega t}e^{-i\delta_\omega} \Big) e^{-i\epsilon_{2S}t/\hbar} \qquad (47b)$$

$$\phi_{2P_0}^P = \Big(D_1|\phi_{2P_0}\rangle + D_2|\phi_{2S}\rangle e^{i\omega t}e^{i\delta_\omega} + D_2|\phi_{2S}\rangle e^{-i\omega t}e^{-i\delta_\omega} \Big) e^{-i\epsilon_{2P}t/\hbar} \qquad (47c)$$

where $D_1 = N$, $D_2 = -i\langle\phi_\beta|\epsilon_o \cdot \mathbf{r}|\phi_\alpha\rangle\frac{N}{\omega}$ and N is a normalization constant. Instead of projecting the dressed states onto field free states, this form of approach assumes that the dressed states collapse onto their field free source (Sharma and Mohan 1990). Taking this

type of approach the T_{1S2S} transition amplitude becomes

$$T_{1S2S} = D_1 V_{1S2S}\ \delta(\tfrac{1}{2\mu}k_f^2 = \tfrac{1}{2\mu}k_{2S}^2)$$
$$+ D_2 V_{1S2P_0} e^{-i\delta_\omega}\ \delta(\tfrac{1}{2\mu}k_f^2 = \tfrac{1}{2\mu}k_{2S}^2 - \hbar\omega)$$
$$+ D_2 V_{1S2P_0} e^{i\delta_\omega}\ \delta(\tfrac{1}{2\mu}k_f^2 = \tfrac{1}{2\mu}k_{2S}^2 + \hbar\omega) \qquad (48)$$

Comparing the Floquet dressed atomic states of eq.(37) with the Perturbative dressed atomic states of eq.(47), it can be seen that each individual dressed state ψ has a very similar form under both treatments. But the Perturbative approach does not predict the infinite set of periodic states. This lack of an infinite set of states makes a great difference in the "measured" transition amplitude, as can be seen by comparing the Floquet transition amplitude of eq.(44) with the Perturbative transition amplitude of eq.(48). Not only does the Floquet transition amplitude have more terms, or more paths for the transition, it also has a δ_ω dependence that will be preserved in the cross sections, whilst the δ_ω dependence of the Perturbative transition amplitude will clearly cancel out in the resulting cross sections.

By first predicting the infinite set of states, and then by writing the "measured" transition amplitude in terms of the "dressed" transition amplitude, this Floquet model provides two distinct areas of possible photon absorption and emission, which can be denoted by the mechanisms (A,$\hbar\omega$) and (e,A,$\hbar\omega$). (A,$\hbar\omega$) refers to the projection of the dressed atomic states onto the field free atomic states, and gives rise to laser photon absorption and emission and Raman photon emission. (e,A,$\hbar\omega$) refers to the transitions between dressed atomic states which requires the influence of the projectile, and which only gives rise to laser photon absorption and emission. There is a third area of possible photon absorption and emission, which is omitted in this model that ignores the laser perturbation

of the projectile. This can be denoted by the mechanism (e,$\hbar\omega$), which refers to photon absorption and emission by the projectile before and after the collision. When the full laser perturbation is included, (section 6) there is no indication of such photon absorption and emission, so that the multiphoton events, associated with the projectile, occur during transitions between dressed states only, or is described by (e,A,$\hbar\omega$). Hence (A,$\hbar\omega$) and (e,A,$\hbar\omega$) adequately describe the mechanisms and sequence of all multiphoton events. It can therefore be seen that this model provides a concise description of the projectile atom collision in a laser field, where the interactions (A,$\hbar\omega$) and (e,A,$\hbar\omega$), as recently described (Newell 1990) are included exactly.

5.RESULTS: $e^- + H(1S) + N\hbar\omega \longrightarrow e^- + H(2S, 2P_0) + M\hbar\omega$

State-to-state cross sections for the 1S-2S and 1S-$2P_0$ transitions, in laser assisted e^--H(1S) collisions, are presented in both the Multichannel Eikonal Treatment and the Born-Wave approximation, as a function of impact energy and laser field intensity. All cross sections shown are a summation over the state-to-state cross sections, for all possible final projectile energies consistent with a given initial relative energy. Changes in the final projectile energy arise from photon absorption and emission. The laser considered is a monotonic, plane polarized CO_2 laser ($\hbar\omega = 0.117$eV), with the polarization direction parallel to the initial projectile velocity. The restricted basis set - 1S, 2S, $2P_0$, and $2P_{\pm 1}$ - is used for the dressing of the states, which in turn provide the basis set used within the Multichannel Eikonal Treatment. The axis of quantization is along the direction of incidence of the projectile electron, and as stated above is also taken as the direction of polarization of the laser field.

Cross sections vs field strength are presented in Fig.6 and Fig.7, for Floquet dressed hydrogen atoms where $\delta_\omega = 0°$. The cross sections are compared over a range of orders of approximation for the dressing of the atomic states. It can be seen that there are very striking differences between the different levels of approximation, especially between the first order cross section (which fails to exhibit a second stationary point) and the higher orders. It is also apparent for both the Born-Wave approximation (Fig.6) and the Multichannel Eikonal Treatment (Fig.7) that at least a third order approximation in the Floquet dressing is needed in order to reach convergence over the range of field strengths studied. The divergence from convergence, for each order of approximation,

occurs at successively higher field strengths. Cross sections vs field strength are presented in Fig.8 and Fig.9 for Perturbatively dressed hydrogen atoms. In contrast to the Floquet dressed atomic states, the Perturbative dressed atomic states produce cross sections with very little significant difference between the successive orders of approximation. Although convergence is not even satisfactorily reached by a fifth order approximation - a fifth order cross section is nearly identical to a third order cross section, but a fourth order cross section is distinctly different - a reasonable qualitative result can be obtained from a first order approximation.

As the field strength ϵ_o rises, cross sections for both the Floquet dressed atomic states (Fig.6 and Fig.7) and the Perturbative dressed atomic states (Fig.8 and Fig.9) show an initial rise for the 1S-2S cross sections and an initial fall for the 1S-$2P_0$ cross sections. This initial trend is due to the dressed atomic states S and P, which show increasing amounts of each others zero field characteristics. The percentage $2P_0$ component in each of the dressed atomic states S and P, presented in Fig.10 as a function of field strength, illustrates this in a very visual manner for third order Floquet dressed and third order Perturbative dressed states, (a) and (b) respectively. The plots of Fig.10 exhibit the play off between the dressed states S and P, with each simultaneously giving up more of its intrinsic zero field character, and adopting more of the other character. For both approaches to the dressed atomic states, this character interchange continues past the point where the dressed state S has a greater $2P_0$ characteristic than the dressed state P. It is to be expected that the scattering cross sections would rise and fall according to the character of the dressed atomic states, ie, the 1S-2S cross section, is expected to rise past the falling 1S-$2P_0$ cross section

as ϵ_o increases. This is the case for the cross sections produced by Perturbatively dressed atomic states, where the plots of Fig.8 and Fig.9 exhibit a monotonic rise and fall in the 1S-2S and 1S-$2P_0$ cross sections. But it is clearly not the case for cross sections produced by Floquet dressed atomic states. The plots of Fig.6 and Fig.7 show cross sections, where there are distinct peaks and dips, which seem to bear no relation to the character of the dressed states. These peaks and dips arise from the contributions to the state-to-state cross sections, from the infinite set of periodic states. The first order cross sections, of Fig.6 and Fig.7, demonstrate very clearly the contribution to the cross section via the first order terms only. As the field strength rises, the contribution to the cross section via the first order terms increases, and these contributions, whilst initially augmenting, eventually begin to curtail the rising change in characterstics, thereby causing the single stationary point. For the second order cross sections, contributions are allowed from both first and second order terms. As the field strength rises, the rising contribution to the cross sections from second order terms is now added to the first order contributions. The second order terms initially curtail, but then augment the rising change in characteristics, and eventually managed to dominate the first order contributions to cause the second stationary point. This distinct difference between the first and second order approximations to the cross sections, emphasizes the role played by the higher order terms through the infinite set of periodic dressed states. Since the infinite set of periodic states is not predicted in a Perturbative dressing of the atom, contributions from higher order terms cannot occur. Thus no stationay points can be expected, for the Perturbative cross sections, as the cross sections follow the character of the dressed atomic states.

It has already been explained in section 3 that any experiment would measure cross sections over a range of phase factors δ_ω. Cross sections are presented in Fig.11 and Fig.12, compared over a range of phase factors from $\delta_\omega = 0°$ to $90°$. Cross sections for phase factors in the range $90°$ to $360°$ are a repeat of those shown. A model attempting to predict experimental results, therefore requires averaging over the reduced range of $0°$ to $90°$ alone. The cross sections pertain to Floquet dressed hydrogen atoms, and are calculated by the Born-Wave approximation (Fig.11) and the Multichannel Eikonal Treatment (Fig.12). Cross sections for Perturbative dressed atomic states are not presented, because of their phase independence. The above results (Fig.6 and Fig.7), which illustrate convergence in the cross sections for rising orders of atomic dressing, justify the use of a third order approximation in the following cross sections. The Born-Wave approximation (Fig.11) and the Multichannel Eikonal Treatment (Fig.12) both show a range of different responses of the cross section to the changing field strength. These range from the two distinct stationary points exhibited by cross sections for $\delta_\omega = 0°$, and the single stationary point of the cross sections for $\delta_\omega = 90°$. For $\delta_\omega = 90°$ there are no contributions to the cross sections from first or third order terms, so that the single observed stationary point is dependent on the second order terms only. For phases between $0°$ and $90°$ the contributions from the different orders vary, giving rise to the range of cross sections between the two extremes described. Both the Born-Wave and the Multichannel Eikonal results are presented in Fig.13 when the cross sections are averaged over the required range of phases, from $\delta_\omega = 0°$ to $90°$. It is immediately noticed, while the dressed atomic states S and P practically exchange zero field characteristics as the electric field strength rises, that the averaged

cross sections for the 1S-2S and 1S-$2P_0$ transitions never cross. Also the field strength at which the two cross sections are identical, is the same as the field strength at which the dressed atomic states S and P each contain a 50:50 combination of 2S and $2P_0$ field free states. This non-crossing of the averaged cross section in Fig.13, is due to the projection of the "dressed" transition amplitudes onto the "measured" transition amplitudes. If the dressed atomic states S and P are dominated by each others zero field characteristics, they will then contribute more to the state-to-state cross section of the character that dominates them, via the infinite set of periodic states, than to the state-to-state cross sections of their own zero field character. Hence a dressed state S, with a predominately $2P_0$ character, contributes mostly to the 1S-$2P_0$ cross section, rather than the 1S-2S cross section. This then leads to viewing the phase dependent state-to-state cross sections, as being variations from these phase averaged cross sections. These variations occur due to constructive and destructive interference. When the cross sections are averaged, the effect of the interference is cancelled out. To contrast with this non-crossing of the cross sections in Fig.13, cross sections vs frequency are presented in Fig.14 for third order Perturbative dressed atomic states. For the Perturbative dressed atomic states, the 1S-2S and the 1S-$2P_0$ cross sections do cross in Fig.14, with the cross sections again being identical at the same field strength that the dressed states S and P each contain a 50:50 mixture of 2S and $2P_0$ field free states.

6.LASER PERTURBATION OF THE PROJECTILE

The full effect of the laser field is now considered by applying the laser perturbation to both the projectile and the target atom. The perturbed Hamiltonian is

$$H = \tfrac{1}{2\mu}P_R^2 - \tfrac{Z}{m_P}\mathbf{P}_R\cdot\mathbf{A}/c + \tfrac{1}{2m_P}(AZ/c)^2$$
$$+ \sum_i \tfrac{1}{2}(\mathbf{p}_{ri} + \mathbf{A}/c)^2 + V(\mathbf{r}) + V(\mathbf{R},\mathbf{r}) \qquad (49a)$$
$$= \tfrac{1}{2\mu}P_R^2 - \tfrac{Z}{m_P}\mathbf{P}_R\cdot\mathbf{A}/c + \tfrac{1}{2m_P}(AZ/c)^2 + H_F + V(\mathbf{R},\mathbf{r}) \qquad (49b)$$

in the center of mass frame of reference, where the Floquet Hamiltonian for the atom

$$H_F = \sum_i \tfrac{1}{2}(\mathbf{p}_{ri} + \mathbf{A}/c)^2 + V(\mathbf{r})$$

has already been considered in section 2. The charge and the mass of the projectile are Z and m_p. For heavy particle collisions, $m_P \neq \mu$ the reduced mass of the collisional system. This difference occurs because the laser perturbation must be applied in the laboratory frame of reference, and the resulting Hamiltonian is then transformed to the center of mass frame of reference. The laser perturbations can be handled by treating the projectile and the atom as isolated systems. The internal atomic portion has already been considered via the solution of $id_t\phi = H_F\phi$ in section 2. Thus a solution for the projectile Hamiltonian

$$H_P = \tfrac{1}{2\mu}P_R^2 - \tfrac{Z}{m_P}\mathbf{P}_R\cdot\mathbf{A}/c + \tfrac{1}{2m_P}(AZ/c)^2 \qquad (50)$$

only is needed. The wave function Φ, which satifies the Schrödinger equation $i\frac{d}{dt}\Phi = H_P\Phi$, is represented by

$$\Phi = \exp\left[\, i\left(\mathbf{P}_R\cdot\mathbf{R} + \tfrac{Z}{m_P}\int_x^t \mathbf{P}_R\cdot(\mathbf{A}_o/c)\cos(\omega\tau+\delta_\omega) - \alpha \right) d\tau\right] \qquad (51)$$

where α is a constant phase shift that cancels out in the collisional S-matrix. In the original paper by Volkov (1935) the solution Φ is expressed in the general form

$$\Phi = \exp\left[i\left(\mathbf{P}_R \cdot \mathbf{R} + \frac{Z}{m_P}\mathbf{P}_R \cdot (\mathbf{A}_o/\omega c)\sin(\omega t + \delta_\omega) - \alpha \right) \right] \cdot Z_o \qquad (52)$$

where Z_o is dependent on $\mathbf{P}_R$, A_o, ω, m_P, δ_ω *and* x. If it is assumed that the only dependence of Z_o on x can be acknowledged by varying δ_ω, then δ_ω can be easily varied for any value of x, to give

$$\omega x + \delta_\omega = 0 \qquad \text{and} \quad Z_o = 1$$

for use in eq.(52) giving rise to the usual Volkov dressed wave function for a laser perturbed plane wave

$$\Phi = \exp\left[i\left(\mathbf{P}_R \cdot \mathbf{R} + \frac{Z}{m_P}\mathbf{P}_R \cdot (\mathbf{A}_o/\omega c)\sin(\omega t + \delta_\omega) - \alpha \right) \right] \qquad (53)$$

In deriving the wave function eq.(53), the assumption has been made that there are no transient effects arising from turn-on or turn-off of the laser, as is reasonable in this soft-photon weak-field regime. Having set $\omega x + \delta_\omega$ and $Z_o = 1$, it must be realized that δ_ω has now taken on a definite and distinct value for each collision. If $t = x$ is defined as being the time at which the point of closest approach for the collision is reached, then δ_ω is the phase shift of the laser field at the point of closest approach, as shown in Fig.1. In any experiment, collisions will occur across a wide range of space and time. Thus δ_ω will not be in general a constant for all collisions. As mentioned in section 3, a theoretical model that purports to predict experimental results, must include an average of the collisions over a range of δ_ω from 0° to 360°.

This dressed projectile wave function can now be combined with the dressed atomic wave functions from section 2, and using the techniques of section 3 the laser perturbed collisional S-matrix

$$S_{pq}(t) = \langle \Phi_p | \Phi_q \rangle \delta_{pq} + i2\pi \, T_{pq} \, \delta(Q_p + \tfrac{1}{2\mu}k_f^2 + (n+x-m)\hbar\omega - Q_q - \tfrac{1}{2\mu}k_i^2) \qquad (54)$$

can be derived. This S-matrix is of exactly the same form as eq.(33), with the new "dressed" transition amplitude

$$T_{pq} = \sum_n \sum_m \sum_\alpha \sum_\beta \sum_x A^m_{p\beta} A^n_{q\alpha} \, \langle \Phi_\beta | V | \Psi^+_\alpha \rangle \, J_x(D) \, e^{ix\delta_\omega} \qquad (55)$$

The Bessel function argument D is $\frac{Z}{m_P}(\mathbf{k}_i - \mathbf{k}_f) \cdot (\mathbf{A}_o/\omega c)$, and as usual arises from a Fourier expansion of the Volkov dressing of the projectile. The new conservation of energy requirement is now

$$\tfrac{1}{2\mu}k_f^2 = \tfrac{1}{2\mu}k_p^2 - (n+x-m)\hbar\omega \qquad (56)$$

where the projectile contribution x, to the number of photons absorbed and emitted during transitions between the dressed wave functions, is also included. The "measured" transition amplitude $T_{\beta\alpha}$ can now be written in terms of this new "dressed" transition amplitude T_{pq}, as outlined in section 3.

Cross sections vs field strength are presented in Fig.15 and Fig.16, for third order Floquet dressed hydrogen atoms, in a Born-Wave approximation of laser assisted e^--H(1S) collisions. Cross sections with the laser perturbation included for both the atom and the projectile, are compared with cross sections that neglect the laser perturbation of the projectile. It has already been shown that the Volkov dressing produces a very significant effect on individual differential and integral cross sections, with a specific final

projectile energy (Weinsgarthofer et al 1979, Byron et al 1987, Jetzke et al 1987, Sarkar and Chakraborty 1988). When the state-to-state transition cross sections are however summed over an increasingly wider range of projectile energies, corresponding to higher order multiphoton events, the fully perturbed collisional cross sections converge on the cross sections that include a laser perturbation of the atom only. This is clearly evident from the cross sections displayed in Fig.15 and Fig.16. As would be expected, this convergence improves as the initial impact energy increases. This study has only been conducted using the Born-Wave approximation, due to the difficulties associated with producing a practical numerical technique that can handle the Volkov dressed states within the Multichannel Eikonal Prescription in a reasonable amount of computer time. Despite the practical problems there is no difficulty in principle from using the new transition amplitude, and there is nothing to indicate that the convergence exhibited by the Born-Wave approximation would not be reproduced by the Multichannel Eikonal Treatment as well.

7.CONCLUSION

This work has studied laser assisted collisions, in a soft-photon weak-field regime, for intermediate energy projectiles. Within this regime, the most appropriate method of incorporating the laser perturbation of the atom, has been found to be the Floquet prescription. This Floquet approach, with its predicted infinite set of periodic states, is considered, by the authors, to be superior to the more traditional time-dependent Perturbation theory with which it was compared, because it provides a very concise description of projectile-atom collisions in a laser field. Unlike the time-dependent Perturbation theory, the Floquet prescription exactly describes the location during the collisional sequence of events at which photons are absorbed and emitted. From section 4, there are two distinct photon absorption and emission processes, allowed within the Floquet approach. The first being absorption and emission by the projectile, during the projectile-atom interaction (e,A,$\hbar\omega$), and the second being absorption and emission by the atom, well before and well after the projectile-atom interaction, (A,$\hbar\omega$). The laser perturbation (e,$\hbar\omega$) of the projectile was also acknowledged in this work, in the form of Volkov dressed projectile wave functions. It has however been shown that these projectile states have very little effect on the state-to-state cross sections, when summed over all possible final projectile energies consistant with a given projectile energy. These dressed wave functions also gave no indication of allowing photon absorption or emission by the projectile, before and after the projectile-atom interaction.

This work has also shown that the Floquet treatment provides cross sections with some very distinct, interesting and new features, the most important of which are summarized

below:

(a): When there is significant coupling between the atomic states, the Floquet approach requires at least a third order approximation in the dressed atomic states, to attain convergence in the state-to-state cross sections over the full range of field strengths studied in this work. This convergence in the higher order dressed states is critical, since the first order approximation does not even yield a qualitative indication of the overall variation of the converged cross sections with field strength, and a second order approximation is often not much better. This indicates that the contribution to the cross sections from the higher terms in the atomic dressed states are important.

(b): The Floquet cross sections display a laser phase dependence of δ_ω. It has also been shown that for comparison with experiment, it is necessary to take an average of the state-to-state cross sections over this phase, from $\delta_\omega = 0°$ to $360°$.

(c): For a third order approximation the Floquet dressed atomic states can be written in the general form.

$$\begin{aligned}|S\rangle = A|2S,n\rangle &+ B\epsilon^{i\delta_\omega}|2P_0,n+1\rangle + B\epsilon^{-i\delta_\omega}|2P_0,n-1\rangle \\ &+ C\epsilon^{i2\delta_\omega}|2S,n+2\rangle + C\epsilon^{-i2\delta_\omega}|2S,n-2\rangle \\ &+ D\epsilon^{i3\delta_\omega}|2P_0,n+3\rangle + D\epsilon^{-i3\delta_\omega}|2P_0,n-3\rangle \end{aligned} \tag{57}$$

and

$$\begin{aligned}|P\rangle = A|2P_0,n\rangle &+ B\epsilon^{i\delta_\omega}|2S,n+1\rangle + B\epsilon^{-i\delta_\omega}|2S,n-1\rangle \\ &+ C\epsilon^{i2\delta_\omega}|2P_0,n+2\rangle + C\epsilon^{-i2\delta_\omega}|2P_0,n-2\rangle \\ &+ D\epsilon^{i3\delta_\omega}|2S,n+3\rangle + D\epsilon^{-i3\delta_\omega}|2S,n-3\rangle \end{aligned} \tag{57}$$

If these dressed atomic states S and P are plotted against field strength then the dressed states practically exchange intrinsic zero field characteristics as the field strength rises. Eventually the dressed state S will have a greater $2P_0$ character than the dressed state P. Despite this character interchange of the dressed states, the 1S-2S state-to-state cross section never rises above the 1S-$2P_0$ state-to-state cross section when the phase averaged 1S-2S and 1S-$2P_0$ cross sections are plotted against field strength. This is demonstrated in Fig.17 for electron hydrogen collisions using Floquet dressed atomic states. It should be noticed that the 1S-2S and 1S-$2P_0$ cross sections have the same value, at precisely the same electric field strength that the dressed states S and P have a 50:50 composition of 2S and $2P_0$ field free states.

Where ever possible, numerical calculations are based on both the Multichannel Eikonal Treatment and the Born-Wave approximation. Both treatments produce similar qualitative variations to the cross sections with electric field strength, and any quantitative difference tends to orginate from the difference between the field free scattering theories adopted.

Acknowledgement: The authors thank Prof. Shakeshaft for bringing his references to our attention after our paper was written. This research was supported by the US Air Force Office of Scientific Research under Grant No AFOSR-89-0426.

BIBLIOGRAPHY

Bauchau H. and Shakeshaft R. (1984) Phys. Rev. A **30** 2752.

Bayfield J.E (1979) Excited Atomic and Molecular states in strong Electromagnetic fields. Phys Reports **55** 334.

Bransden B.H (1983) Atomic Collision Theory 2nd edn (NewYork: W.A.Benjamin) Ch4.

Burke P.G, Francken P and Joachain C.J (1991) J.Phys B:At Mol Opt Phys **24** 761.

Byron F. W. and Joachain C. J. (1984) J. Phys. B: At. Mol. Phys. **17** L295.

Byron F.W Jr, Francken P and Joachain C.J (1987) J.Phys B:At Mol Opt Phys **20** 5487.

Chu S.I (1985) Recent developments in Semi-Classical Floquet theories for intense field multiphoton processes. Adv At Mol Phys **21** 197.

Flannery M.R and McCann K.J (1975) J.Phys B:At Mol Phys **7** L223, 2518, L522.

Geltman S and Macquet A (1989) J.Phys B:At Mol Opt Phys **22** L419.

Jetzke S, Broad J and Macquet A (1987) J.Phys B:At Mol Opt Phys **20** 2887.

Kroll N.M and Watson K.W (1973) Phys Rev A **8** 804.

Mansky E.J and Flannery M.R (1990) J.Phys B:At Mol Opt Phys **23** 4549, 4572.

Newell W.R (1989) 16th Int Conf in the Phys of Electronic and Atomic Collisions. (N.Y) **205** (A.Dalgarno, R.S.Freund, P.M.Kock, M.S.Lubell and T.B.Lucatorto, eds) 122.

Sambe H (1973) Phys Rev A **7** 2203.

Sarkar S and Chakraborty M (1988) Phys Rev A **37** 1456.

Sharma B and Mohan M (1990) J.Phys B:At Mol Opt Phys **23** 3361.

Shirley J.H (1965) Phys Rev **138** B979.

Smith P.H.G (1991) Ph.D Thesis (Georgia Institute of Technology).

Smith P.H.G and Flannery M.R (1991) Nuc Inst and Meth in Phys Res (In Press).

Volkov D.V Z.Phys (1935) **94** 250.

Weinsgartshofer A, Clarke E.M, Holmes J.K and Jung C (1979) Phys Rev A **19** 2371.

Weissbluth M (1989) Photon-Atom interaction (Boston: Academic Press) P261.

FIGURE AND TABLE CAPTIONS

Figure (1): Vector potentials _____ $\mathbf{A}_o \cos(\omega t + \delta_\omega)$ and .. .. $\mathbf{A}_o \cos \omega t$, for a monotonic plane polarized laser field of frequency ω, positioned in time relative to the orbit's pericenter at time t = 0.

Figure (2): A restricted two state Floquet matrix for the 2S and $2P_0$ states of a hydrogen atom in a laser field, is shown for Floquet N^{o} n= -1, 0, and 1, where an unrestricted matrix would have Floquet N^{o} up to $\pm\infty$. The matrix is diagonalized to determine the "Quasi" energies Q_q and the dressed atomic states ψ_q.

Figure (3 a-c): Radial distribution functions of the dressed atomic states S and P, for a third order Floquet dressed hydrogen atom, are compared for increasing electric field strengths of a monotonic CO_2 laser field of photon energy $\hbar\omega = 0.0043$au.

Figure (4): The percentage $2P_0$ component vs field strength, of the dressed atomic states S _____ and P _ _ _ _ _ , are compared for a hydrogen atom in a laser field of photon energy $\hbar\omega = 0.0043$au.

Figure (5): Energy level diagram, $E = E_0 + \hbar\omega$, of the hydrogen dressed atomic states S and P at a photon energy of $\hbar\omega = 0.0043$au.

Figure (6): Cross sections vs field strength for the 1S-2S and 1S-$2P_0$ transitions, (a) and (b) respectively, in e^--H(1S) collisions in a laser field, using Floquet dressed hydrogen atoms and a Born-Wave approximation, are compared over a range of orders of approximation

for the Floquet dressing (.—.—. = 1st, ... = 2nd, - - - - - = 3rd and ——— = 4th order) at a photon energy $\hbar\omega$ = 0.0043au and $\delta_\omega = 0°$. The laser perturbation is included for the atom only.

Figure (7): Cross sections vs field strength for the 1S-2S and 1S-2P$_0$ transitions, (a) and (b) respectively, in e^--H(1S) collisions in a laser field, using Floquet dressed hydrogen atoms and a Multichannel Eikonal Treatment, are compared over a range of orders of approximation for the Floquet dressing (.—.—. = 1st, ... = 2nd, - - - - - = 3rd and ——— = 4th order) at a photon energy $\hbar\omega$ = 0.0043au and $\delta_\omega = 0°$. The laser perturbation is included for the atom only.

Figure (8): Cross sections vs field strength for the 1S-2S and 1S-2P$_0$ transitions, (a) and (b) respectively, in e^--H(1S) collisions in a laser field, using Perturbative dressed hydrogen atoms and a Born-Wave approximation, are compared over a range of orders of approximation for the Floquet dressing (-——-——- = 1st, —.—. = 2nd, ... = 3rd, - - - - - = 4th and ——— = 5th order) at a photon energy $\hbar\omega$ = 0.0043au. The laser perturbation is included for the atom only.

Figure (9): Cross sections vs field strength for the 1S-2S and 1S-2P$_0$ transitions, (a) and (b) respectively, in laser assisted e^--H(1S) collisions using Perturbative dressed hydrogen atoms and a Multichannel Eikonal Treatment, are compared over a range of orders of approximation for the Floquet dressing (-——-——- = 1st, — — = 2nd, . . . = 3rd, - - - - - = 4th and ——— = 5th order) at a photon energy $\hbar\omega$ = 0.0043au. The laser perturbation is included for the atom only.

Figure (10): The percentage $2P_0$ component vs field strength, for the dressed states S _____ and P _ _ _ _ _ , are compared for both Floquet and Perturbative dressed hydrogen atoms, (a) and (b) respectively, in a laser field of photon energy $\hbar\omega = 0.0043$au.

Figure (11): Cross sections vs field strength for the 1S-2S and 1S-$2P_0$ transitions, (a) and (b) respectively, in laser assisted e^--H(1S) collisions using third order Floquet dressed hydrogen atoms and a Born-Wave approximation, are compared over a range of phases δ_ω (_____ $= 0°$, _ _ _ _ _ $= 22.5°$, ... $= 45°$, . __ . __ . $= 67.5°$ and _ ____ _ ____ _ $= 90°$) at a photon energy $\hbar\omega = 0.0043$au. The laser perturbation is included for the atom only.

Figure (12): Cross sections vs field strength for the 1S-2S and 1S-$2P_0$ transitions, (a) and (b) respectively, in laser assisted e^--H(1S) collisions using third order Floquet dressed hydrogen atoms and a Multichannel Eikonal Treatment, are compared over a range of phases δ_ω (_____ $= 0°$, _ _ _ _ _ $= 22.5°$, ... $= 45°$, . __ . __ . $= 67.5°$ and _ ____ _ ____ _ $= 90°$) at a photon energy $\hbar\omega = 0.0043$au. The laser perturbation is included for the atom only.

Figure (13): Cross sections vs field strength for the 1S-2S _____ and 1S-$2P_0$ _ _ _ _ _ transitions in laser assisted e^--H(1S) collisions using third order Floquet dressed hydrogen atoms are compared in the Born-Wave approximation and the Multichannel Eikonal Treatment, (a) and (b) respectively, at a photon energy $\hbar\omega = 0.0043$au. The cross sections are an average of phase dependent cross sections for $\delta_\omega = 0°$ to $90°$, and the laser perturbation is included for the atom only.

Figure (14): Cross sections vs field strength for the 1S-2S _____ and 1S-2P_0 _ _ _ _ _ transitions in laser assisted e^--H(1S) collisions using third order Perturbative dressed hydrogen atoms are compared in the Born-Wave approximation and the Multichannel Eikonal Treatment, (a) and (b) respectively, at a photon energy $\hbar\omega = 0.0043$au. The laser perturbation is included for the atom only.

Figure (15): Cross sections vs field strength for 1S-2S and 1S-2P_0 transitions, (a) and (b) respectively, in laser assisted e^--H(1S) collisions using third order Floquet dressed hydrogen atoms and a Born-Wave approximation are compared with the laser perturbation included for the atom only (_____) and the laser perturbation included for both the atom and the projectile, where the later cross sections are a summation over a range of final projectile energies (_ _ _ = $\pm 20\hbar\omega$, ... = $\pm 25\hbar\omega$ and _ _ _ _ _ = $\pm 30\hbar\omega$ about the field-free final projectile energy). The phase $\delta_\omega = 0°$ and the photon energy $\hbar\omega = 0.0043$au.

Figure (16): Cross sections vs field strength for 1S-2S and 1S-2P_0 transitions, (a) and (b) respectively, in laser assisted e^--H(1S) collisions using third order Floquet dressed hydrogen atoms and a Born-Wave approximation are compared with the laser perturbation included for the atom only (_____) and the laser perturbation included for both the atom and the projectile, where the later cross sections are a summation over a range of final projectile energies (_ _ _ = $\pm 20\hbar\omega$, = $\pm 25\hbar\omega$ and _ _ _ _ _ = $\pm 30\hbar\omega$ about the field-free final projectile energy). The phase $\delta_\omega = 90°$ and the photon energy $\hbar\omega = 0.0043$au.

Figure (17): Cross sections in e^--H(1S) collisions are compared against the $2P_0$ component of the dressed atomic states, (a) and (b) respectively, over a range of electric field strengths for third order Floquet dressed hydrogen atoms in a laser field. The cross sections 1S-2S ——— and 1S-$2P_0$ - - - - - are an average of the phase dependent cross sections over a range of phases from $\delta_\omega = 0°$ to 90°, using a Multichannel Eikonal Ttreatment. For the percentage $2P_0$ component ——— represent the dressed state S and - - - - - represent the dressed state P.

Table (1): "Dressed" transition amplitude elements T_{pq}, final projectile energies $\frac{1}{2\mu}k_f^2$ and coefficients of the "dressed" transition amplitude T_{pq} within the "measured" transition amplitude T_{1S2S}.

Table (1): "Dressed" transition amplitude elements T_{pq}. final projectile energies $\frac{1}{2\mu}k_f^2$ and coefficients of the "dressed" transition amplitude T_{pq} within the "measured" transition amplitude T_{1S2S}.

"Dressed" transition amplitude matrix elements T_{pq}	Final projectile energy	Projection operator probability amplitude from T_{pq} onto T_{1S2S}
$T_{41} = AV_{1S2S}$	$\frac{1}{2\mu}k_f^2 = \frac{1}{2\mu}k_{2S}^2$	A
$T_{41} = BV_{1S2P_0}e^{-i\delta_\omega}$	$\frac{1}{2\mu}k_f^2 = \frac{1}{2\mu}k_{2S}^2 + \hbar\omega$	A
$T_{41} = BV_{1S2P_0}e^{+i\delta_\omega}$	$\frac{1}{2\mu}k_f^2 = \frac{1}{2\mu}k_{2S}^2 - \hbar\omega$	A
$T_{31} = AV_{1S2P_0}$	$\frac{1}{2\mu}k_f^2 = \frac{1}{2\mu}k_{2P_0}^2$	$Be^{+i\delta_\omega}$
$T_{31} = BV_{1S2S}e^{-i\delta_\omega}$	$\frac{1}{2\mu}k_f^2 = \frac{1}{2\mu}k_{2P_0}^2 + \hbar\omega$	$Be^{+i\delta_\omega}$
$T_{31} = BV_{1S2S}e^{+i\delta_\omega}$	$\frac{1}{2\mu}k_f^2 = \frac{1}{2\mu}k_{2P_0}^2 - \hbar\omega$	$Be^{+i\delta_\omega}$
$T_{71} = AV_{1S2P_0}$	$\frac{1}{2\mu}k_f^2 = \frac{1}{2\mu}k_{2P_0}^2$	$Be^{-i\delta_\omega}$
$T_{71} = BV_{1S2S}e^{-i\delta_\omega}$	$\frac{1}{2\mu}k_f^2 = \frac{1}{2\mu}k_{2P_0}^2 + \hbar\omega$	$Be^{-i\delta_\omega}$
$T_{71} = BV_{1S2S}e^{+i\delta_\omega}$	$\frac{1}{2\mu}k_f^2 = \frac{1}{2\mu}k_{2P_0}^2 - \hbar\omega$	$Be^{-i\delta_\omega}$

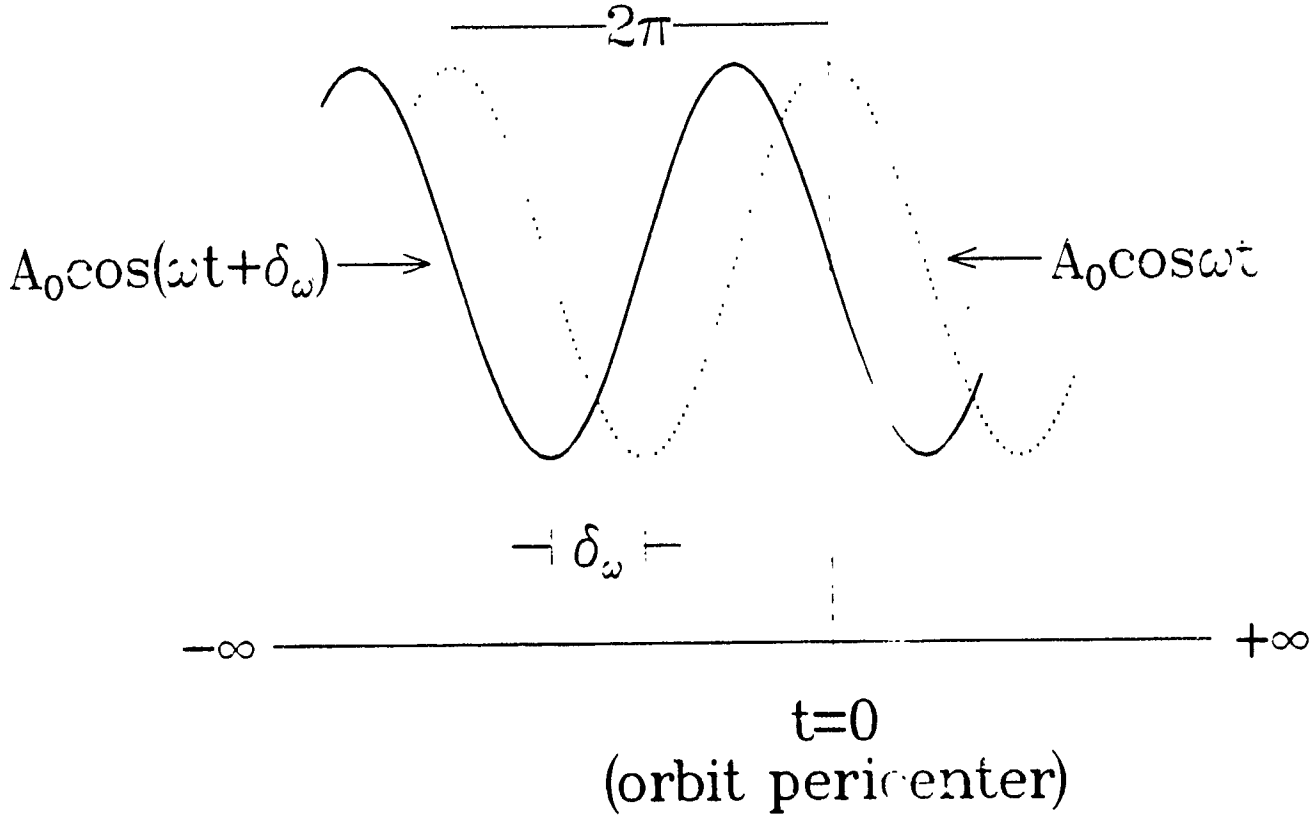

Figure(1): Vector potentials _____ $\mathbf{A}_o \cos(\omega t - \delta_\omega)$ and $\mathbf{A}_o \cos\omega t$. for a monotonic plane polarized laser field of frequency ω. positioned in time relative to the orbit's pericenter at time t = 0.

FIGURE 1: SMITH AND FLANNERY

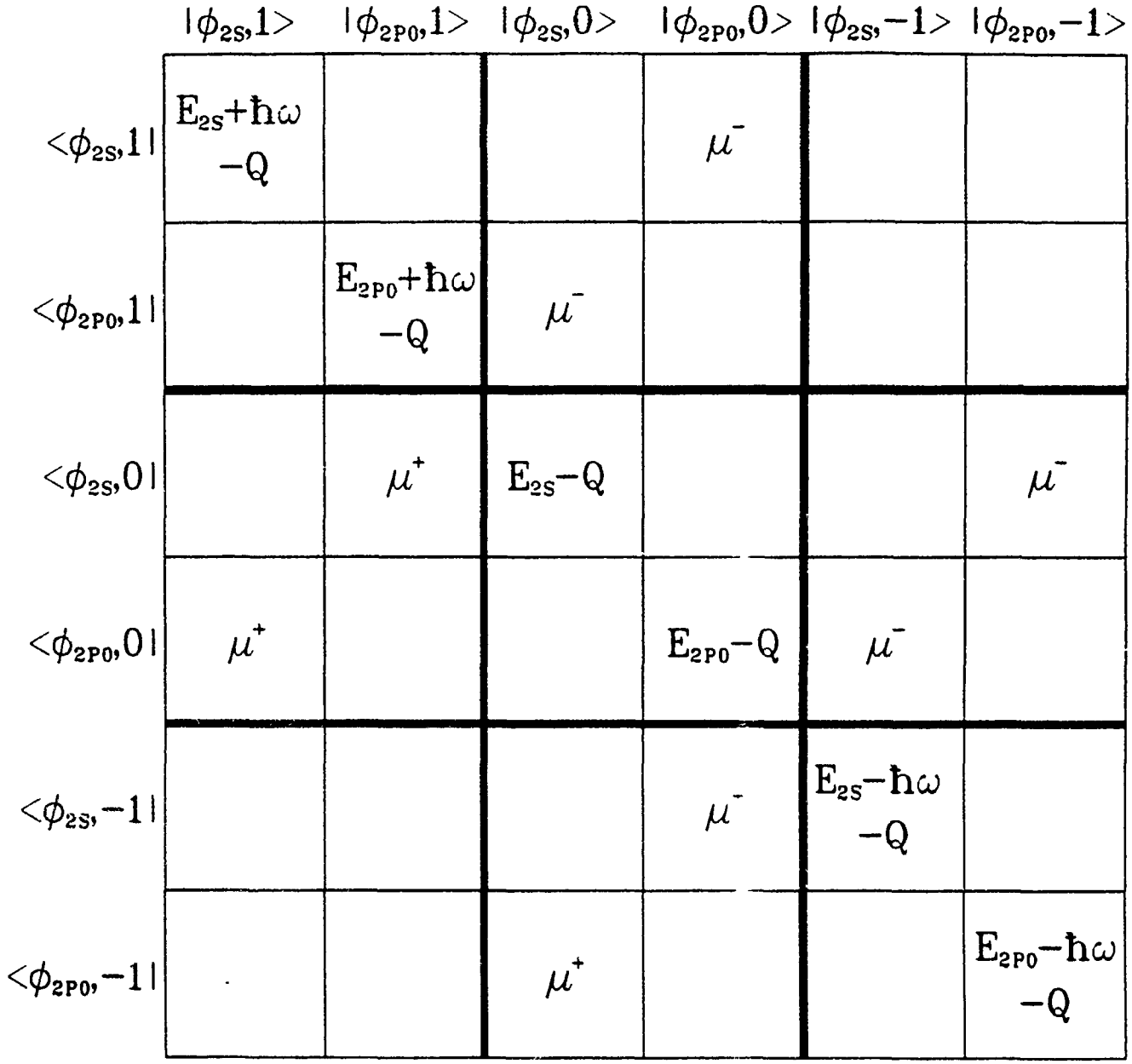

Figure(2): A restricted two state Floquet matrix for the 2S and $2P_0$ states of a hydrogen atom in a laser field. is shown for Floquet №s n= -1, 0, and 1, where an unrestricted matrix would have Floquet №s up to $=\infty$. The matrix is diagonalized to determine the "Quasi" energies Q_q and the dressed atomic states ψ_q.

FIGURE 2: SMITH AND FLANNERY

of a monotonic CO_2 laser field of photon energy $\hbar\omega = 0.0043$au.

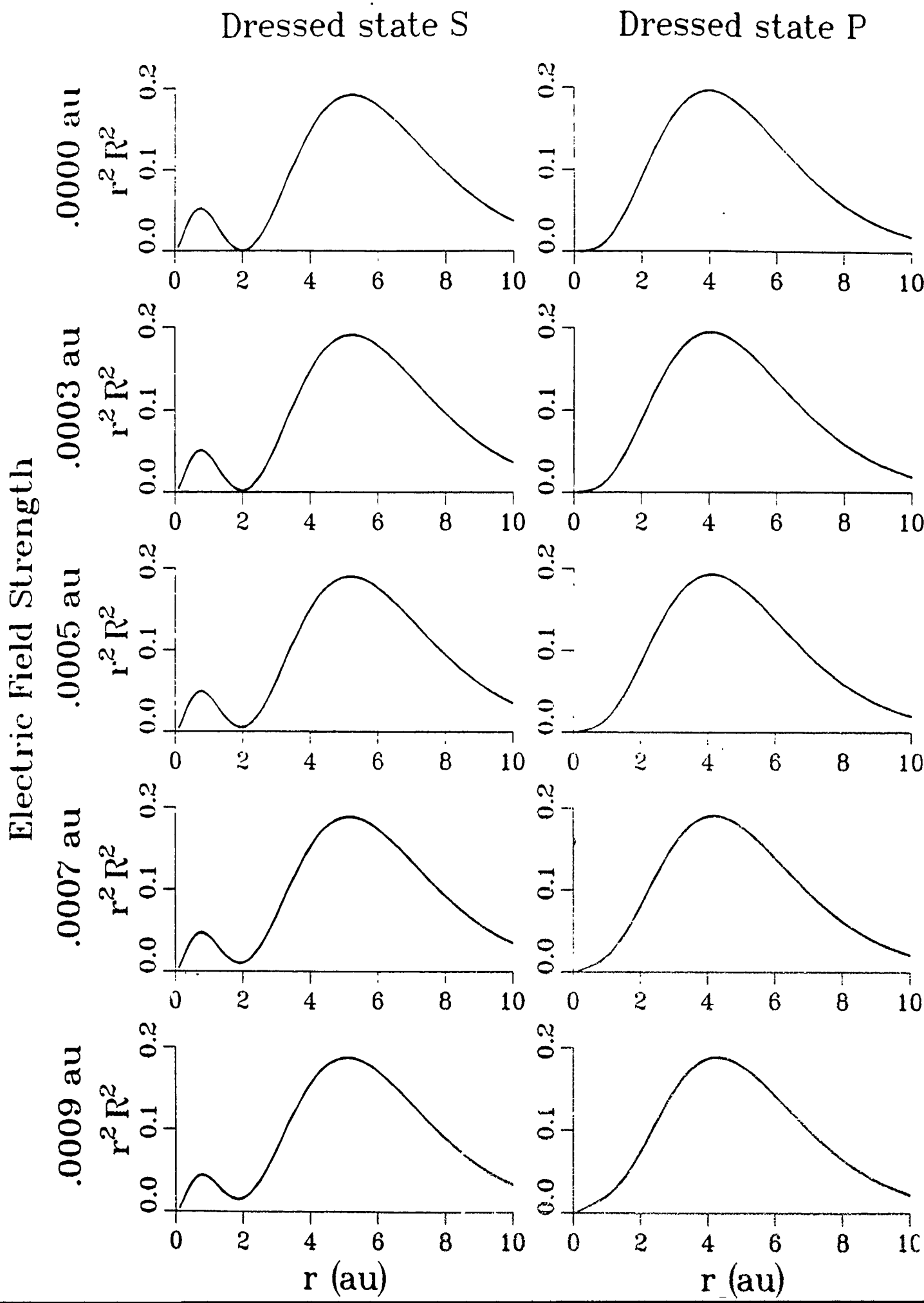

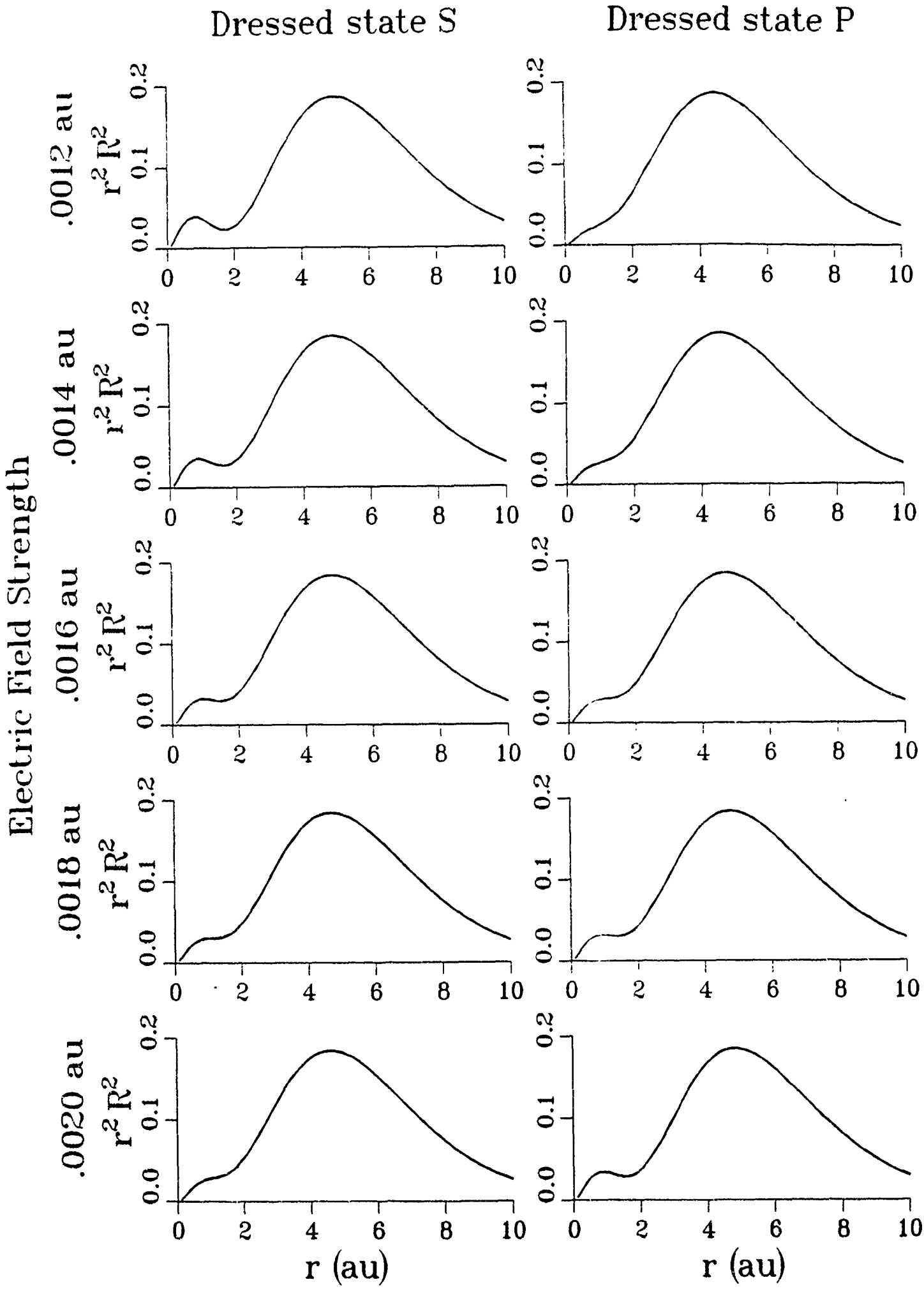
Dressed state S
Dressed state P
Electric Field Strength
.0012 au
.0014 au
.0016 au
.0018 au
.0020 au
r² R²
0.0
0.1
0.2
0
2
4
6
8
10
r (au)

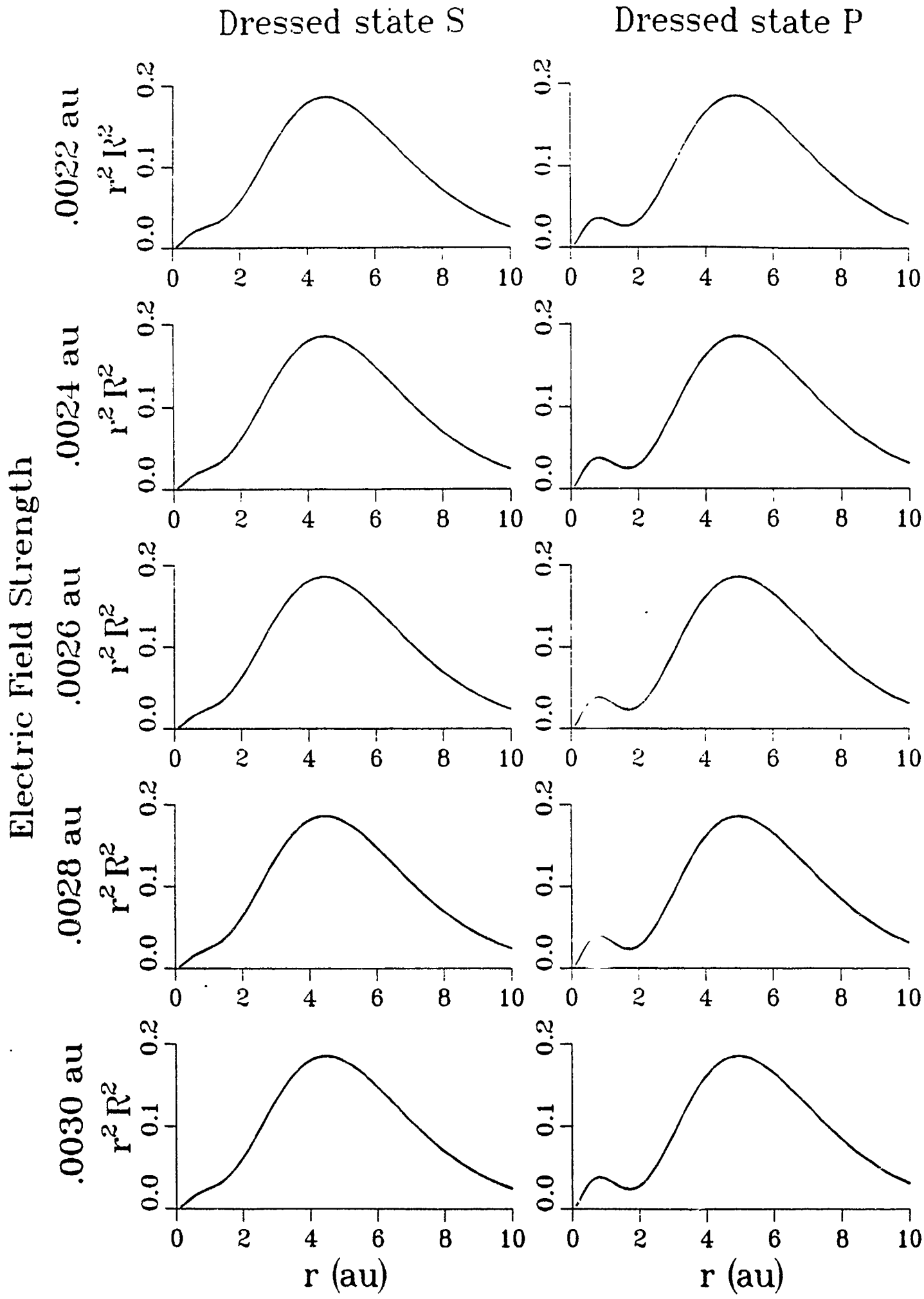
Dressed state S
Dressed state P
Electric Field Strength
.0022 au
.0024 au
.0026 au
.0028 au
.0030 au
r² R²
0.0
0.1
0.2
0
2
4
6
8
10
r (au)

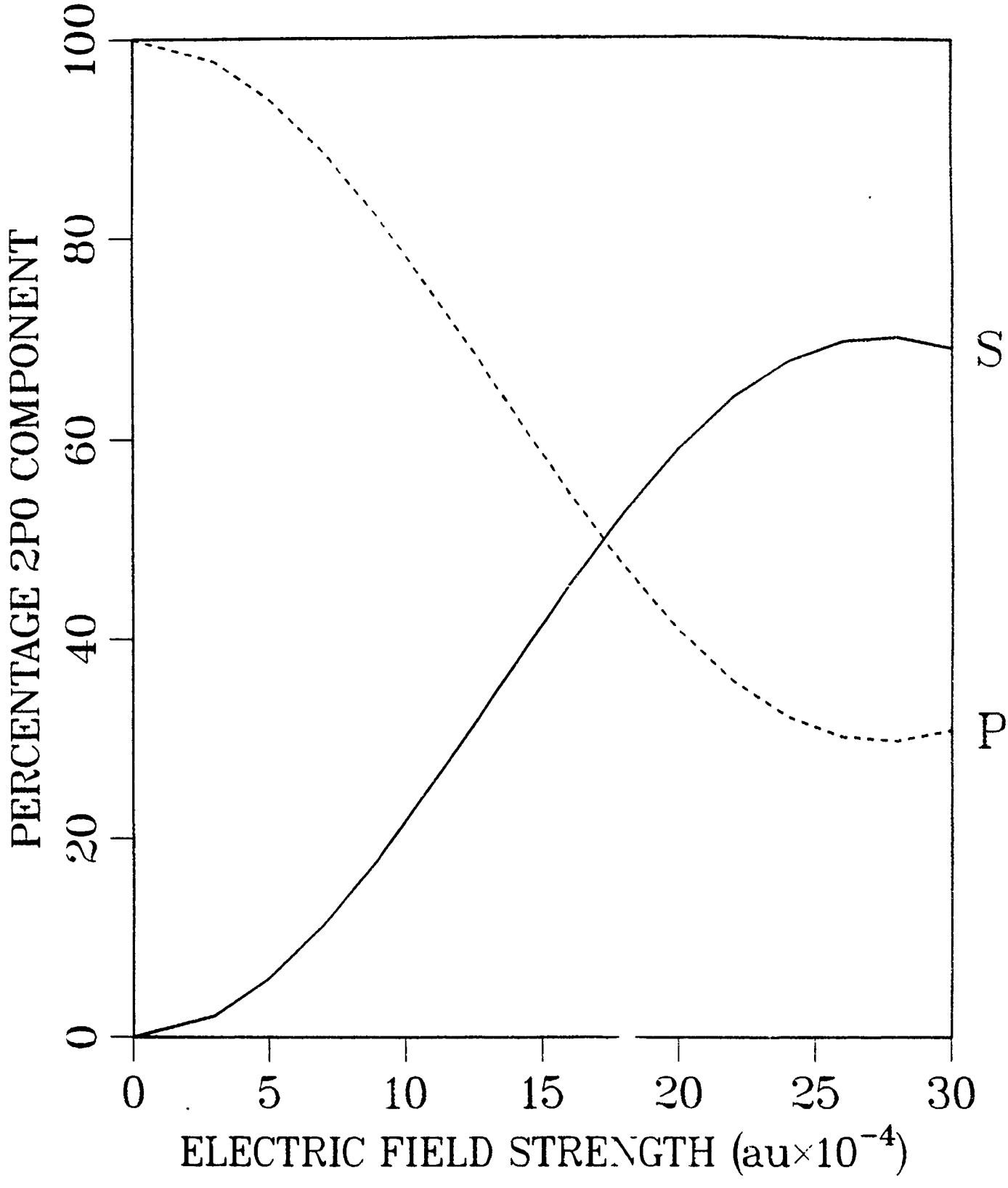

Figure(4): The percentage $2P_0$ component vs field strength. of the dressed atomic states S _____ and P _ _ _ _ _ . are compared for a hydrogen atom in a laser field of photon energy $\hbar\omega = 0.0043$au.

FIGURE 4: SMITH AND FLANNERY

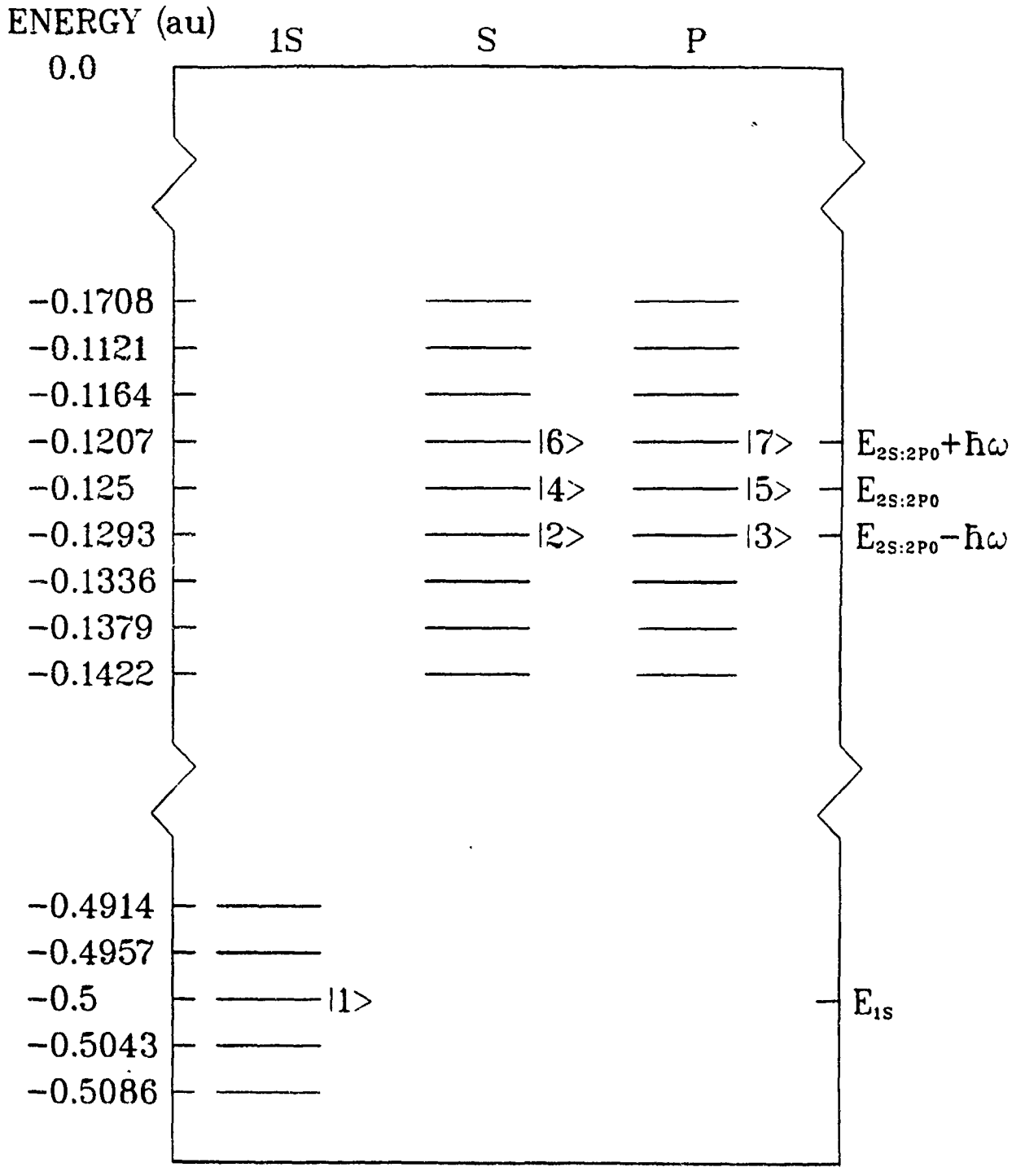

Figure(5): Energy level diagram, $E = E_0 - \hbar\omega$, of the hydrogen dressed atomic states S and P at a photon energy of $\hbar\omega = 0.0043$au.

FIGURE 5: SMITH AND FLANNERY

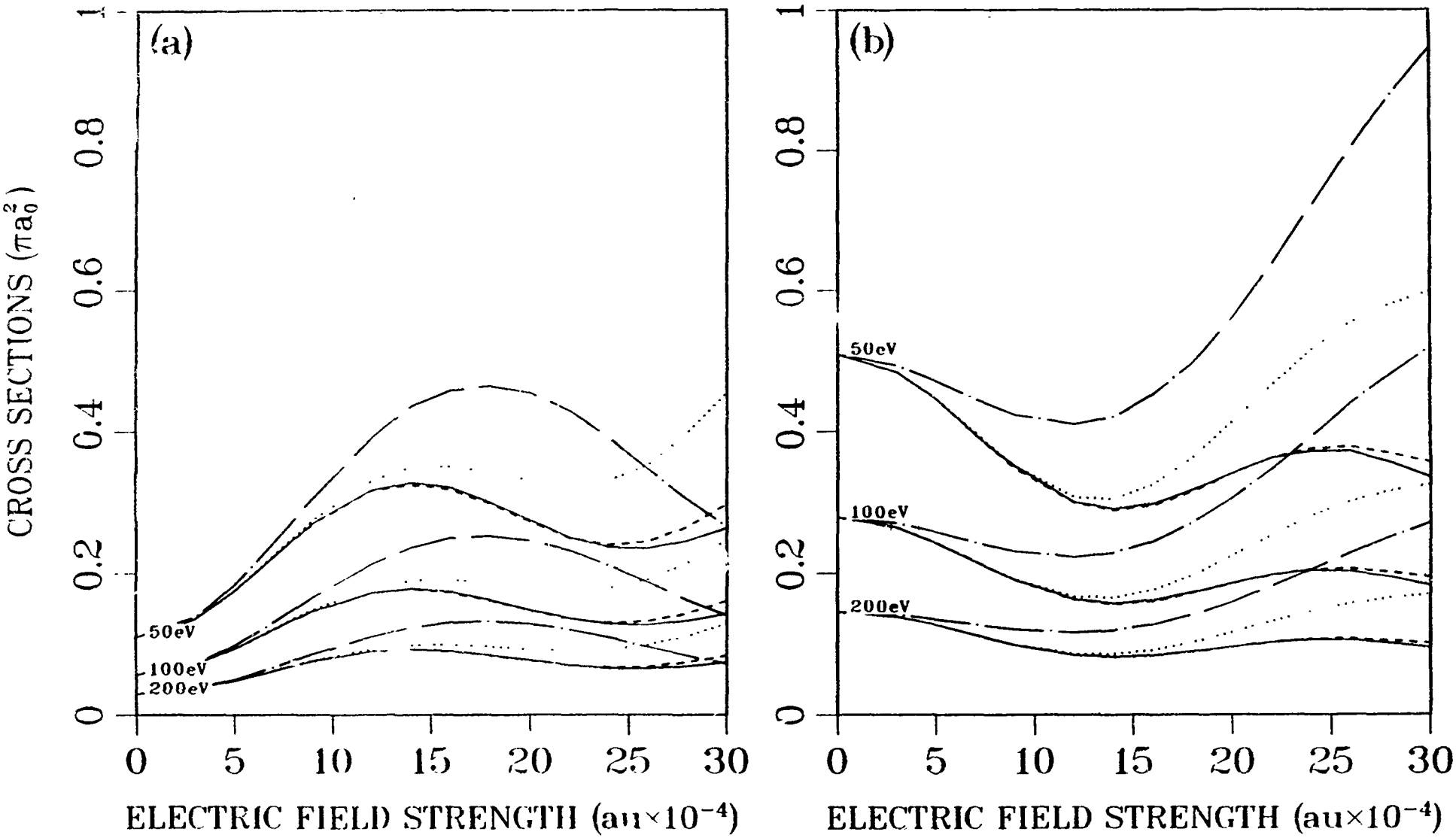

Figure(6): Cross sections vs field strength for the 1S-2S and 1S-2P_0 transitions, (a) and (b) respectively, in e^--H(1S) collisions in a laser field, using Floquet dressed hydrogen atoms and a Born-Wave approximation. are compared over a range of orders of approximation for the Floquet dressing (— — = 1st, . . . = 2nd, - - - - - = 3rd and ——— = 4th order) at a photon energy $\hbar\omega = 0.0043$au and $\delta_\omega = 0°$. The laser perturbation is included for the atom only.

IGURE 6: SI

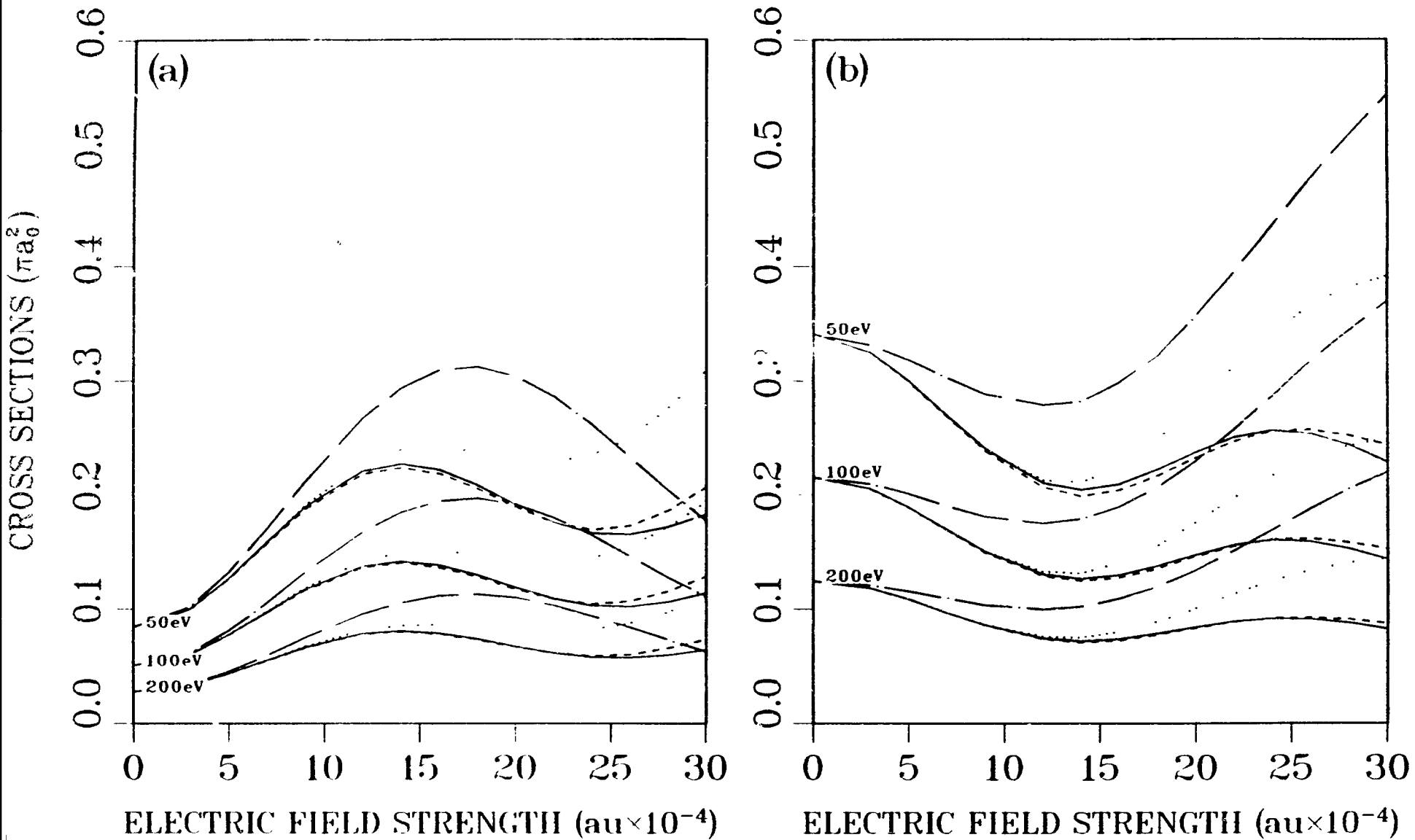

Figure(7): Cross sections vs field strength for the 1S-2S and 1S-2P_0 transitions, (a) and (b) respectively, in e^--H(1S) collisions in a laser field, using Floquet dressed hydrogen atoms and a Multichannel Eikonal Treatment, are compared over a range of orders of approximation for the Floquet dressing (— — — = 1^{st}, — — — = 2^{nd}, - - - - - = 3^{rd} and ——— = 4^{th} order) at a photon energy $\hbar\omega$ = 0.0043au and δ_ω = 0°. The laser perturbation is included for the atom only.

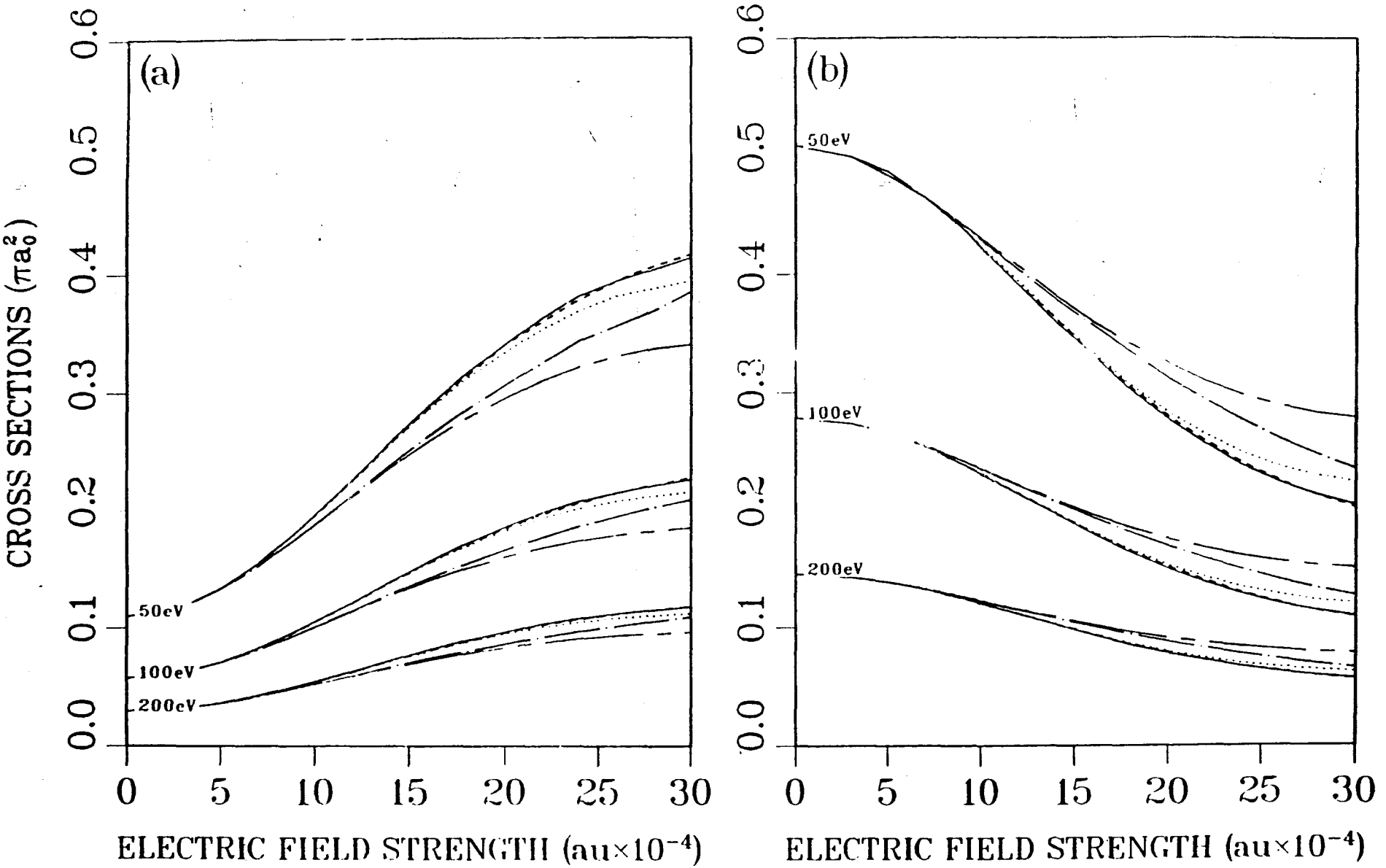

Figure(8): Cross sections vs field strength for the 1S-2S and 1S-$2P_0$ transitions, (a) and (b) respectively, in e^--H(1S) collisions in a laser field, using Perturbative dressed hydrogen atoms and a Born-Wave approximation, are compared over a range of orders of approximation for the Floquet dressing (_ — _ — _ — _ = 1st, — — — = 2nd, ... = 3rd, - - - - - = 4th and _____ = 5th order) at a photon energy $\hbar\omega$ = 0.0043au. The [illegible]ion is inclu[illegible]

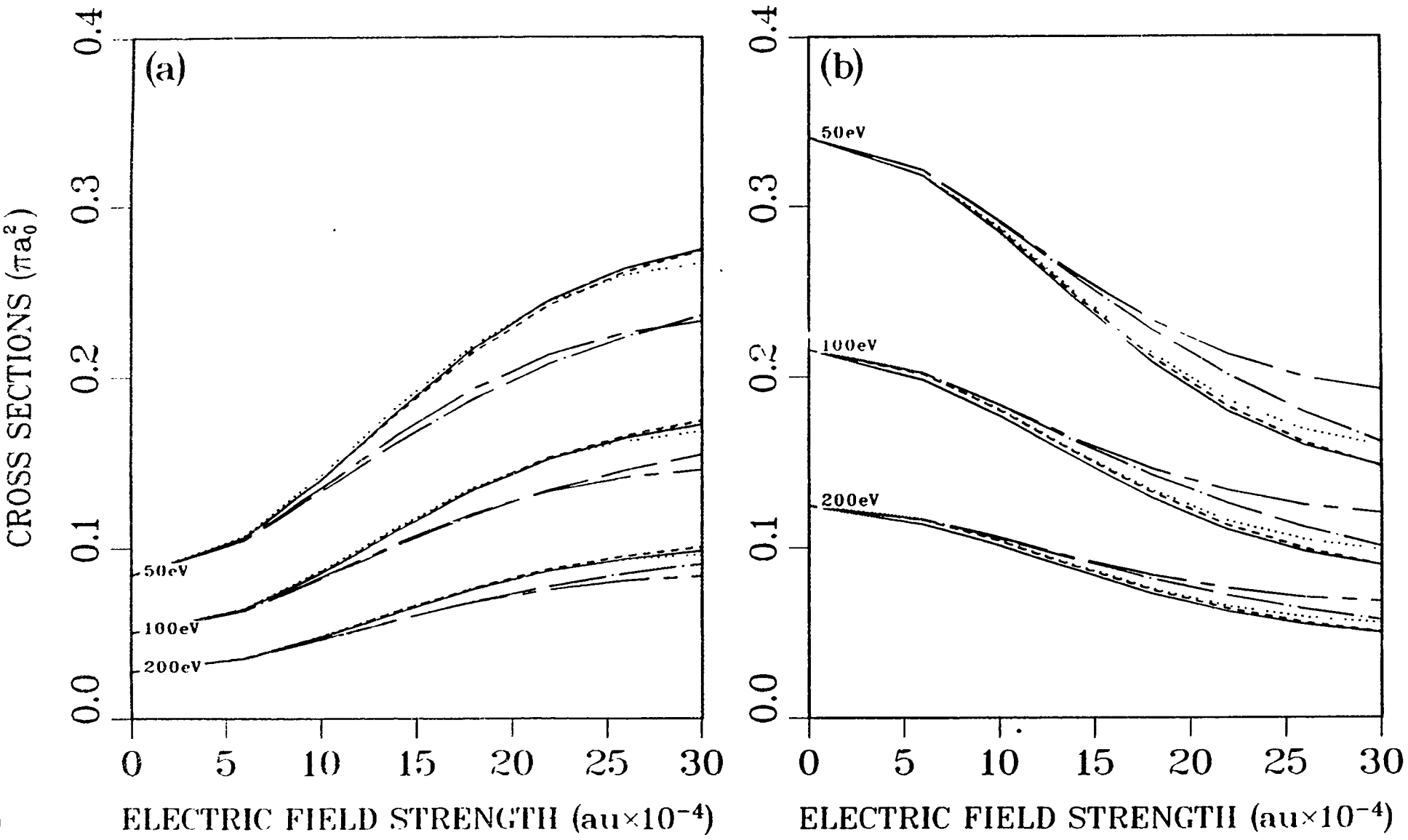

Figure(9): Cross sections vs field strength for the 1S-2S and 1S-2P$_0$ transitions. (a) and (b) respectively, in laser assisted e^--H(1S) collisions using Perturbative dressed hydrogen atoms and a Multichannel Eikonal Treatment. are compared over a range of orders of approximation for the Floquet dressing (_ ___ - ____ = 1st, ___ ___ = 2nd, ... = 3rd, - - - - = 4th and _____ = 5th order) at a photon energy $\hbar\omega$ = 0.0043au. The [illegible] perturbation is incl[illegible]

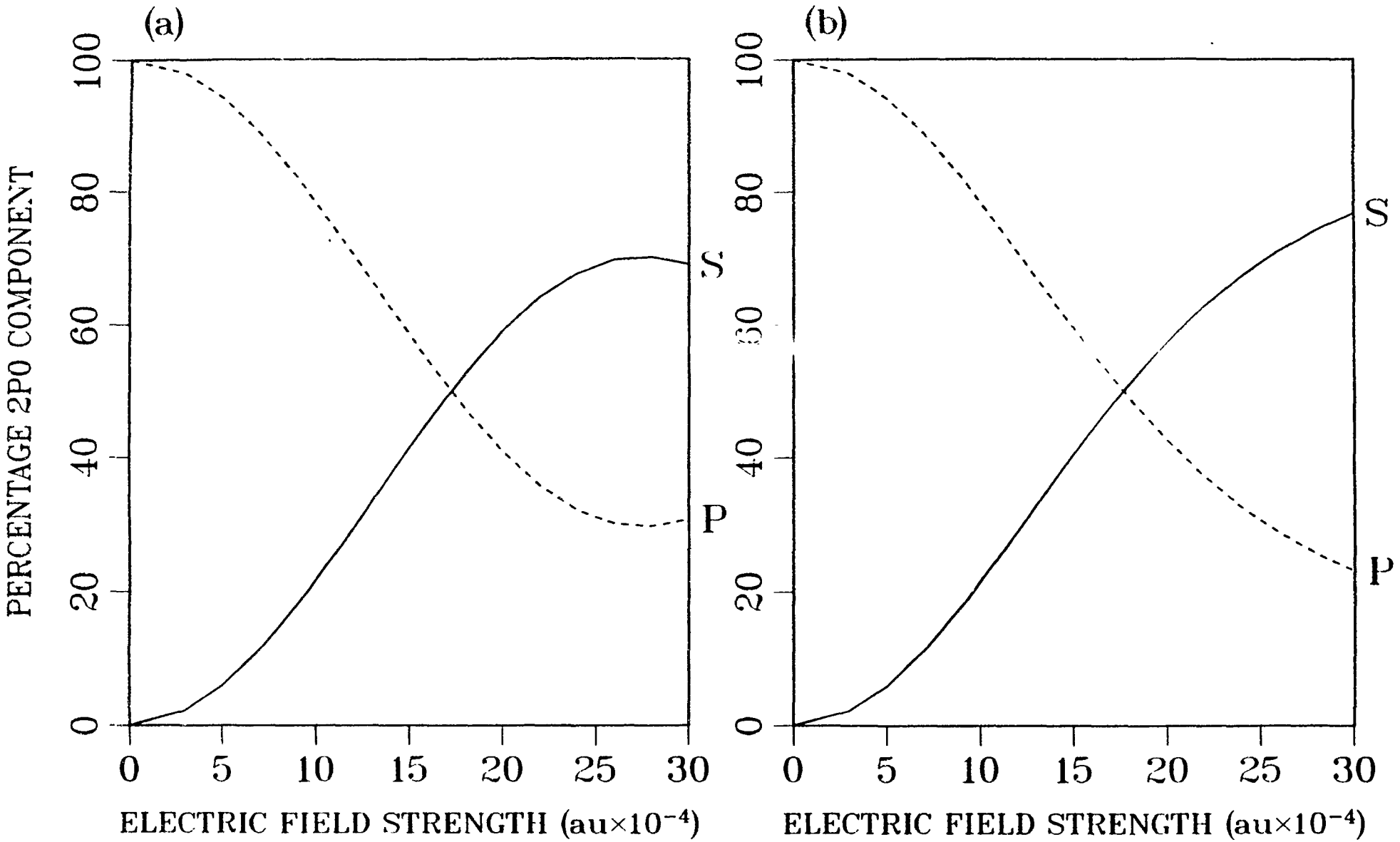

Figure(10): The percentage $2P_0$ component vs field strength, for the dressed states S ——— and P - - - - - , are compared for both Floquet and Perturbative dressed hydrogen atoms, (a) and (b) respectively, in a laser field of photon energy $\hbar\omega = 0.0043$au.

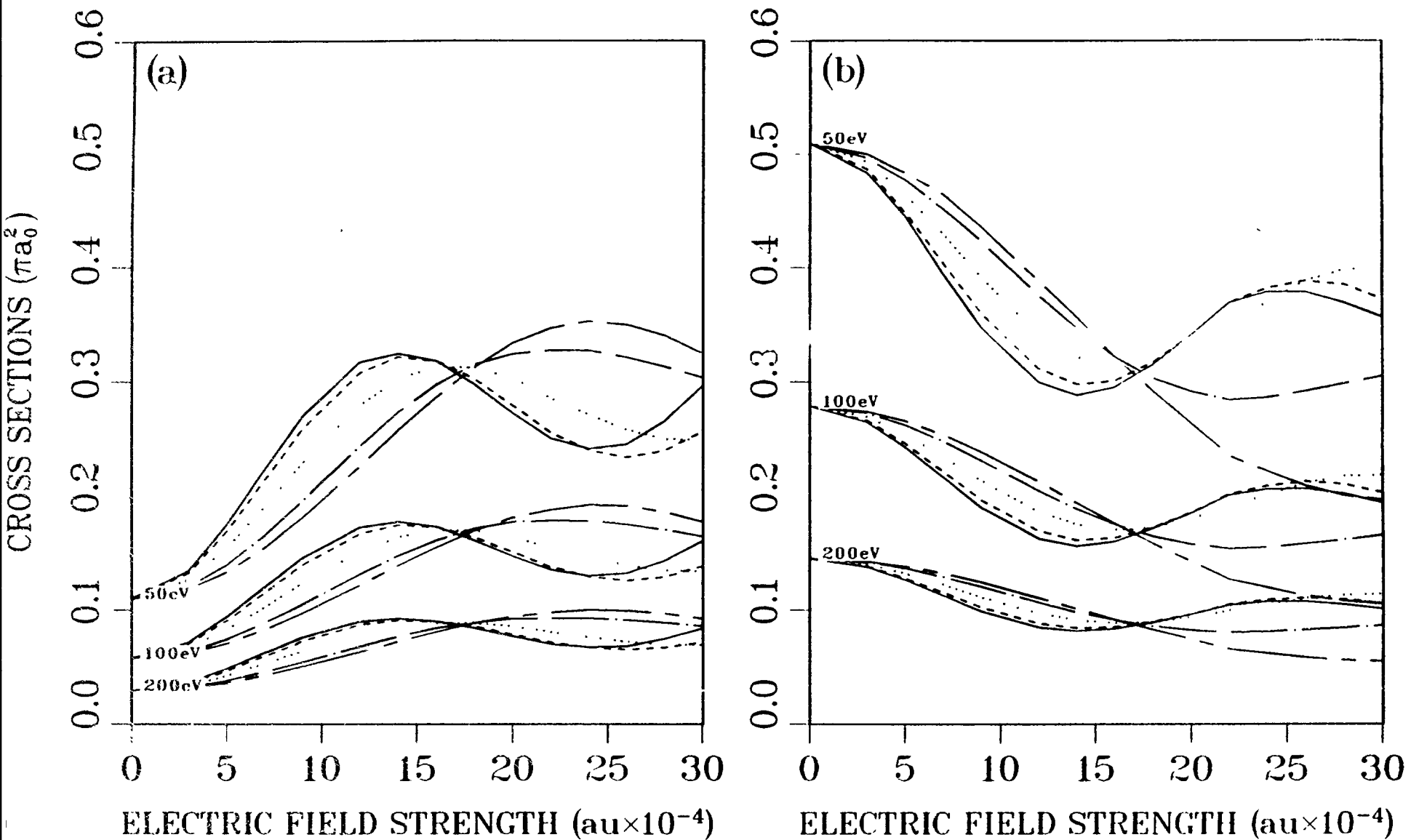

Figure(11): Cross sections vs field strength for the 1S-2S and 1S-2P_0 transitions, (a) and (b) respectively, in laser assisted e^--H(1S) collisions using third order Floquet dressed hydrogen atoms and a Born-Wave approximation, are compared over a range of phases δ_ω (——— = 0°, - - - - - = 22.5°, ——— = 45°, — — — = 67.5° and _ ——— _ ——— _ = 90°) at a photon energy $\hbar\omega$ = 0.0043au. The laser perturbation is included for the atom

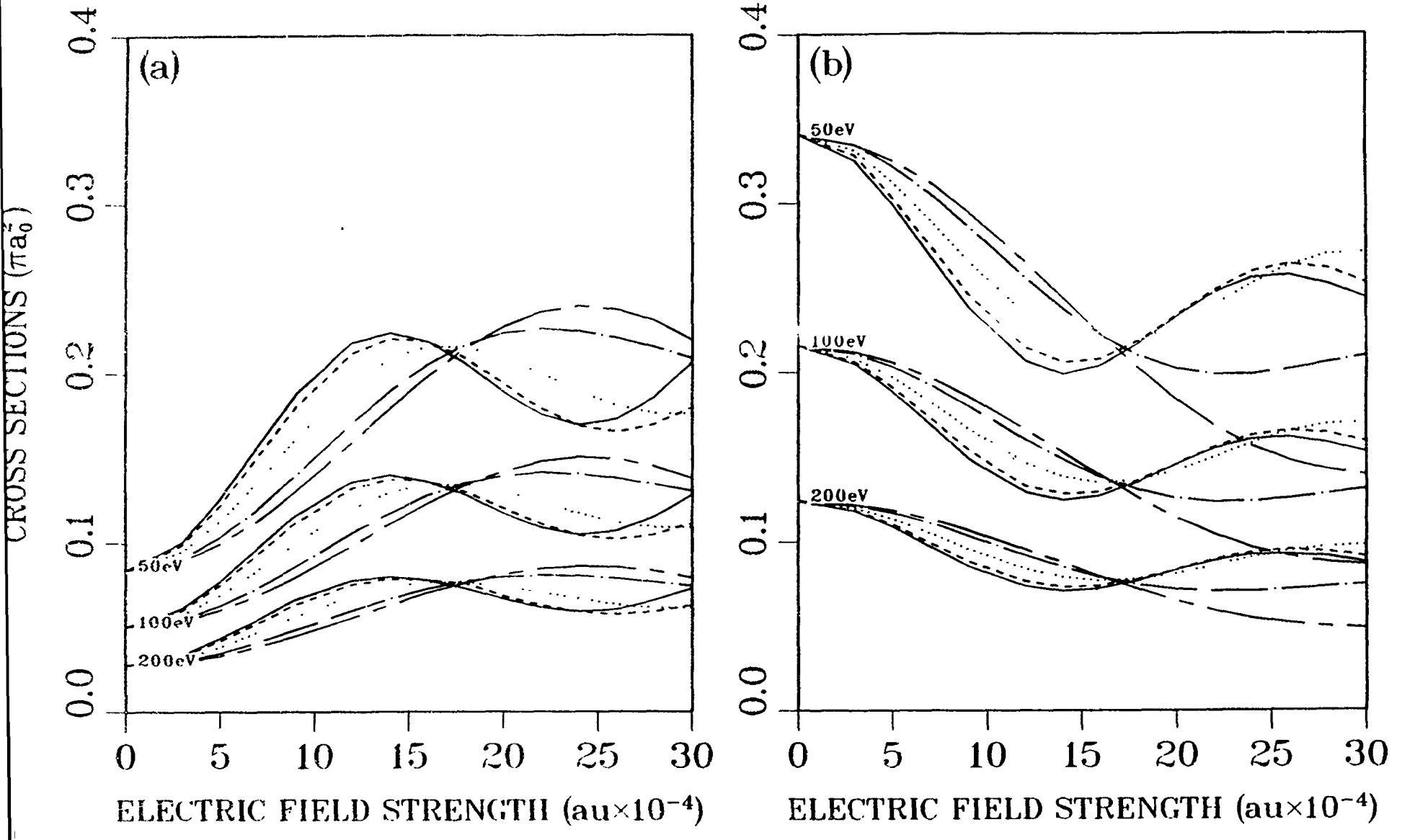

Figure(12): Cross sections vs field strength for the 1S-2S and 1S-2P$_0$ transitions, (a) and (b) respectively, in laser assisted e^--H(1S) collisions using third order Floquet dressed hydrogen atoms and a Multichannel Eikonal Treatment, are compared over a range of phases δ_ω (——— = 0°, - - - - - = 22.5°, ... = 45°, — — . = 67.5° and _ —— - —— . = 90°) at a photon energy $\hbar\omega = 0.0043$au. The laser perturbation is included for

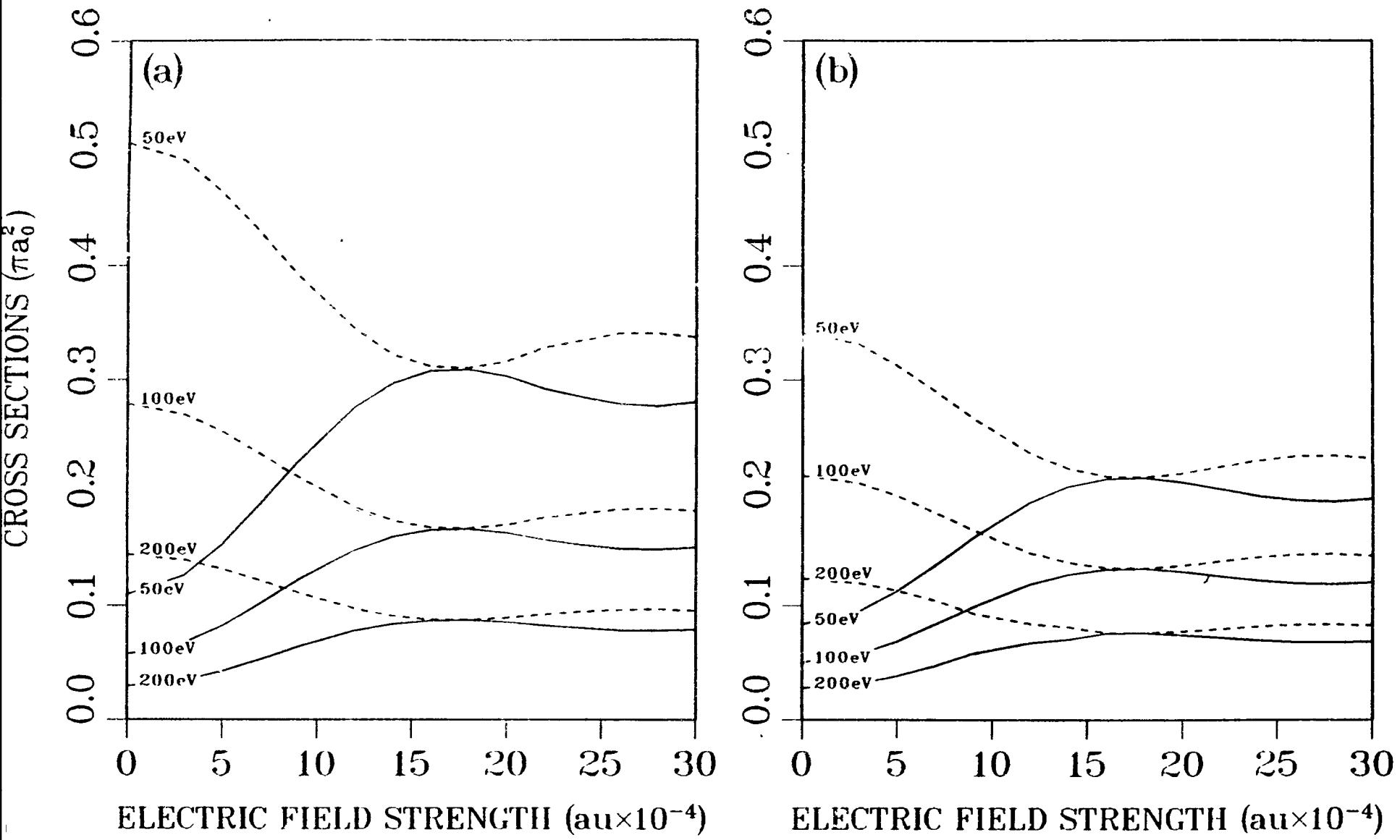

Figure(13): Cross sections vs field strength for the 1S-2S _____ and 1S-2P_0 - - - - - transitions in laser assisted e^--H(1S) collisions using third order Floquet dressed hydrogen atoms are compared in the Born-Wave approximation and the Multichannel Eikonal Treatment, (a) and (b) respectively, at a photon energy $\hbar\omega = 0.0043$au. The cross sections are an average of phase dependent cross sections for $\delta_\omega = 0°$ to 90°, and the laser perturbation is included for the atom only.

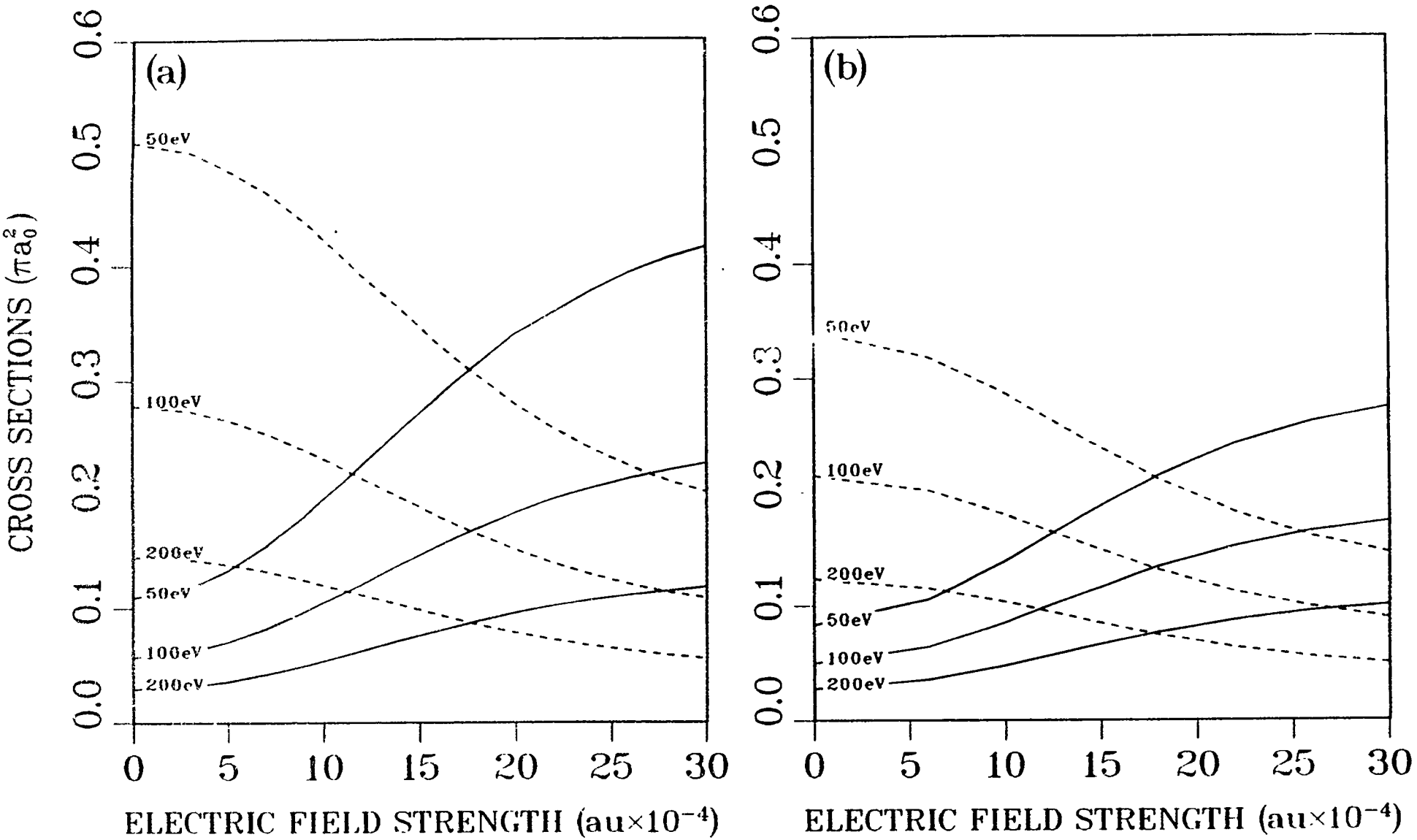

Figure(14): Cross sections vs field strength for the 1S-2S _____ and 1S-2P_0 - - - - transitions in laser assisted e^--H(1S) collisions using third order Perturbative dressed hydrogen atoms are compared in the Born-Wave approximation and the Multichannel Eikonal Treatment, (a) and (b) respectively, at a photon energy $\hbar\omega = 0.0043$au. The laser perturbation is included for the atom only.

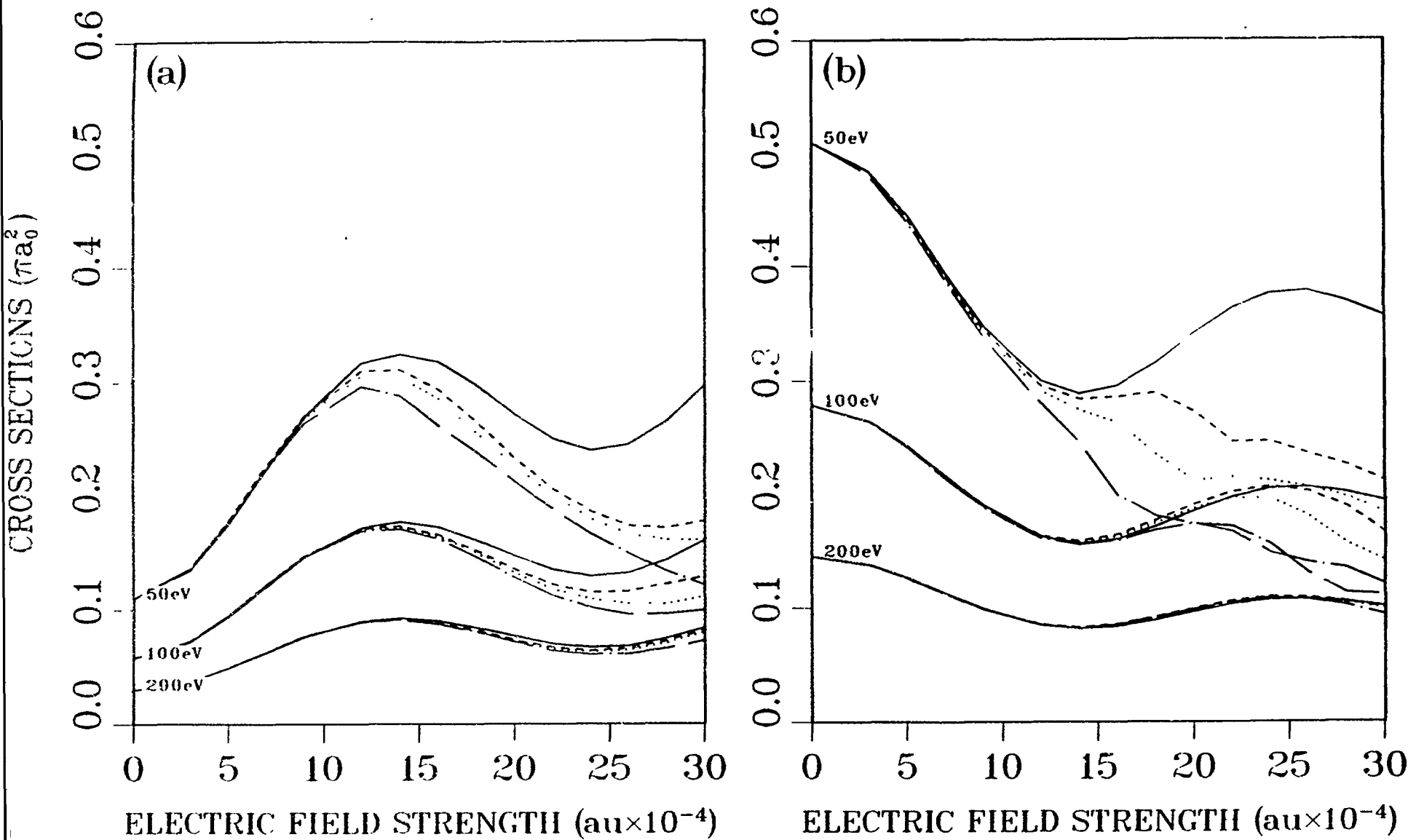

Figure(15): Cross sections vs field strength for 1S-2S and 1S-2P$_0$ transitions. (a) and (b) respectively, in laser assisted e^--H(1S) collisions using third order Floquet dressed hydrogen atoms and a Born-Wave approximation are compared with the laser perturbation included for the atom only (_____) and the laser perturbation included for both the atom and the projectile, where the later cross sections are a summation over a range of final projectile energies (__ __ = $\pm 20\hbar\omega$, = $\pm 25\hbar\omega$ and _ _ _ _ _ = $\pm 30\hbar\omega$ about the field-free final projectile energy). The phase $\delta_\omega = 0$ and the photon energy

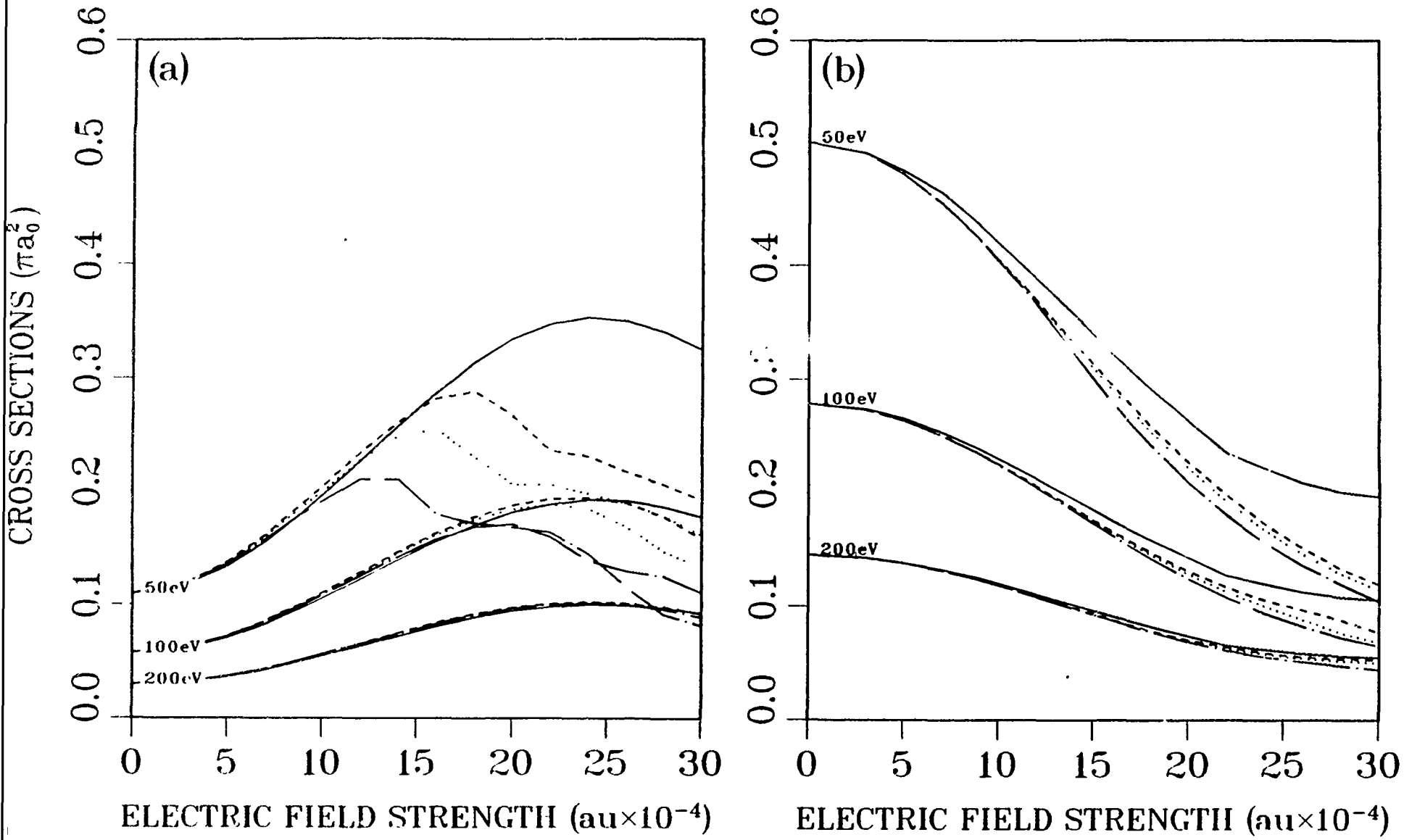

Figure(16): Cross sections vs field strength for 1S-2S and 1S-2P$_0$ transitions, (a) and (b) respectively, in laser assisted e^--H(1S) collisions using third order Floquet dressed hydrogen atoms and a Born-Wave approximation are compared with the laser perturbation included for the atom only (_____) and the laser perturbation included for both the atom and the projectile, where the later cross sections are a summation over a range of final projectile energies (__ __ = $\pm 20\hbar\omega$, = $\pm 25\hbar\omega$ and _ _ _ _ _ = $\pm 30\hbar\omega$ about the field-free final projectile energy). The phase $\delta_\omega = 90°$ and the photon energy

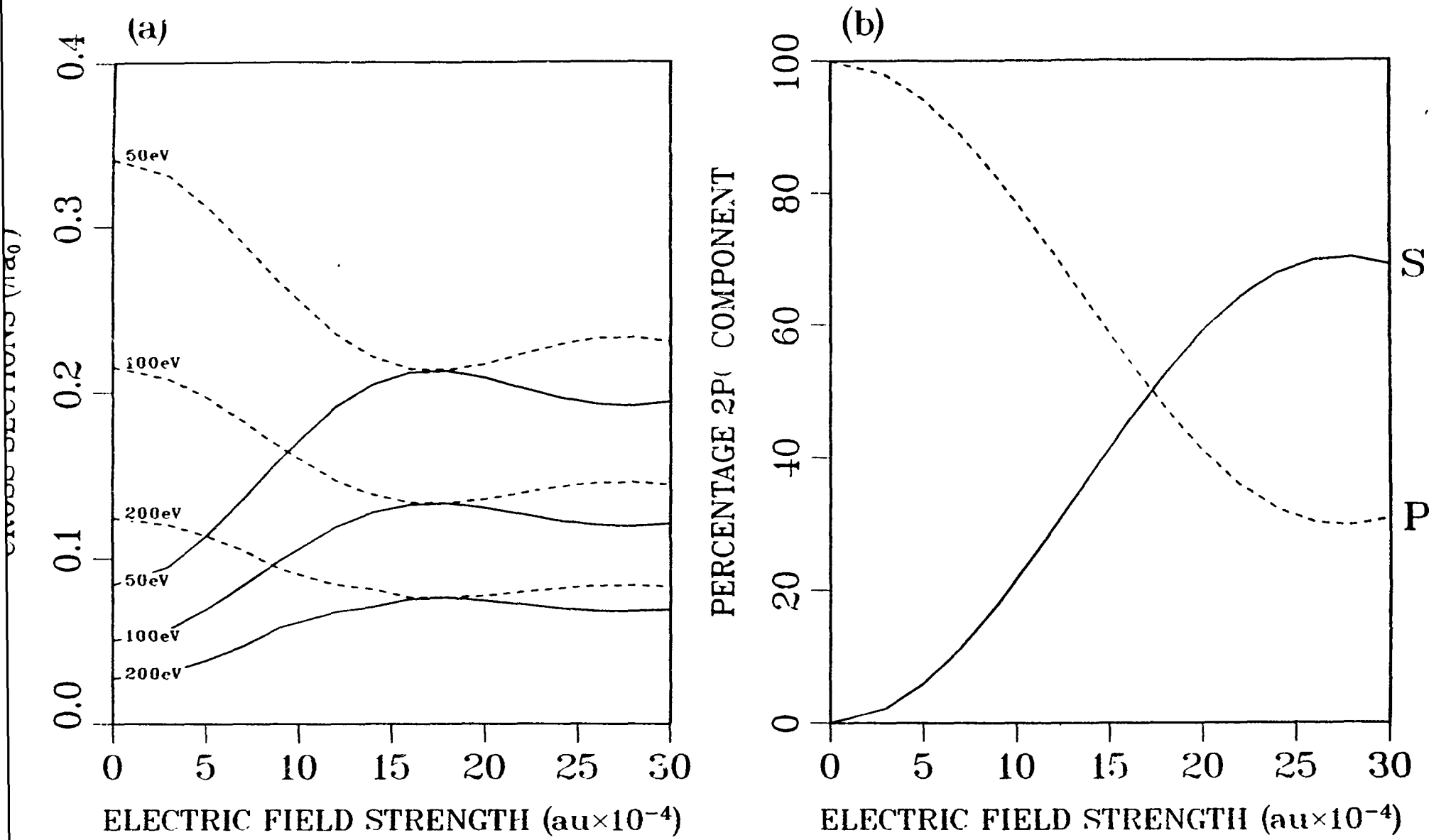

Figure(17): Cross sections in e^--H(1S) collisions are compared against the $2P_0$ component of the dressed atomic states, (a) and (b) respectively, over a range of electric field strengths for third order Floquet dressed hydrogen atoms in a laser field. The cross sections 1S-2S ——— and 1S-$2P_0$ - - - - - are an average of the phase dependent cross sections over a range of phases from $\delta_\omega = 0°$ to 90°, using a Multichannel Eikonal treatment. For the percentage $2P_0$ component ——— represent the dressed state S and - - - - - represent the dressed state P.

APPENDIX D

Transport-Collisional Master Equations for Termolecular Recombination as a Function of Gas Density

M. R. Flannery

Transport-Collisional Master Equations for Termolecular Recombination

M. R. Flannery
School of Physics
Georgia Institute of Technology
Atlanta, Georgia 30332-0430

Abstract

Sets of Transport-Collisional Master Equations are developed for the microscopic distribution $n(R, E, L)$ of pairs over internal separation R, energy E and orbital angular momentum L of (A-B) pairs in a background gas M of variable density. Expressions are also provided for the rate of recombination of A and B as a function of gas density. Analytical solutions for the pair distributions n and microscopic probabilities for recombination are obtained in the classical absorption limit. They pertain to exact (A-B) trajectories under general symmetric interaction $V(R)$ between A and B and are applied to ion-ion and electron-ion collisional recombination in a gas. A classical variational method is also presented.

1. Introduction

In previous papers[1-4], the rate α for termolecular recombination,

$$A + B + M \underset{k_d}{\overset{\alpha}{\rightleftharpoons}} AB + M \tag{1.1}$$

of species A and B (assumed structureless) in a low density gas M was considered by exact (quasi-steady-state[1] and variational[2]) treatments and by various approximate methods based on energy-diffusion[3], bottleneck[1] and electrical analogues[4]. The exact treatments[1,2] involve the solution of either a one-dimensional set of integral equations for the relaxation of the (A-B) pair distribution $n(E)$ in relative energy E or a variational determination of $n(E)$ with respect to external parameters varied to yield the minimum rate α. Both procedures[1,2] are equivalent to a quasi-steady-state distribution $n(E)$ among highly excited levels E. Ion-atom association[5] at low gas density involves the solution of a two-dimensional set of integral equations in E and in relative (orbital) angular momentum L of the associating (A-B) pair.

The aim of this paper is to develop the appropriate generalization to all gas densities, when there is *non-equilibrium* not only in the E and L degrees of freedom but also in the (A-B) internal separation **R**.This inhibited relaxation arises from the increased difficulty of transport of A towards B by diffusional-drift through the gas M. The two particle phase-space distribution $n(\mathbf{R}, \mathbf{p}; t)$ of (A-B) pairs with respect to **R** and relative (orbital) momentum $\mathbf{p} = M_{AB}\mathbf{v}$ is then governed by the microscopic transport equation[6],

$$\frac{d}{dt} n(\mathbf{R}, \mathbf{p}; t) = \frac{\partial n}{\partial t} + \mathbf{v} \cdot \nabla_{\mathbf{R}} n - \nabla_{\mathbf{R}} V \cdot \nabla_{\mathbf{p}} n \tag{1.2a}$$

$$= \frac{\partial n}{\partial t} + [\nabla_{\mathbf{R}} \cdot (n\mathbf{v})]_{\mathbf{p}} - \nabla_{\mathbf{R}} V \cdot [\nabla_{\mathbf{p}} n]_{\mathbf{R}} \tag{1.2b}$$

where $V(\mathbf{R})$ is the energy of mutual interaction between A and B with reduced mass M_{AB}. This transport rate is then set equal to the input-output rate for the net collisional production at fixed **R** of state p from all states p′ of the pair (A-B). A Boltzmann equation for $n(\mathbf{R}, \mathbf{p}; t)$ is then obtained[6] and is valid for dilute concentrations of reactants A and B in a gas bath M of general gas density N so that (A-B) collisions with the gas M provide the dominant state changing mechanism. Naumann[7] has recently reproduced the same basic equation[6] via an alternative stochastic route.

The next development[8] was the transformation of (1.2) for *symmetric* $V(R)$ to the more natural form,

$$\frac{d}{dt}n(\mathbf{R}, E_i, L_i^2; t) = \frac{\partial n_i}{\partial t} + \frac{1}{R^2}\frac{\partial}{\partial R}\left[R^2 n(\mathbf{R}, E_i, L_i^2; t)v_R\right]_{E_i, L_i^2} \tag{1.3}$$

for the resulting R-symmetric (A-B) pair distribution $n_i(R) \equiv n(\mathbf{R}, E_i, L_i^2)$ over $\mathbf{R}$, E_i and L_i^2. The radial speed dR/dt is v_R so that the microscopic radial current of pairs expanding and contracting at R is $j_i = 4\pi R^2 n_i v_R$ per unit interval $dE_i dL_i^2$, which is conserved and which depends only on E_i under equilibrium in $\mathbf{R}$, E_i and L_i^2 (Appendix A). The collisional RHS of the Boltzmann equation[6] may now be written in the collisional input-output form,

$$\frac{d}{dt}n(\mathbf{R}, E_i, L_i^2; t) \equiv \frac{dn_i(\mathbf{R})}{dt} = -\int dE_f \int dL_f^2 \left[n_i(R)\nu_{if}(R) - n_f(R)\nu_{fi}(R)\right] \tag{1.4}$$

where ν_{if} is the frequency per unit $dE_f dL_f^2$ of state changing $E_i, L_i \rightarrow E_f, L_f$ transitions produced by collision between the (A-B) pairs in state i and the gas species M and the integrations are over all E_f and L_f accessible at a given R.

The above two developments[6,8] of (1.2) and (1.3) now facilitate the construction in this paper of two sets of Transport-Collisional Master Equations for the pair microscopic distribution $n(R, E, L^2)$ and the L^2-integrated distribution $n(R, E)$. The sets essentially represent three-dimensional (R, E, L^2) and two-dimensional (R, E) integral equations respectively. The two-dimensional (R, E) set is however composed of two separate sets, each valid in exclusive regions of (R, E) space which become coupled via boundary conditions at the (R, E)-interface. The full sets are in general difficult to solve by customary numerical algorithms.

In this paper analytical solutions are obtained in the absorption or classical limit, when the back-coupling terms ν_{fi} in (1.4) are consistently neglected. Analytical expressions are then derived for the probability $P^A(R_0, E, L^2)$ for association of (E, L^2)-pairs with internal separations $R \leq R_0$ and for the various L^2- and E-averaged probabilities, $P^A(R_0, E)$ and $P^A(R_0)$ respectively, as a function of gas density. Not only does this analytical route provide further detailed insight into recombination but also the strategy therein suggest procedures valuable for eventual detailed numerical solution of the full Transport-Collisional Master Equations.

In this paper the recombining species A and B are assumed structureless and the recombination proceeds via collisional and transport relaxation in the relative (A-B) coordinates $\mathbf{R}$, E and L^2 in the (atomic or molecular) gas. Even with this simplification the resulting set of three-dimensional transport-collisional equations are quite complicated. Generalization is however required to cover the possibility of recombination process to cover the possibility of recombination process

$$Xe_2^+ + Cl^- + Xe \rightarrow XeCl + 2Xe \tag{1.5}$$

where the new two-body tidal mechanism introduced by Bates and Morgan[10],

$$\{Xe_2^+(v_i, J_i) - Cl^-\}_{E_i} \rightarrow \{Xe_2^+(v_f, J_f) - Cl^-\}_{E_f} \rightarrow XeCl + Xe \tag{1.6}$$

is mediated by collisions with the third bodies M and was shown by their recent computer simulation[10] to be necessary in order to explain the observed[11] production of $XeCl$ rather than Xe_2Cl as implied by (1.1). Although the 'two-body' rate of (1.6) involving orbital $\rightarrow$ internal energy conversion can in principle be added directly to the collisional RHS of (1.4), the interaction $V(\mathbf{R})$ between $Xe_2^+ - Cl^-$ is however orientation dependent and the transport side (1.3) must be so modified. Inclusion of this aspect within the present theory is feasible, but implementation involves an additional order of complexity to what is already a multilayered structure. The detailed inclusion of *orientation dependent* (A-B) interactions $V(\mathbf{R})$ will be considered at a later stage.

Since the time-dependent set of equations based on (1.3) and (1.4) can be reduced to a time-independent set via a quasi-steady state (QSS) criterion for highly excited bound (A-B) pairs, some background discussion of QSS is useful.

1.1 Quasi-Steady-State (QSS) Approximation :

Association (1.1) which proceeds at forward rate $\alpha(cm^3s^{-1})$ is coupled with the reverse process of dissociation which occurs at frequency $k_d(s^{-1})$. Both processes are naturally time dependent and the measured rate constants α and k_d satisfy

$$\frac{dN_{A,B}(t)}{dt} = -\alpha N_A(t)N_B(t) + k_d N_{AB}(t) \tag{1.7}$$

where N_A, N_B and N_{AB} are the time varying concentrations (cm^{-3}) of reactant and product species. The rate constants α and k_d can however be determined by a time independent procedure[1,9] in which association and dissociation can be treated separately.

Association emerges[1,9] in the time independent picture as if equilibrium concentrations $\tilde{N}_A$ and $\tilde{N}_B$ of the dissociated species A and B with relative energies E in the range $0 \leq E_i \leq \infty$ (which defines a reactant block $\mathcal{C}$) are collisionally transferred via an intermediate block $\mathcal{E}$ of highly excited states in the energy range $0 \geq E_f \geq -S$ to a product block $\mathcal{S}$ of fully stabilized molecular levels in the energy range $-S \geq E \geq -D$ where -D is the lowest energy level of the molecule AB (cf. Fig. 1 of ref. 1). The energy level -S lies within[1] at most $20kT$ below the dissociation limit. The intermediate block $\mathcal{E}$ is in quasi-steady state (QSS) since collisions occur in a time scale much shorter than the characteristic time for overall recombination and the stabilized product block $\mathcal{S}$ is considered to have zero population in the time-independent treatment. The $\mathcal{C}$ block is depleted and the $\mathcal{S}$ block is filled at a rate $\alpha\tilde{N}_A\tilde{N}_B$ via the steady state conduit of $\mathcal{E}$-block levels.

Dissociation emerges[1,9] in the time-independent picture as if a thermal concentration $\tilde{N}_{AB}$ of pairs in the $\mathcal{S}$ block are collisionally transferred through block $\mathcal{E}$ to block $\mathcal{C}$ maintained at zero population. The rate constants so deduced satisfy the detailed balance relation,

$$\alpha\tilde{N}_A\tilde{N}_B = k_d\tilde{N}_{AB}. \tag{1.8}$$

The QSS procedure is equivalent to seeking the lowest eigenvalue $\lambda_0 = k_d$ in the expansion of the time-dependent distribution $n_i(t)$ of level i in terms of the basis set $e^{-\lambda_j t}$ with j=1, 2, ... which define various timescales of relaxation. After initial transients described by the rapid time decay dependencies $\exp(-\lambda_1 t)$, $\exp(-\lambda_2 t)$, etc. the internal degrees of freedom then quickly relax into a quasi-steady-state which is slowly decaying as $\exp(-k_d t)$. It is this final relaxation which is of interest here.

2.1 Basic Theory: Exact Rate in Collisional and Transport Representations

On assuming that (A-B) pairs in the block $\mathcal{E}$ of highly excited bound levels are in quasi-steady-state, the rate of collisional termolecular recombination is the collisional net current,

$$\alpha\tilde{N}_A\tilde{N}_B = \int_E^{\infty} dE_i \int_0^{L_{im}^2} dL_i^2 \int_{R_i^-}^{R_i^+} d\mathbf{R} \left(\int_{V(R)}^{E} dE_f \int_0^{L_{fm}^2(R)} dL_f^2 \left[n_i(\mathbf{R})\nu_{if}(R) - n_f(\mathbf{R})\nu_{fi}(R) \right] \right) \tag{2.1}$$

which is constant across an arbitrary level $E = -\mid E \mid$ embedded in block $\mathcal{E}$. When $E = 0$, (2.1) is simply the net collisional rate of production of bound pairs, or depletion rate (1.8) of dissociated pairs and is appropriate for pure (A-B) Coulombic attraction $V(R) = -e^2/R$ which does not support any bound levels with positive energies.

Here $n_i(\mathbf{R}) \equiv n(\mathbf{R}, E_i, L_i^2)$ and $n_i(\mathbf{R})dE_i\ dL_i^2\ d\mathbf{R}$ is the number density of (A-B) pairs with internal relative energy E_i, internal relative angular momentum squared L_i^2, and internal separation $\mathbf{R}$ in the interval $dE_i\ dL_i^2\ d\mathbf{R}$ about $(E_i, L_i^2, \mathbf{R})$. The frequency of collisions with third bodies for $(E_i, L_i^2 \rightarrow E_f + dE_f, L_f^2 + dL_f^2)$ transitions at fixed (A-B) separation R is $\nu_{if}(R)dE_f dL_f^2$. Also $R_i^{\pm}$ denote the orbit's pericenter $(-)$ and apocenter $(+)$ or turning points of radial motion under the effective interaction

$$V_i(R) = V(R) + \frac{L_i^2}{2M_{AB}R^2} \tag{2.2}$$

The maximum value L_{im} of angular momentum $\mathbf{L} = \mathbf{R} \times \mathbf{p}_i$ accessible at fixed E_i and R is Rp_i and is determined also from $E_i = V_i(R)$ so that

$$L_{im}^2(R) = 2M_{AB}R^2[E_i - V(R)] = R^2p_i^2 = M_{AB}^2R^2v_i^2(R), \tag{2.3}$$

where p_i is the momentum for relative (A-B) motion with speed v_i. The maximum L^2 accessible overall at given E_i is either infinite for dissociated pairs ($E_i > 0$) or is L_{i0}^2 given by (2.3) evaluated at the radius R_0 for bound ($E_i < 0$) circular orbits (where $\partial V_i/\partial R = 0$). In thermodynamic equilibrium at temperature T the distribution of pairs over $\mathbf{R}$, E_i and L_i^2 is (Appendix A),

$$\tilde{n}_i(\mathbf{R}) \equiv \tilde{n}_i(\mathbf{R}, E_i, L_i^2) = \frac{\tilde{N}_A\tilde{N}_B e^{-E_i/kT}}{(2\pi M_{AB}kT)^{3/2}} \frac{2\pi}{R^2v_R} \tag{2.4}$$

where the radial speed v_R of relative (A-B) motion is determined from the energy relation,

$$E_i = \frac{1}{2}M_{AB}v_R^2 + V(R) + \frac{L_i^2}{2M_{AB}} = \frac{1}{2}M_{AB}v_i^2(R) + V(R). \tag{2.5}$$

The one-way equilibrium collisional rates,

$$C_{if}(R) = \tilde{n}_i(\mathbf{R})\nu_{if}(R) = \tilde{n}_f(\mathbf{R})\nu_{fi}(R) = C_{fi}(R) \tag{2.6}$$

satisfy the principle of detailed balance. The recombination rate (2.1) then vanishes under equilibrium conditions. The rate (2.1) with $E = 0$ may now be rewritten in terms of the fractional distribution,

$$\rho_i(R) = n_i(\mathbf{R})/\tilde{n}_i(\mathbf{R}), \tag{2.7}$$

which represents the departure of i-pairs from thermodynamic equilibrium, as

$$\alpha\tilde{N}_A\tilde{N}_B = \int_0^\infty dE_i \int_0^\infty dL_i^2 \int_{R_i^-}^\infty d\mathbf{R} \int_{V(R)}^0 dE_f \int_0^{R^2p_f^2} dL_f^2 \left[\rho_i(R) - \rho_f(R)\right] C_{if}(R). \tag{2.8}$$

This rate may alternatively be rewitten in terms of,

$$P_{fi}^S(R) = 1 - \frac{n_f\nu_{fi}}{n_i\nu_{if}} = 1 - \frac{\rho_f(R)}{\rho_i(R)}, \tag{2.9}$$

introduced here as the *probability for subsequent collisional stabilization of an f-pair collisionally produced in a bound level* $f \equiv (E_f, L_f^2)$ *from a dissociated i-pair.* Then,

$$\alpha\tilde{N}_A\tilde{N}_B = \int_0^\infty dE_i \int_0^\infty dL_i^2 \int_{R_i^-}^\infty d\mathbf{R} \int_{V(R)}^0 dE_f \int_0^{L_{fm}^2} n_i(R)\nu_{if}(R)P_{fi}^S(R)dL_f^2, \tag{2.10a}$$

in the *collisional representation*, which in turn can be rewritten as,

$$\alpha\tilde{N}_A\tilde{N}_B = \lim_{R_0\to\infty} \int_0^\infty dE_i \int_0^{R_0^2p_0^2} dL_i^2 \int_{R_i^-}^{R_0} d\mathbf{R} \int_{V(R)}^0 dE_f \int_0^{L_{fm}^2} n_i(R)\nu_{if}(R)P_{fi}^S(R)dL_f^2, \tag{2.10b}$$

where $p_0^2 = 2M_{AB}(E_i - V(R_0))$. Provided R_0 is large enough so that equilibrium in (E_i, L_i^2) is collisionally maintained then the distribution $\rho_i(R) = \rho_f(R) = \rho(R)$ for $R \geq R_0$ is independent of (E_i, L_i^2) and P_{fi}^S of (2.9) then vanishes for $R \geq R_0$. As $R_0 \to \infty$, then $\rho(R) \to \rho_\infty$, the normalized distribution maintained to preserve steady-state.

From (1.3) and (1.4) the microscopic steady-state distributions satisfy the collisional-transport set of Master equations[8]

$$\pm\frac{1}{R^2}\frac{\partial}{\partial R}\left[R^2n_i^\pm(R) \mid v_R \mid\right]_{E_i,L_i^2} = -\int_{V(R)}^\infty dE_f \int_0^{L_{m,f}^2} dL_f^2 \left[n_i^\pm(R)\nu_{if}(R) - n_f^\pm(R)\nu_{fi}(R)\right] \tag{2.11}$$

when $n_i^+(R)$ and $n_i^-(R)$ are the respective distributions of pairs which are radially expanding (+) or radially contracting (−) at R, ie. n^+ and n^- are respectively characterized by postive ($v_R > 0$) and negative ($v_R < 0$) radial speeds v_R. These distributions are coupled via the boundary conditions,

$$\begin{aligned} n_i^-(R \to \infty) &= \tilde{n}_i^-(R) \\ n_i^-(R_i^-) &= n_i^+(R_i^-) \end{aligned} \tag{2.12}$$

at infinity and the pericenter R_i^- for dissociated states i, and by

$$\begin{aligned} n_f^-(R_f^-) &= n_f^+(R_f^-) \\ n_f^-(R_f^+) &= n_f^+(R_f^+) \end{aligned} \tag{2.13}$$

at the apses $R_f^\pm$ of bound orbits f. Within each set, the collision frequency ν_{if} couples the distributions $n_i^\pm$ with all (E_f, L_f^2) state-distributions. The two sets of integro-differential coupled equations (2.11) for n_i^+ and n_i^- are coupled via their boundary values (2.12) and (2.13). Simple as (2.11) appears, this general class of partial integro-differential equations involving *boundary-value* conditions are notoriously difficult to solve. The Volterra type equation (2.11) has as yet not been solved theoretically or numerically. Simpler versions of (2.11) are currently receiving much attention in the mathematical literature[12].

Addition of (2.11) for n_i^+ and n_i^- provides the microscopic continuity equation in terms of the microscopic net radial current,

$$J_i(R) = J(R, E_i, L_i^2) = [n_i^+(R) - n_i^-(R)]v_R \tag{2.14}$$

across R as,

$$\frac{1}{R^2}\frac{\partial}{\partial R}\left[R^2(n_i^+ - n_i^-) \mid v_R \mid\right]_{E_i, L_i^2} = -\int_{V(R)}^{\infty} dE_f \int_0^{L_{fm}^2} dL_f^2 \left[n_i(R)\nu_{if}(R) - n_f(R)\nu_{fi}(R)\right] \tag{2.15a}$$

or as,

$$\frac{1}{R^2}\frac{\partial}{\partial R}\left[R^2 J_i(R)\right] = -\int_{V(R)}^{\infty} dE_f \int_0^{L_{fm}^2} dL_f^2 \left[\rho_i(R) - \rho_f(R)\right] C_{if}(R), \tag{2.15b}$$

which is expressed in general terms by,

$$\nabla \cdot \mathbf{J}_i = n_i(R) \int_{V(R)}^{\infty} dE_f \int_0^{L_{fm}^2} dL_f^2 \nu_{if}(R) P_{fi}^S(R). \tag{2.15c}$$

Collisional depletion and production terms involve the summed distribution $n_i = (n_i^+ + n_i^-)$ which appears on the right hand sides of (2.15), while the difference $(n_i^+ - n_i^-)$ appears on the transport side. Upon integration of (2.15) between R_i^- and ∞, the rate (2.1) or (2.8) across the dissociation limit E = 0 may then be expressed in the equivalent *transport representation* as,

$$\alpha \tilde{N}_A \tilde{N}_B = \lim_{R_0 \to \infty} \int_0^{\infty} dE_i \int_0^{R_0^2 P_0^2} dL_i^2 \left[4\pi R_0^2 \tilde{n}_i^-(R_0) v_R\right] \rho_i^-(R_0) P_i^A(R_0) \tag{2.16}$$

where the one-way equilibrium flux (Appendix A)

$$4\pi R^2 \tilde{n}_i^- v_R = 4\pi^2 \tilde{N}_A \tilde{N}_B e^{-E_i/kT}/(2\pi M_{AB} kT)^{3/2} \tag{2.17}$$

across R is, by (2.4) independent of R and L_i^2. Also the normalized distributions are,

$$\rho_i^\pm(R) \equiv \rho^\pm(R, E_i, L_i^2) = \frac{n^\pm(R, E_i, L_i^2)}{\tilde{n}^\pm(R, E_i, L_i^2)} \equiv \frac{n_i^\pm(R)}{\tilde{n}_i^\pm(R)} \tag{2.18}$$

and

$$P_i^A(R) = 1 - \frac{n_i^+(R)}{n_i^-(R)} = 1 - \frac{\rho_i^+(R)}{\rho_i^-(R)}, \tag{2.19}$$

is introduced here as the *probability for association within a sphere of radius R of all contracting i-pairs which enter the R-sphere.* Of the radial microscopic flux $4\pi R^2 n_i^- \mid v_R \mid$ at R only a fraction $P_i^A(R)$ eventually becomes associated as exhibited by (2.16).

The set of Master Equations (2.11) yield, for the normalized distributions (2.18) to

$$\frac{1}{R^2}\frac{\partial}{\partial R}\left(R^2 \tilde{j}_i^{\pm} \rho_i^{\pm}(R)\right) = \mp \int_{V(R)}^{\infty} dE_f \int_0^{L^2_{mf}} dL_f^2 \left[\rho_i^{\pm}(R) - \rho_f^{\pm}(R)\right] C_{if}^{\pm}(R) \tag{2.20}$$

where the one-way equilibrium current $\tilde{j}_i^{\pm} = \tilde{n}_i^{\pm} v_R$, and where the forward and backward one-way equilibrium collisional rates between levels $i \equiv (E_i, L_i^2)$ and f are,

$$C_{if}^{\pm}(R) = \tilde{n}_i^{\pm}(R)\nu_{if}(R) = \tilde{n}_f^{\pm}(R)\nu_{fi}(R) = C_{fi}^{\pm}(R) \tag{2.21}$$

which satisfy detailed balance.Then (2.20) with (2.17) reduces to,

$$\left[\frac{\partial \rho_i^{\pm}(R)}{\partial R}\right]_{E_i, L_i^2} = \mp \int_{V(R)}^{\infty} dE_f \int_0^{L^2_{mf}} dL_f^2 \left[\rho_i^{\pm}(R) - \rho_f^{\pm}(R)\right] (\nu_{if}(R)/v_R) \tag{2.22}$$

This set is solved according to boundary conditions,

$$\rho_i^-(R \to \infty) = 1; \qquad \rho_i^-(R, E_i \to \infty) = 1 \tag{2.23}$$

and

$$\begin{aligned} \rho_i^-(R_i^-) &= \rho_i^+(R_i^-) \\ \rho_i^+(R_i^+) &= \rho_i^-(R_i^+) \end{aligned} \tag{2.24}$$

which in effect serve to couple both ($\pm$) sets of integro-differential equations (2.22). Since $L_i^2 = (2mE_i)\rho^2$ where ρ is the impact parameter, then the transport representation (2.16) of the rate can be rewritten as the $(R_0 \to \infty)$ limit of

$$\alpha = \left[\frac{8kT}{\pi M_{AB}}\right]^{1/2} \int_0^{\infty} \epsilon\, e^{-\epsilon}\, d\epsilon \int_0^{\rho_0(\epsilon, R_0)} 2\pi\rho\, d\rho \quad \rho_i^-(R_0) P_i^A(R_0) \tag{2.25}$$

where $\epsilon = E_i/kT$, and where

$$\rho_0^2 = R_0^2[1 - V(R_0)/E_i] \tag{2.25}$$

is the maximum impact parameter accessible for formation of pairs with $R \leq R_0$ at energy E_i.

Many mathematical complexities exist in determining the theoretical and numerical solution of the general class of equations subject to boundary (not initial !) conditions, as represented by (2.22)-(2.24). While investigations into appropriate numerical procedures are currently in progress, it is important now to contruct simplified models suggested by the respective collisional and transport forms (2.10) and (2.16) for the rates and reported in the following sections with the aim that new insight and conclusions will emerge, without the necessity of detailed solution. The models will then in turn suggest various procedures valuable for eventual detailed numerical solution.

3. Improved Classical Treatment

Treatments which include forward collisional couplings ν_{if} and neglect backward collisional couplings ν_{fi} are termed classical in the sense that the set of coupled equations (2.11) or (2.20) are then replaced by the two sets of uncoupled equations in n_i^+ and n_i^- which contain only absorption (loss) terms and which can

be solved in closed analytical form. Classical solutions in the sense as defined here therefore only include collisional absorption from dissociated states (E_i, L_i^2).

3.1 Analytical Rate with Collisional Absorption. Physical Assumption:

Neglect the redissociation terms $n_f \nu_{fi}$ which collisionally populate continuum level i in (2.1) from the bound states f for $R \leq R_0$. Thus $P_{fi}^S(R)$ the stabilization probability (2.9), is unity for $R \leq R_0$. Assume that thermodynamic equilibrium in E_i, L_i^2 (but *not* in R) is collisionally maintained at fixed R for pairs with $R \geq R_0$, so that $\rho_i(R) = \rho_f(R)$ for $R > R_0$ is independent of (E_i, L_i^2). The stabilization probability $P_{fi}^S(R \geq R_0)$ of (2.9) then vanishes. Thus R_0 is assumed to be sufficiently small that the net effect of collisions at $R \leq R_0$ is pure absorption, depleting the dissocation channels, and yet is sufficiently large that the net (input-output) effect of collisions at $R \geq R_0$ is to maintain thermodynamic equilibrium in E_i and L_i^2, whereby preventing any stabilization from occurring outside R_0.

The total frequency for collisional destruction of continuum states i in (2.11) may be taken for small $R < R_0$ as the total collisional frequency in (2.10) for *direct* formation of all bound levels, ie.

$$\nu_i(R) = \int_{V(R)}^{\infty} dE_f \int_0^{L_{mf}^2} \nu_{if}(R) dL_f^2 \approx \int_{V(R)}^{0} dE_f \int_0^{L_{mf}^2} \nu_{if}(R) dL_f^2 \tag{3.1}$$

In this approximation the bound pairs are now fully stabilized against redissociation for $R \leq R_0$ and are therefore considered as the recombined products. The recombination rate (2.9b) then reduces to,

$$\alpha \tilde{N}_A \tilde{N}_B = \alpha(R_0) n(R_0) = \int_0^{\infty} dE_i \int_0^{R_0^2 p_0^2} dL_i^2 \int_{R_i^-}^{R_0} \left[4\pi R^2 n_i(R) \mid v_R \mid\right] \frac{\nu_i(R)}{\mid v_R \mid} dR, \tag{3.2}$$

in the *collisional representation*. Even though both representations, *collisional* (2.10) and *transport* (2.16), are equivalent, physical insight and algebraic development is facilitated more readily via the transport form.

3.2 Analytical Solution for $R < R_0$: Nonequilibrium in E_i, L_i^2 and R.

On ignoring therefore, the backward rates $n_f^{\pm} \nu_{fi}$ for collisional repopulation of level i, each set of coupled Master equations (2.11) reduces to

$$\pm \frac{1}{R^2} \frac{\partial}{\partial R} \left[R^2 n_i^{\pm} v_R\right]_{E_i, L_i^2} = -n_i^{\pm}(R) \nu_i(R), \; R \leq R_0 \tag{3.3}$$

for pure absorption within $R \leq R_0$. Here and below, v_R is now used to denote the positive radial speed $\mid v_R \mid$. Eqns. (3.3) are coupled by boundary conditions (2.12) and (2.13). Since $\rho_i^{\pm} = n_i^{\pm} / \tilde{n}_i^{\pm}$, (3.3) is then

$$\left[\frac{\partial \rho_i^{\pm}(R)}{\partial R}\right]_{E_i, L_i^2} = \mp \frac{\nu_i(R)}{v_R} \rho_i^{\pm}, \; R \leq R_0 \tag{3.4}$$

which follows also from (2.22). When integrated subject to boundary conditions $\rho_i^-(R_0)$ at R_0 and $\rho_i^-(R_i^-) = \rho_i^+(R_i^-)$ at the pericenter R_i^- (3.4) provides the distributions

$$\rho_i^-(R) = \frac{n_i^-(R)}{\tilde{n}_i(R)} = \rho_i^-(R_0) \exp\left[-\int_R^{R_0} \frac{\nu_i(R)}{v_R} dR\right] \tag{3.5}$$

for pairs contracting at R, and

$$\begin{aligned} \rho_i^+(R) = \frac{n_i^+(R)}{\tilde{n}_i^+(R)} &= \rho_i^-(R_i) \exp\left[-\int_{R_i}^{R} \frac{\nu_i(R)}{v_R} dR\right] \\ &= \rho_i^-(R_0) \exp\left\{-\int_R^{R_0} \frac{\nu_i(R)}{v_R} dR\right\} \exp\left\{-\oint_{R_i}^{R_0} \frac{\nu_i(R)}{v_R} dR\right\}, \; P \leq R_0, \end{aligned} \tag{3.6}$$

for pairs expanding at R, respectively. It is now simpler to insert these distributions into the two-dimensional transport representation (2.16) rather than into the equivalent three-dimensional collisional representation (3.2). In either case however the rate reduces to,

$$\alpha \tilde{N}_A \tilde{N}_B = \int_0^\infty dE_i \int_0^{R_0^2 p_0^2} dL_i^2 \left[4\pi R_0^2 \tilde{n}_i^-(R_0) v_R\right] \rho_i^-(R_0) P_i^A(R_0) \tag{3.7}$$

where,

$$p_0^2 = 2m[E_i - V(R_0)] \tag{3.8}$$

and where the probability (2.19) for association within R_0 of $(R \leq R_0)$ pairs now takes the simple form

$$P_i^A(R_0) = 1 - \exp\left\{ - \oint_{R_i^-}^{R_0} \frac{\nu_i(R)}{v_R} dR \right\} \tag{3.9}$$

for absorption within the segment $R_i^- \leq R \leq R_0$ of the trajectory enclosed by the sphere of radius R_0. The integrand,

$$\frac{\nu_i(R)}{v_R} dR = \nu_i(R) dt = \frac{ds_i}{\lambda_i} = \frac{v_i}{\lambda_i} dt, \tag{3.10}$$

is the elemental probability that A-B collides with M during time interval dt, or within trajectory element ds_i of their actual (E_i, L_i^2)-orbit s_i for A-B relative motion at speed v_i. Hence,

$$P_i^A(R_0) = 1 - \frac{\rho_i^+(R_0)}{\rho_i^-(R_0)} = \left[1 - \exp\left(- \oint_{R_i^-}^{R_0} \frac{ds_i}{\lambda_i} \right) \right] \tag{3.11}$$

is simply the probability for (A-B)-M collisions with microscopic free path length $\lambda_i = v_i/\nu_i$ towards any collision within the portion of the orbit enclosed by a sphere of radius R_0.

Binary Decomposition: When the (A-B)-M collisions at a given pair separation R(A-B) can be decomposed as binary (A-M and B-M) collisions (an excellent decomposition for ionic species $A^+ - B^-$ in a neutral gas), then $\nu_i = \nu_{iA} + \nu_{iB}$ so that $\lambda_i^{-1} = \lambda_{iA}^{-1} + \lambda_{iB}^{-1}$. Then (3.11) factors as,

$$P_i^A(R_0) = 1 - S_A S_B \tag{3.12}$$

which decomposes as,

$$P_i^A(R_0) = P_i^A(R_0, \lambda_{iA}) + P_i^A(R_0, \lambda_{iB}) - P_i^A(R_0, \lambda_{iA}) P_i^A(R_0, \lambda_{iB}), \tag{3.13}$$

where the probability of survival against either (A-M) or (B-M) collisions within the segment is

$$S_{A,B} = \exp\left\{ - \oint_{R_i^-}^{R_0} ds_i / \lambda_{iA,B} \right\}. \tag{3.14}$$

This decomposition holds only at this (E, L^2) microscopic level (cf. §3.3). The corresponding probability for association arising from an individual collision within the trajectory is

$$P_i^A(R_0, \lambda_{iA,B}) = 1 - S_{A,B} \tag{3.15}$$

The above *binary assumption* leads quite naturally to the decomposition in (3.13) of the (E_i, L_i^2) microscopic probabilities for individual collisions. Since the sum $P_i^A(\lambda_A) + P_i^A(\lambda_B)$ includes the probability $P_i^A(\lambda_A) P_i^A(\lambda_B)$ for simultaneous collisions twice, the simultaneous probability must be subtracted as in (3.13). Note that the above solutions (3.5) and (3.6) of (3.3) for the normalized distributions $\rho^\pm$ and (3.11) for the microscopic probability of association show quite directly that these E_i, L_i^2-pairs are not in

equilibrium with respect to L_t^2 in this classical approximation since $\rho_t^{\pm}$ are clearly dependent on L. The distribution $\rho_t^-(R_0)$ of pairs contracting at R_0 may be in L^2-equilibrium.

3.3 Averaged Association Rates and Probabilities

With the aid of Appendix A, the rate (3.7),

$$\alpha \tilde{N}_A \tilde{N}_B = \int_0^\infty dE \int_0^{R_0^2 p_0^2} dL^2 \left[4\pi R^2 \tilde{n}^-(R_0, E, L^2) v_R\right] \rho^-(R_0, E, L^2) P^A(R_0; E, L^2) \tag{3.16}$$

may be rewritten as,

$$\alpha = \pi \bar{v} \int_0^\infty \epsilon\, e^{-\epsilon}\; d\epsilon \int_0^{\rho_0^2} \rho_t^-(R_0, E, \rho) P^A(R_0; E, \rho) d\rho^2 \tag{3.17}$$

where ρ is the impact parameter associated with the (E_t, L_t)- trajectory. Here $L^2 = (2M_{AB}E)\rho^2$, $\epsilon = E/kT$, $\bar{v}$ is the mean speed $(8kT/\pi M_{AB})^{1/2}$ and $\rho_0^2 = R_0^2[1 - V(R_0)/E]$. On performing the L_t^2 and E-integrations, then with the aid of Appendix A,

$$\alpha = \left(\tilde{N}_A \tilde{N}_B\right)^{-1} \int_0^\infty dE \left[4\pi R_0^2 \tilde{n}^-(R_0, E) \frac{v}{2}\right] \rho^-(R_0, E) P^A(R_0, E) \tag{3.18}$$

$$= \pi \bar{v} \int_0^\infty \epsilon\, e^{-\epsilon}\; d\epsilon\; \rho_0^2\; \rho^-(R_0, E) P^A(R_0, E) \tag{3.19}$$

$$= \pi \rho_{max}^2 \bar{v} \rho^-(R_0) P^A(R_0); \qquad \rho_{max}^2 = R_0^2[1 - V(R_0)/kT] \tag{3.20}$$

where the integrated densities and distributions are given by

$$n^-(R_0, E) = \int_0^{R_0^2 p_0^2} n^-(R_0, E, L^2) dL^2 = \rho^-(R_0, E) \tilde{n}^-(R_0, E) \tag{3.21}$$

and,

$$n^-(R_0) = \int_0^\infty n^-(R_0, E) dE = \rho^-(R_0) \tilde{n}^-(R_0). \tag{3.22}$$

Also,

$$\pi \rho_0^2 \rho^-(R_0, E) P^A(R_0, E) = \pi \int_0^{\rho_0^2} \rho^-(R_0, E, \rho) P^A(R_0; E, L^2) d\rho^2 \tag{3.23}$$

and

$$\pi \rho_{max}^2 \rho^-(R_0) P^A(R_0) = \int_0^\infty \epsilon\, e^{-\epsilon}\; d\epsilon\; \pi \rho_0^2 \rho^-(R_0, E) P^A(R_0, E), \tag{3.24}$$

define the appropriate L_t^2 and (L_t^2, E_t) averages, $P^A(R_0, E)$ and $P^A(R_0)$, respectively, of the original microscopic association probability (2.19).

In the absorption limit,

$$P^A(R_0, E, L^2) = 1 - \exp\left\{ - \oint_{R_t^-}^{R_0} \frac{ds_t}{\lambda_t} \right\}; \tag{3.25}$$

and for general interactions $V(R)$, analytical expressions for $P^A(R_0, E)$ and $P^A(R_0)$ can be deduced under various equilibrium conditions.

For R_0 sufficiently large, the distribution of pairs contracting at R_0 is in equilibrium with respect to L. Then

$$n_i^-(\mathbf{R},E,L^2)=\frac{\tilde{n}^-(\mathbf{R},E,L^2)}{\tilde{n}^-(\mathbf{R},E)}n^-(\mathbf{R},E) \tag{3.26}$$

so that $\rho^-(R_0,E,L^2)=\rho^-(R_0,E)$ is now independent of L. The L^2-averaged probability in (3.23) becomes

$$P^A(R_0,E)=\frac{1}{\rho_0^2}\int_0^{\rho_0^2}\left\{1-\exp\left(-\oint_{R_i^-}^{R_0}\frac{ds_i}{\lambda_i}\right)\right\}d\rho^2=1-\frac{n^+(R_0,E)}{n^-(R_0,E)}. \tag{3.27}$$

If in addition the incoming R_0-pairs are also in equilibrium with respect to E so that $\rho^-(R_0,E)=\rho^-(R_0)$. The E-averaged or macroscopic probability is then,

$$P^A(R_0)=\frac{1}{\pi\rho_{max}^2}\int_0^\infty \epsilon\, e^{-\epsilon}\; d\epsilon\pi\rho_0^2P^A(R_0,E)=1-\frac{n^+(R_0)}{n^-(R_0)}. \tag{3.28}$$

Although the microscopic absorption probability (3.25) satisfies the rule (3.13) for decomposition into probabilities for individual A and B collisions with the gas, the trajectory ρ and energy E-averaged probabilities (3.27) and (3.28) do not satisfy this decomposition. That is,

$$P^A(R_0,\lambda;E)\neq 1-(1-P_1)(1-P_2)=P_1+P_2-P_1P_2 \tag{3.29}$$

where $P_1=P^A(R_0,\lambda_A;E)$ and $P_2=P^A(R_0,\lambda_B;E)$. The equality has always been tacitly assumed in previous macroscopic treatments[13-15]. The breakdown is directly apparent from comparison of the corresponding expr ssions derived explicitly for straight-line trajectories ($E\gg V(R)$ for weak interactions). Here, the Thomson straight-line (E,ρ) microscopic probability[13] is

$$P_{SL}^A(R_0;\lambda;E\to\infty,\rho)=1-\exp\{-2(R_0^2-\rho^2)^{1/2}/\lambda\} \tag{3.30}$$

with ρ-average[14],

$$P_{SL}^A(X;E\to\infty)=P_{SL}^A(X)=1-\frac{1}{2X^2}[1-e^{-2X}(1+2X)];\quad X=R_0/\lambda \tag{3.31}$$

which does not rigorously satisfy the decomposition rule (3.13). The decomposition (3.13) however is satisified numerically fairly closely. While the Thomson microscopic probability (3.30) depends on L (via ρ), the L^2-average (3.31) is independent of E since $E\gg V(R)$. The Thomson distributions within R_0 are therefore in E-equilibrium but not in L^2- equilibrium. The distributions which yield (3.25) are in general not in (E,L^2)-equilibrium.

For ion-neutral (hard-sphere) collisions with constant (speed independent) path length $\lambda_i=\lambda$ then (3.25) reduces to,

$$P^A(R_0,E,L^2)=1-\exp\left[-\mathcal{L}(R_0,E,L^2)/\lambda\right] \tag{3.32}$$

where $\mathcal{L}$ is the length of the segment of the (E,L^2)-trajectory enclosed by the sphere. For (ion-induced dipole) collisions at constant frequency $\nu_i=\nu$ then

$$P^A(R_0,E,L^2)=1-\exp\left(-\nu T\right) \tag{3.33}$$

where T is the transit time. Figure 1(a,b) illustrate the variation with $X=R_0/\lambda$ of the ρ^2 and (ρ^2,E)-averaged values (3.27) and (3.28) of the microscopic probability (3.32) associated with ion-ion recombination under Coulombic attraction $V(R)=-e^2/R=-(R_e/R)kT$ within a characteristic radius $R_0=0.408R_e$ (cf. §4.4 and ref. 4). Various analytical expressions for the microscopic segment length $\mathcal{L}$ of the (E,L)-trajectory have been derived in Appendix B (cf. (B6), (B9), (B15) and (B19)), together with corresponding L^2 or ρ^2 averages (B31) for general interactions $V(R)$.

As E increases, the ρ^2-averaged probability (3.27) decreases monotonically (see Fig. 1) from the parabolic ($E\ll V(R)$) envelope,

$$P^A(X = R_0/\lambda, E \to 0) = 2\int_0^1 \left[y/\sqrt{1-y^2}\right]^{Xy} \exp\left(-2X(1-y^2)^{1/2}\right) y\, dy, \tag{3.34}$$

obtained from (B15b) for $\mathcal{L}$ in (3.32) with (B22), to the straight line ($E \gg V(R)$) envelope (3.31). This monotonic decrease between the two limiting envelopes essentially arises from the decrease of the ρ^2-averaged segment $\mathcal{L}(E, \rho; R_0)$ of the enclosed trajectory from $2R_0$ (cf. B23) for parabolic motion (cf. B23) to $\frac{4}{3}R_0$ for rectilinear motion. The envelopes increase initially with density $N \sim \lambda^{-1}$ as the collision probabilities $2R_0/\lambda$ and $\frac{4}{3}R_0/\lambda$ in the parabolic and straight line limits, respectively. For intermediate energies E the gradients are confined to within these limits (cf. Fig. 1a, inset). Fig. (1b) illustrates that the E-averaged probability (3.28) is graphically indistinquishable (to within three significant figures) from $P^A(R_0, E = kT)$ and is much closer to the parabolic limit (3.34), than to the straight-line limit (3.31).

The use of (B19) for $\mathcal{L}$ in (3.27) is universal in that the variation of $P^A(R_0, E)$ with R_0 at a *fixed* gas density N, in addition to the above variation with N at a fixed R_0, can be illustrated also by Fig. 1 simply by regarding the selected values of the normalized energy as values of $\epsilon' = r_0\epsilon$, and the absissa X as linear in R_0. As $R_0 = r_0 R_e$ increases from zero, P^A follows for all ϵ the initial increase of the $\epsilon' = 0$ parabolic envelope and eventually falls onto the straight-line envelope. The R_0-variation of P is shown in Fig. (2a) for $E = kT$ at one density ($f = R_e/\lambda = 1$) and in Fig. (2b) at several densities ranging from high to low.

There are as yet no analytical results for the averaged probabilities (3.27) for $P^A(R_0, E)$ and (3.28) for $P^A(R_0)$ for general V(R), not even for the Coulomb interaction. Figs. (1a,b) are based on numerical ρ^2-integrations over Elliptic Integrals (Appendix B). New analytical expressions now will be developed for general V(R) for the following two cases: (a) The low-gas density limit (when $P_i^A \to \mathcal{L}/\lambda_i$) in §4.1 and (b) The case of pairs in L^2-equilibrium (§6.1).

4. Low Density Limit: Classical Analytical Rates and Probabilities Under Exact (A-B) Trajectories

The association probability (3.11) tends, as $N \to 0$ ie. as $\lambda_i/R_e \to \infty$, where R_e is a characteristic length given by the outermost root of $|\, V(R_e) \,| = kT$, to

$$P^A(R_0, E_i, L_i^2) \to \oint_{R_i^-}^{R_0} \frac{ds_i}{\lambda_i} \tag{4.1}$$

which is linear in N. The *transport form* (3.16) of the classical rate then tends to,

$$\alpha_{Low}\tilde{N}_A\tilde{N}_B = \int_0^\infty dE_i \int_0^{R_0^2 p_0^2} dL_i^2 \left[4\pi R_0^2 \tilde{n}_i^-(R_0, E_i, L_i^2) v_R\right] \oint_{R_i^-}^{R_0} \frac{ds_i}{\lambda_i} \tag{4.2}$$

which provides the required linear increase with N. Since the collision frequency,

$$\nu_i(R) = \frac{v_i(R)}{\lambda_i} = \frac{[2(E_i - V(R))/M_{AB}]^{1/2}}{\lambda_i} \tag{4.3}$$

is already linear in N via λ_i, the low-density limit of the *collisional form* is obtained from (3.2) by simply setting $n_i(R) = \tilde{n}_i(R)$, the zero-order approximation for all dissociated pairs, to give the low density N linear limit,

$$\alpha_{Low}\tilde{N}_A\tilde{N}_B = \int_0^\infty dE_i \int_0^{R_0^2 p_0^2} dL_i^2 \int_{R_i^-}^{R_0} \left[4\pi R^2 \tilde{n}_i(R, E_i, L_i^2)\right](v_i/\lambda_i) dR \tag{4.4}$$

which is identical with (4.2) since $dt = dR/v_R = ds_i/v_i$. Since the one-way equilibrium flux,

$$4\pi R^2 \tilde{n}_i^-(R, E_i, L_i^2) \,|\, v_R \,| = \frac{4\pi^2 \tilde{N}_A \tilde{N}_B \exp(-E_i/kT)}{(2\pi M_{AB} kT)^{3/2}} \tag{4.5}$$

across a sphere of radius R is independent of R and L_i and since

$$L_i^2 = (2mE_i)\rho^2 \tag{4.6}$$

in terms of the impact parameter ρ, then (4.2) is also

$$\alpha_{Low} = \left[\frac{8kT}{\pi M_{AB}}\right]^{1/2} \int_0^\infty \epsilon\, e^{-\epsilon}\, d\epsilon \int_0^{\rho_0} 2\pi\rho\, d\rho \oint_{R_i}^{R_0} \frac{ds_i}{\lambda_i} \tag{4.7}$$

where $\epsilon = E_i/kT$ is the normalized energy. The maximum impact parameter ρ_0 accessible for formation of the R_0-complexes at energy E_i is given by,

$$\rho_0^2 = R_0^2 p_0^2/(2mE_i) = R_0^2\left(1 - \frac{V(R_0)}{E_i}\right) \tag{4.8}$$

Even when λ_i is independent of R and ρ, (4.7) involves knowledge of the length $\mathcal{L}(E,\rho)$ of the enclosed trajectory as a function of E and ρ. For pure Coulombic attraction $\mathcal{L}(E,\rho)$ can be provided (Appendix B) in terms of incomplete Elliptic Integrals of the first and second kind, but the double (E,ρ)-integration remaining in (4.7) appears intractable. A more elegant approach is based on the recognition that the innermost double integral of (4.7) is simply,

$$2\pi \int_0^{\rho_0} \rho d\rho \oint_{R_i}^{R_0} ds_i = 4\pi \int_0^{R_0} R^2\left[1 - \frac{V(R)}{E_i}\right] dR \tag{4.9}$$

This identity is proven directly in Appendix B (B32-B36), but follows most conveniently by reversing the order of the (L_i^2, R)-integrations in the collisional form (4.4) of the rate. Upon assuming λ_i is independent only of L_i, then (4.4) gives

$$\alpha_{Low}\tilde{N}_A\tilde{N}_B = \int_0^\infty dE_i \int_0^{R_0} 4\pi R^2 v_i\,(dR/\lambda_i) \int_0^{R^2 p_i^2(R)} \tilde{n}_i(\mathbf{R}, E_i, L_i^2) dL_i^2. \tag{4.10}$$

The L_i^2-integrated equilibrium distribution here is then the standard Maxwell-Boltzmann distribution,

$$\tilde{n}_i(\mathbf{R}, E_i)dE_i = \frac{2}{\sqrt{\pi}}\left[\frac{E_i - V(R)}{kT}\right]^{1/2} \tilde{N}_A\tilde{N}_B \exp(-E_i/kT) d(E_i/kT) \tag{4.11}$$

such that

$$\tilde{n}_i(\mathbf{R}, E_i)v_i dE_i = \left[\frac{8kT}{\pi M_{AB}}\right]^{1/2}\left[1 - \frac{V(R)}{E_i}\right]\tilde{N}_A\tilde{N}_B \epsilon\, e^{-\epsilon}\, d\epsilon, \tag{4.12}$$

with the result that (4.10) then reduces to

$$\alpha_{Low} = \left[\frac{8kT}{\pi M_{AB}}\right]^{1/2} \int_0^\infty \epsilon\, e^{-\epsilon}\, d\epsilon \int_0^{R_0(E_i)} 4\pi R^2\left[1 - \frac{V(R)}{E_i}\right] \frac{dR}{\lambda_i(R, E_i)}. \tag{4.13}$$

Comparison with the transport form (4.7) provides the valuable relation (4.9) valid for all (curved) trajectories under general V(R) when the *radius* R_0 *is independent of* L_i, but not necessarily of E_i. When λ_i and R_0 are both independent of ϵ then integration of (4.13) over ϵ yields,

$$\alpha_{Low} = \left[\frac{8kT}{\pi M_{AB}}\right]^{1/2} \int_0^{R_0} 4\pi R^2\left[1 - \frac{V(R)}{kT}\right] dR/\lambda(R) \tag{4.14}$$

Both (4.13) and (4.14) are exact (new) classical results for all trajectories under general V(R) valid when the path length λ_i is or is not dependent of E_i, respectively. The customary classical (Thomson straight-line) result follows from the direct use of rectilinear paths in (4.7) or by setting $E_i \gg V(R)$ in (4.13).

4.1 Averaged Association Probabilties

The rate (3.18) may also be written as,

$$\alpha_{Low}\tilde{N}_A\tilde{N}_B = \int_0^\infty \left[\frac{1}{4}\tilde{n}_i(R_0,E_i)v_i(R_0)4\pi R_0^2\right] P_i^A(E_i;R_0)dE_i \tag{4.15}$$

where $P_i^A(E_i,R_0)$, the microscopic probability (4.1) averaged over ρ (or L_i^2), is the probability for association of an equilibrium number of E_i-pairs contracting across R_0. By comparison with (4.12) and (4.13), the probability at low gas density is given exactly by,

$$P_i^A(E_i,R_0) = \frac{1}{\pi\rho_0^2}\int_0^{R_0(E_i)} 4\pi R^2\left[1-\frac{V(R)}{E_i}\right]\frac{dR}{\lambda_i(R,E_i)} \tag{4.16}$$

where ρ_0^2 is given by (4.8). Since the E_i-averaged flux

$$\int_0^\infty \left[\frac{1}{4}\tilde{n}_i(R_0,E_i)v_i(R_0)4\pi R_0^2\right] dE_i = \pi\rho_{max}^2\overline{v} \tag{4.17}$$

where

$$\rho_{max}^2 = R_0^2\left(1-\frac{V(R_0)}{kT}\right), \tag{4.18}$$

and where $\overline{v}$ is the mean relative speed $(8kT/\pi M_{AB})^{1/2}$, then (4.15) reduces simply to,

$$\alpha_{Low}\tilde{N}_A\tilde{N}_B = \pi\rho_{max}^2\overline{v}P^A(R_0), \tag{4.19}$$

where P^A is the (E_i,ρ)-averaged of the microscopic probability (3.28) given exactly by,

$$P^A(R_0) = \frac{1}{\pi\rho_{max}^2}\int_0^{R_0} 4\pi R^2\left[1-\frac{V(R)}{kT}\right]dR/\lambda(R) \tag{4.20}$$

when R_0 and λ_i are assumed independent of E_i. The probability (4.16) and its E_i-average (4.20) hold for any curved trajectory under V(R). Expressions (4.16) and (4.20) are new analytical results for the probabilities under general V(R).

4.2 Ion-Ion Recombination Under Coulombic Attraction:

For hyperbolic motion under Coulombic attraction $V_c(R) = -e^2/R$, the E_i-microscopic probability (4.16) reduces to,

$$P_i^A(E_i,R_0) = \frac{4}{3}\frac{R_0(E_i)}{\lambda_i(E_i)}\left(1-\frac{3}{2}\frac{V_c(R_0)}{E_i}\right)\Big/\left(1-\frac{V_c(R_0)}{E_i}\right) \tag{4.21}$$

where both R_0 and λ_i may be functions of E_i. The macroscopic probability (4.20) is,

$$P^A(R_0) = \frac{4}{3}\frac{R_0}{\lambda}\left[1-\frac{3}{2}\frac{V_c(R_0)}{kT}\right]\Big/\left[1-\frac{V_c(R_0)}{kT}\right] \tag{4.22}$$

for constant R_0 and λ. The rate (4.14) or (4.19) is exactly,

$$\alpha_{Low}(R_0) = \pi\rho_{max}^2\overline{v}P^A(R_0) = \frac{4}{3}\pi R_0^3\frac{\overline{v}}{\lambda}\left[1-\frac{3}{2}\frac{V_c(R_0)}{kT}\right] \tag{4.23}$$

for Coulomb attraction. This is appropriate for termolecular ion-ion recombination,

$$A^+ + B^- + M \rightarrow AB + M \tag{4.24}$$

in a low density gas M. For straight-line trajectories, Thomson obtained the rate,

$$\alpha_T = \pi R_0^2 \overline{v} P_T^A(R_0) \tag{4.25}$$

where the Thomson (straight-line) probability is

$$P_T^A = \frac{4}{3}\frac{R_0}{\lambda} \tag{4.26}$$

The corresponding probability (4.22) and cross section ($\pi\rho_{max}^2$) for the correct hyperbolic trajectory are greater than the corresponding straight-line Thomson probability P_T^A and cross section πR_0^2 by the enhancement factors,

$$F_p = P^A/P_T^A = \left(1+\frac{3}{2}\frac{R_e}{R_0}\right)\Big/\left(1+\frac{R_e}{R_0}\right), \tag{4.27a}$$

and

$$F_c = \rho_{max}^2/R_0^2 = \left(1+\frac{R_e}{R_0}\right), \tag{4.27b}$$

respectively, where $R_e = e^2/kT$ is the natural unit of length. The probability factor F_p remains bounded, increasing from 1 for large $R_0 \gg R_e$ to 1.5 in the limit of small $R_0 \ll R_e$. The focusing factor F_c is unlimited increasing from 1 to R_e/R_0 over the same range of R_0. The two factors however combine to give the amplified ratio,

$$\alpha_L/\alpha_T = \left(1+\frac{3}{2}\frac{R_e}{R_0}\right) \rightarrow \begin{cases} 1, & R_0 \gg R_e \\ 1.5(R_e/R_0) & R_0 \ll R_e \end{cases} \tag{4.28}$$

For typical $R_0 \approx R_e/2$ characteristic[4] of ion-ion recombination this trajectory-correction for α is quite large (~ 4).

Consideration of the inner integral of (4.7) in isolation presumedly hindered previous efforts to obtain the correct generalization of Thomson's straight-line result (4.26) to actual hyperbolic trajectories. It can be seen however that the cross section focusing factor F_c to the cross section is the main correction. Natanson's result[15],

$$\alpha_N = \pi\rho_{max}^2 \overline{v} P_T^A(R_0) \tag{4.29}$$

which accounts for F_c but retains the Thomson straight-line association probability (4.26) therefore remains quite accurate by being lower than the correct rate (4.23) by the F_p-correction of between 1 and 1.5 .

4.3 Electron-Ion Recombination

For termolecular recombination electron-ion recombination,

$$e^- + A^+ + B \rightarrow A + B, \tag{4.30}$$

the kinetic energy of the electron of mass m changes by an amount $(T_i - T_f) = (2m/M)T_i$ after an elastic (low-energy, isotropic) collision with the gas atom B of mass M. The change in internal energy E_i of the $(e^- - A^+)$ pair is $E_i - E_f = T_i - T_f = (2m/M)[E_i - V(R)]$. Hence the pair is bound ($E_f \leq 0$) provided[16],

$$E_i \leq \frac{2m}{M}\frac{e^2}{R} = \delta\frac{e^2}{R} = E_m \tag{4.31}$$

where E_m rather than ∞, is now the upper limit to E_i in (4.13).

On rearranging the order of integrations to reflect this R-dependent limit to E_i, the rate (4.13) for constant λ_i is then,

$$\alpha_L^e = \left[\frac{8kT}{\pi M_{AB}}\right]^{1/2}\frac{1}{\lambda}\int_0^{R_0} 4\pi R^2 dR \int_0^{\delta R_e/R}\left(1+\frac{R_e}{R\epsilon}\right)\epsilon\, e^{-\epsilon}\, d\epsilon \tag{4.32}$$

which, with the aid of $e^{-(\delta R_e/R)} \approx 1 - \delta R_e/R$ for small $\delta = (2m/M)$, yields,

$$\alpha_L^e = 8\pi \frac{m}{M} \frac{\dot{R}_0 R_e^2}{\lambda} \left[\frac{8kT}{\pi M_{AB}}\right]^{1/2} \tag{4.33}$$

where $R_e = e^2/kT$. When $R_0 = \frac{2}{3}R_e$ the Thomson radius, this classical rate α_L^e agrees exactly with Pitaevskii's rate[17] derived from a Fokker- Planck analysis of diffusion in energy space. A previous classical treatment[16] of (4.30) established the important result that α^e varies linearly with R_0 (as above) rather than R_0^3 as in (4.23) for ion-ion recombination (4.24). The formulation[16] adopted however a less rigorous weighting procedure which differed from (4.13) by a factor of 2/3 (in the inner integral) and which therefore resulted in a rate $\frac{2}{3}\alpha_P$ rather than α_P as found here.

The main difficulty in applying (4.23) and (4.33) to the collisional recombination processes (4.24) and (4.30) is that the trapping radius R_0 is uncertain. The rates increase without limit as R_0^3 and R_0 for each case, respectively. The radius may be assigned de-facto by comparison with results[4] of more elaborate theories based on accurate numerical solution of the full Collisional Input-Output Master Equation. It would however be advantageous if a classical treatment were formulated where R_0 appears as a variational parameter. Such a treatment is now developed in the following section.

4.4 Classical Variational Treatment

Let the bound level $V(R_0)$ separate the reaction zone from the product zone. The one-way rate across this transition state from (2.1) with $E = V(R_0)$ is,

$$\alpha_V(R_0)\tilde{N}_A\tilde{N}_B = \int_{V(R_0)}^{\infty} dE_i \int_0^{R_0^2 p_0^2} dL_i^2 \int_{R_i^-}^{R_i^+} n_i(\mathbf{R})\nu_i'(R)d\mathbf{R} \tag{4.34}$$

where the frequency of collisional transitions across the boundary is

$$\nu_i'(R, R_0) = \int_{V(R)}^{V(R_0)} dE_f \int_0^{L_{f_m}^2} \nu_{if}(R) dL_f^2 \tag{4.35}$$

and where R_i^+ is the apocenter for bounded motion ($0 > E_i \geq V(R)$) and is R_0 for dissociated pairs. The contribution α_C to (4.34) from the continuum states is given by (4.13) with ν_i replaced by ν_i' and is supplemented by the additional contribution α_B from the bound states between 0 and $V(R_0)$ to give,

$$\alpha_V = \alpha_C + \alpha_B \tag{4.36}$$

where,

$$\alpha_B = \int_{V(R_0)}^{0} dE_i \int_0^{R_0} \left[4\pi R^2 n_i(\mathbf{R}, v_i)v_i\right] \frac{dR}{\lambda_i'(R, E_i)} \tag{4.37}$$

which with the aid of (4.12) for bound states reduces to

$$\alpha_B(\epsilon_0) = \bar{\nu} \int_0^{\epsilon_0} \epsilon\, e^{\epsilon} \rho(\epsilon)\, d\epsilon \int_0^{R_0} 4\pi R^2 \left(\frac{|V(R)|}{|E_i|} - 1\right) \frac{dR}{\lambda_i'} \tag{4.38}$$

where $\rho(\epsilon) = n_i/\tilde{n}_i$, $\epsilon_0 = -V(R_0)/kT$ and $\lambda_i'(\epsilon_0) = \nu_i'/v_i$ is in principle a function of ϵ_0. At low gas densities ρ is independent of R due to **R**-equilibrium.

For Coulomb attraction and constant λ_i', then the contribution to (4.34) from the continuum states is,

$$\alpha_C(R_0) = \frac{4}{3}\pi R_0^3 \frac{\bar{\nu}}{\lambda'} \left(1 + \frac{3}{2}\epsilon_0\right) \qquad , \epsilon = R_e/R_0 \tag{4.39}$$

as before in (4.23). When $\rho(\epsilon) = 1$ and the contribution from bound levels is,

$$\alpha_B(R_0) = \frac{4}{3}\pi R_0^3 \frac{\overline{v}}{\lambda'}\left(\left[1+\frac{1}{2}\epsilon_0\right]e^{\epsilon_0} - \left[1+\frac{3}{2}\epsilon_0\right]\right) \tag{4.40}$$

The summed rate (4.36) is therefore

$$\alpha_V(R_0) = \frac{4}{3}\pi R_0^3 \frac{\overline{v}}{\lambda'}\left[1-\frac{V_c(R_0)}{2kT}\right]\exp\left(-V(R_0)/kT\right) \tag{4.41}$$

as a function of R_0, or is

$$\alpha_V(\epsilon_0) = \frac{4}{3}\pi R_e^3 \frac{\overline{v}}{\lambda'}\left(\frac{1}{\epsilon_0^3}+\frac{1}{2\epsilon_0^2}\right)e^{\epsilon_0} \tag{4.42}$$

when expressed as a function of the binding energy $\epsilon_0 = e^2/(R_0kT)$ of the transition level. Since upward transitions past this level $V(R_0)$ are neglected by (4.41) and since n_i is set equal to $\overline{n}_i$ which is an upper limit for the distribution of bound levels in the range $0 \geq E_i \geq V(R_0)$, the rate (4.41) is therefore an upper limit. On assuming that the variation of $\lambda'(\epsilon_0)$ in (4.42) with ϵ_0 is much slower than the remaining ϵ_0-dependence, (4.42) displays a minimum at $\epsilon_0^* = \sqrt{6}$ which corresponds to $R_0^* = 0.408R_e$. This level ϵ_0 then acts as a bottleneck to the recombination as in the bottleneck method of Byron et al. This value compares very favorably with exact assignment of R_0 (cf. Fig. 2 of reference 4).

The bound levels between $V(R_0) \sim 2.45kT$ and the dissociated limit are in general not in energy equilibrium as assumed in (4.40) and also in the original bottleneck method[16]. On setting a trial (variational) non-equilibrium distribution,

$$\rho(\epsilon) = \left(1+\frac{\epsilon}{\epsilon_0}\right)\exp(-\epsilon/\epsilon_0) \tag{4.43}$$

which is physically realistic[4], in (4.38) then (4.34) yields,

$$\alpha_V = \frac{4}{3}\pi R_e^3 \frac{\overline{v}}{\lambda'}\left[\frac{1}{\epsilon_0^3}+\frac{1}{2\epsilon_0^2}+\frac{(7\epsilon_0-3\epsilon_0^2)-(2\epsilon_0^2-\epsilon_0-5)\exp(\epsilon_0-1)}{2\epsilon_0(\epsilon_0-1)^3}\right] \tag{4.44}$$

which displays a minimum at $\epsilon_0^* = 2.55$ which corresponds to $R_0^* = 0.392R_e$. The choice of R_0^* is therefore rather insensitive to $\rho(\epsilon)$. The ratios of (4.42) and (4.44) to $\frac{4}{3}\pi R_e^3(\overline{v}/\lambda')$ are however 1.75 and 1.56, respectively.

Since $\lambda_i' = v_i/\nu_i'$ is in general different from the mean path λ_i for production of bound from dissociated pairs, and is in general unknown, the present strategy is to assign the unknown radius R_0 in §4.2 and §4.3 as the above variationally determined R_0^*. Hence (4.23) yields,

$$\alpha_L(R_0^*) = 0.3178\frac{4}{3}\pi R_e^3 \frac{\overline{v}}{\lambda} \tag{4.45}$$

This result is only within a factor of 2 higher than previous numerical results[4] of the exact treatment in which the quasi-steady state solutions (n_f of a collisional input-output integral equation for bound-pairs E_f is used in equation (2.11) of §2) over a wide range ($0.1 \leq a \leq 1$) of mass parameters,

$$a = M_g/(2M_i + M_g) \tag{4.46}$$

for recombination of ions of equal mass M_i in a gas of mass M_g.

It is also interesting to note that agreement of (4.45) with the Thomson straight-line rate-equation (4.25) with $R_0 = \frac{2}{3}R_e$ but with $\overline{v}$ set equal to the customary RMS value of $1.0854\,\overline{v}$,

$$\alpha_T = 0.3216\frac{4}{3}\pi R_e^3 \frac{\overline{v}}{\lambda} \tag{4.47}$$

must be regarded as fortuitous in that the Coulomb focusing factor of 4.676 (neglected in (4.45)) offsets the considerable reduction $(R_0/R_T)^3 \sim 0.23$ of the reaction volume. It is also interesting to note that the variational value $R_0 = 0.408R_e$ agrees closely with the value $R_N = 0.417R_e$ in Natanson's rate,

$$\alpha_N = \pi R_N^2 \bar{v}\left[1 - \frac{V_c(R_N)}{kT}\right] P_T^A(R_N) \tag{4.48}$$

which differs from (4.19) only in the use in P_T^A of Thomson's straight- line probability (4.26) rather than the exact probability (4.22) associated with hyperbolic orbits.

5. Angular-Momentum Integration: L_i^2-Equilibrium, (R, E)-Nonequilibrium

5.1 Master Equations

Integration of the basic set (2.11) of Master Equations for $n_i^{\pm}(\mathbf{R}, E_i, L_i^2)$ over the full range $0 \leq L_i^2 \leq R^2 p_i^2 = 2mR^2[E_i - V(R)] = L_{mi}^2(R)$ of L_i^2 accessible for given R and E_i is facilitated by Leibnitz's rule which provides,

$$\int_0^{L_{mi}^2} \frac{1}{R^2}\frac{\partial}{\partial R}\left[R^2 n_i^{\pm}(R) \mid v_R \mid\right] dL_i^2 = \frac{1}{R^2}\frac{\partial}{\partial R}\left\{\int_0^{L_{mi}^2}\left[R^2 n_i^{\pm}(R) \mid v_R \mid\right] dL_i^2\right\}$$
$$- n_i^{\pm}(\mathbf{R}, E_i, L_{mi}^2)\left[\frac{\partial L_{mi}^2}{\partial R}\right]_{E_i} \tag{5.1}$$

for differentiation with respect to R of an integral with R-dependent limits. The distribution $n_i^{\pm}(\mathbf{R}, E_i, L_{mi}^2)$ in (5.1) is evaluated for that maximum angular momentum $L_{mi}^2(R) = R^2 p_i^2(R)$ associated with the (E_i, L_{mi}^2)-orbit which just reaches R at either turning point $R_i^{\pm}$. Since contracting pairs n_i^- are transformed into expanding pairs n_i^+ at the pericenter and expanding n_i^+ pairs are transformed into contracting pairs at the apocenter, the R-space must be divided into two Regions I and II which exclusively contain the pericenters R_i^- and the apocenters R_i^+, respectively for a given E_i and all accessible L_i. In Region I sources of $n_i^+(R_i^-)$ originate from $n_i^-(R_i^-)$, while in Region II sources of $n_i^-(R_i^+)$ originate from $n_i^+(R_i^+)$. The effective interaction (2.2) associated with L_{mi}^2 is,

$$V_{mi}(R) = V(R) + \frac{L_{mi}^2}{2M_{AB}R^2} \tag{5.2}$$

Region I which contains the pericenters of all L_i^2-orbits with a given E_i has range $R_{i0}^- \leq R \leq R_b$ and Region II which contains the apocenters is $R_b \leq R \leq R_{i0}^+$ where the boundary radius R_b is the radius of the circular orbit given by the minimum of V_{mi}, ie. by the zero of

$$\frac{dV_{mi}}{dR} = \frac{dV}{dR} - \frac{2(E_i - V)}{R} \equiv -\frac{1}{2M - ABR^2}\frac{dL_{mi}^2}{dR} \tag{5.3}$$

and $R_{i0}^{\pm}$ are the turning points associated with the most penetrating $L_i = 0$ orbit. Thus $R_b = e^2/2 \mid E_i \mid$ for a bound orbit under Coulombic attraction. Region II does not exist for dissociated pairs. The boundary conditions (2.12) and (2.13) can therefore be incorporated into (5.1) by setting the distribution evaluated at the turning points to be,

$$n_i^*(R, E_i, L_{mi}^2) = \begin{cases} n_i^-(R, E_i, R^2 p_i^2); & \text{Region I } (dV_{mi}/dR \leq 0) \\ n_i^+(R, E_i, R^2 p_i^2) & \text{Region II } (dV_{mi}/dR \geq 0) \end{cases} \tag{5.4}$$

since n_i^- is the precursor (source) of n_i^+ in the pericenter Region I and n_i^+ is the precursor of n_i^- in the apocenter Region II when it exists. Integration of (2.10) with the aid of (5.1) and (5.4) therefore yields,

$$\pm\frac{1}{R^2}\frac{\partial}{\partial R}\left[R^2 j_i^{\pm}\right] = \pm\left[n_i^* \mid v_R \mid \frac{\partial L_{mi}^2}{\partial R}\right] - \int_{V(R)}^{\infty} dE_f \int_0^{L_{mf}^2} dL_f^2 \int_0^{L_{mi}^2} dL_i^2 \left[\rho_i^{\pm}(R) - \rho_f^{\pm}(R)\right] C_{if}^{\pm}(R) \tag{5.5}$$

where $C_{if}(R) = \bar{n}_i \nu_{if}(R)$ is the one-way equilibrium collisional rate and where,

$$j_i^{\pm}(R) \equiv j^{\pm}(R, E_i) = \int_0^{R^2 p_i^2} n_i(\mathbf{R}, E_i, L_i^2) \mid v_R \mid dL_i^2 \tag{5.6}$$

is the current per unit $d\mathbf{R}\, dE_i$ across the R-sphere.

Addition of the two equations in (5.5) eliminates n_i^- and shows that the E_i-microscopic net current

$$J_i(R) = J(R, E_i) = \left[j_i^+(R) - j_i^-(R)\right] \tag{5.7}$$

across R satisfies the microscopic continuity equation,

$$\frac{1}{R^2}\frac{\partial}{\partial R}\left[R^2 J_i(R)\right] = -\int_{V(R)}^{\infty} dE_f \int_0^{L_{mf}^2} dL_f^2 \int_0^{L_{mi}^2} dL_i^2 \left[\rho_i(R) - \rho_f(R)\right] C_{if}(R) \tag{5.8}$$

in general. The net effect on the net current (5.7) of the conversions at the turning points are null. For (E_i, L_i^2)-equilibrium, $\rho_i(R) = \rho_f(R) = \rho(R)$ and (5.8) then implies *constant* flux $4\pi R^2 J_i(R)$ across the R-sphere.

L^2-Equilibrium: For equilibrium in L_i^2, then

$$n_i(\mathbf{R}, E_i, L_i^2) = \left[\frac{\tilde{n}_i(\mathbf{R}, E_i, L_i^2)}{\tilde{n}_i(\mathbf{R}, E_i)}\right] n_i(\mathbf{R}, E_i) \tag{5.9}$$

which is (Appendix A),

$$n_i(\mathbf{R}, E_i, L_i^2) = \left(\frac{1}{2R^2 p_i p_R}\right) n_i(\mathbf{R}, E_i) \tag{5.10}$$

where p_i and p_R are the relative and radial momenta, and where the L_i^2-integrated distribution is

$$n_i(\mathbf{R}, E_i) = \int_0^{L_{mi}^2} n_i(\mathbf{R}, E_i, L_i^2) dL_i^2 \tag{5.11}$$

The normalized distribution $\rho_i(R, E_i, L_i^2)$ of (2.7) is then independent of L_i^2. The current (5.6) is then,

$$j_i^{\pm}(R, E_i) = \frac{1}{2} n^{\pm}(\mathbf{R}, E_i) v_i = (L_{mi}^2) n_i^{\pm}(\mathbf{R}, E_i, L_{mi}^2) \mid v_R \mid . \tag{5.12}$$

Under L_i^2-equilibrium (5.5) therefore reduces to the set,

$$\pm\frac{1}{R^2}\frac{\partial}{\partial R}\left[R^2 j_i^{\pm}(R, E_i)\right] = \pm\frac{1}{L_{mi}^2}\left[\frac{\partial L_{mi}^2}{\partial R}\right]_{E_i} j_i^-(R, E_i) + \int_{V(R)}^{\infty}\left[\rho_f^{\pm}(R) - \rho_i^{\pm}(R)\right] C_{if}^{\pm}(R) dE_f, \; R \le R_b \tag{5.13}$$

for R in Region I (where $\partial L_{mi}^2/\partial R \ge 0$), and to,

$$\pm\frac{1}{R^2}\frac{\partial}{\partial R}\left[R^2 j_i^{\pm}(R, E_i)\right] = \mp\frac{1}{L_{mi}^2}\left|\frac{\partial L_{mi}^2}{\partial R}\right|_{E_i} j_i^+(R, E_i) + \int_{V(R)}^{\infty}\left[\rho_f^{\pm}(R) - \rho_i^{\pm}(R)\right] C_{if}^{\pm}(R) dE_f, \; R \ge R_b \tag{5.14}$$

for R in Region II (where $\partial L_{mi}^2/\partial R \le 0$). The one-way equilibrium rate (per unit $dE_i dE_f$) for $E_i \to E_f$ collisional transitions is,

$$C_{if}^{\pm}(R) = \int_0^{R^2 p_i^2} dL_i^2 \int_0^{R^2 p_f^2} \tilde{n}_i^{\pm} \nu_{if}(E_i, L_i^2; E_f, L_f^2; R) dL_f^2 = \tilde{n}_i^{\pm}(\mathbf{R}, E_i) \nu_{if}(E_i, E_f, R) \tag{5.15}$$

Note that $dL_{mi}^2(R)$ at constant E_i in (5.13) is simply the increase (if positive) or decrease (if negative) in the number of orbits (states) L_{mi}^2 with their turning points within the range between R and R + dR. In Region I which contains the pericenters, this number increases as R is increased and in Region II which contains

the apocenters this number decreases as R increases. Thus $dL^2_{m_i}/L^2_{m_i}$ in (5.13) and (5.14) is the fractional increase (or decrease) in the current $j^{\pm}(\mathbf{R}, E_i)$ across the R-sphere as R is increased to R + dR. Equation (5.13) therefore incorporates directly the boundary conditions (2.12) and (2.13) by including the appropriate source/sink terms. Contracting (−) pairs which disappear as (−) pairs reappear as sources of expanding (+) pairs in the pericenter region. Equation (5.14) acknowledges that (+) pairs are sources of (−) pairs in apocenter Region II. For Coulombic attraction, Region I comprises all R for $E_i \geq 0$ and $0 \leq R \leq R_b$ for $E_i < 0$ while Region II comprises the range $R_b \leq R \leq 2R_b$ for $E_i < 0$. The boundary radius $R_b = e^2/2 \mid E_i \mid$ is the radius of the circular orbit of energy E_i.

The net radial microscopic current,

$$J_i(R) = J(R, E_i) = \frac{1}{2}(n_i^+ - n_i^-)v_i = \frac{1}{2}\tilde{n}_i^{\pm}(\rho_i^+ - \rho_i^-)v_i = \left[\rho_i^+(R) - \rho_i^-(R)\right]\tilde{j}_i^{\pm} \tag{5.16}$$

satisfies the equation

$$\frac{1}{R^2}\frac{\partial}{\partial R}\left[R^2 J_i(R)\right]_{E_i} = \int_{V(R)}^{\infty}\left[\rho_f(R) - \rho_i(R)\right]C_{if}(R)dE_f, \tag{5.17}$$

since $\rho_i = (\rho_i^+ + \rho_i^-)/2$ and $C_{if} = 2C_{if}^{\pm}(R)$. The net effect of the geometrical (+) → (−) conversions in (5.13) and (5.14) to the net current J_i is obviously null, in accord with (5.17).

The rate (2.1) can then be written in terms of the association probability

$$P_i^A(E_i, R_0) = 1 - \frac{n_i^+(\mathbf{R}, E_i)}{n_i^-(\mathbf{R}, E_i)} = 1 - \frac{\rho_i^+(R)}{\rho_i^-(R)} \tag{5.18}$$

in the *transport representation* as,

$$\alpha\tilde{N}_A\tilde{N}_B = \lim_{R\to\infty}\int_0^{\infty} dE_i\left[4\pi R^2 n_i^-(R)\frac{v_i}{2}\right]\rho_i^-(R)P_i^A(R) \tag{5.19}$$

where i labels E_i-state quantities. In terms of the probability,

$$P_{fi}^S(R) = 1 - \frac{n_f\nu_{fi}}{n_i\nu_{if}} = 1 - \frac{\rho_f(R)}{\rho_i(R)} \tag{5.20}$$

for subsequent collisional stabilization of E_f-pairs originally produced collisionally from a dissociated E_i-pair, the *collisional* representation of the rate is,

$$\alpha\tilde{N}_A\tilde{N}_B = \lim_{R\to\infty}\int_0^{\infty} dE_i\int_0^{R_0} d\mathbf{R}\int_{V(R)}^{0} n_i(R)\nu_{if}(R)P_{fi}^S(R)dE_f \tag{5.21}$$

In terms of the one-way equilibrium flux

$$4\pi R^2\tilde{j}_i^{\pm}(\mathbf{R}, E_i) = 4\pi R^2\left(\tilde{n}_i^{\pm}(\mathbf{R}, E_i)\frac{v_i}{2}\right) = 4\pi R^2 L^2_{m_i}\left[\frac{\exp(-E_i/kT)}{(2\pi M_{AB}kT)^{3/2}}\right] \tag{5.22}$$

per unit interval dE_i across the R-sphere, then the source-sink terms of (5.13) and (5.14) are,

$$\frac{1}{L^2_{m_i}}\left[\frac{\partial L^2_{m_i}}{\partial R}\right]_{E_i} j_i^{\pm}(\mathbf{R}, E_i) = -\frac{1}{R^2}\frac{j_i^{\pm}(R, E_i)}{\tilde{j}_i^{\pm}(\mathbf{R}, E_i)}\frac{\partial}{\partial R}\left(R^2\tilde{j}_i^{\pm}(\mathbf{R}, E_i)\right) \tag{5.23}$$

The set (5.13) and (5.14) then reduce to the following equations in Region I and Region II, respectively.

$$\pm\frac{1}{R^2}\frac{\partial}{\partial R}\left(R^2\tilde{j}_i^{\pm}\rho_i^{\pm}(R)\right) \mp \rho_i^-(R)\frac{1}{R^2}\frac{\partial}{\partial R}\left(R^2\tilde{j}_i^{\pm}\right) = \int_{V(R)}^{\infty}\left[\rho_f^{\pm}(R) - \rho_i^{\pm}(R)\right]C_{if}^{\pm}(R)dE_f, \tag{5.24}$$

$$\pm\frac{1}{R^2}\frac{\partial}{\partial R}\left(R^2\tilde{j}_i^{\pm}\rho_i^{\pm}(R)\right) \mp \rho_i^+(R)\frac{1}{R^2}\frac{\partial}{\partial R}\left(R^2\tilde{j}_i^{\pm}\right) = \int_{V(R)}^{\infty}\left[\rho_f^{\pm}(R) - \rho_i^{\pm}(R)\right]C_{if}^{\pm}(R)dE_f. \tag{5.25}$$

When $(-)$ and $(+)$ pairs are simultaneously in E_i-equilibrium then $\rho_i^{\pm}(R) = \rho_f^{\pm}(R) = \rho^{\pm}(R)$, and the collisional RHS of (5.24) and (5.25) vanishes. The LHS then predicts constant flux $4\pi R^2 \bar{j}_i^{\pm}[\rho^+(R) - \rho^-(R)]$ for the exterior $R > R_0$ region. The above set (5.24) and (5.25) for L^2-equilibrium is identical with that deduced previously[19] from conservation considerations.

Classical solutions are now developed in §6 under L^2-equilibrium in the interior $(R < R_0)$ region. Dissociated pairs belong only to pericenter Region II and classical (full absorption) solutions to (5.24) will be provided in §6. Bound pairs with energy $E \leq E_b = V(R) + (1/2)R\,dV/dR$ and $R > R_b$, the zero of (5.3), are in Region II governed by (5.25), which is also solved in §6.2 in the absorption limit.

6. L^2-Equilibrium: Analytical Expressions for Classical Association Rates and Probabilities for a General Interaction $V(R)$

Assume as in §3.1 that $P_{f_i}^S$, the probability (5.20) for stabilization of the bound state f collisionally produced from dissociated state i is unity for $R \leq R_0$ and is zero for $R > R_0$. The rate (5.21) in the collisional representation is then,

$$\alpha \tilde{N}_A \tilde{N}_B = \int_0^{\infty} dE_i \int_0^{R_0} n_i(R)\nu_i(R)d\mathbf{R} \tag{6.1}$$

where,

$$\nu_i(R) = \int_{V(R)}^{0} \nu_{if}(R)dE_f \tag{6.2}$$

is the frequency for collisional production of bound levels.

6.1 Pericenter Region I ($E \geq E_b = V(R) + \frac{1}{2}\frac{dV}{dR}; R \leq R_b$ for $E \geq 0$ and all R): Microscopic Distribution of Dissociated and Bound Pairs.

The absorption form of (5.24) is then,

$$\frac{\partial \rho_i^-}{\partial R} = \frac{2\nu_i(R)}{v_i(R)}\rho_i^-(R) \equiv \frac{2}{\lambda_i}\rho_i^-(R) \tag{6.3}$$

where for small R,

$$\nu_i(R) = \int_{V(R)}^{0} \nu_{if}(R)dE_f \approx \int_{V(R)}^{\infty} \nu_{if}(R)dE_f \tag{6.4}$$

is close to the total collision frequency to all levels. On integrating (6.3) between R and R_0, the solution is,

$$\rho_i^-(R) = \rho_i^-(R_0)\exp\left(-2\int_R^{R_0}\frac{dR}{\lambda_i}\right) \equiv \rho_i^-(R_0)P_S^-(R_0, R), \tag{6.5}$$

which in effect defines $P_S^-(R_0, R)$, the probability of survival against collision of $(-)$ pairs from R_0 to R. By comparison with (3.5), the main consequence of L_i^2-equilibrium on the distribution is to simply replace the radial speed v_R by its L^2-average of $\frac{1}{2}v_i$.

The outgoing distribution ρ_i^+ satisfies (5.24) which reduces in the collisional absorption limit to,

$$\frac{\partial}{\partial R}\left[R^2p^2\rho_i^+\right] + \frac{2}{\lambda_i}\left(R^2p^2\rho_i^+\right) = \frac{\partial}{\partial R}\left[R^2p^2\right]\rho_i^-(R) \tag{6.6a}$$

which is,

$$\frac{\partial}{\partial R}\left[R^2p^2\rho_i^+\epsilon^{2R/\lambda_i}\right] = \frac{\partial}{\partial R}\left(R^2p^2\right)\rho_i^-(R)\epsilon^{2R/\lambda_i} \tag{6.6b}$$

The above equations (6.3) and (6.6) also follow directly from L_i-integration of the corresponding (E_i, L_i^2)-equations (3.3) over all L_i^2, use of Leibnitz's integration rule and setting $\rho_i^{\pm}(R, E, R^2p_i^2) = \rho_i^-(R, E_i)$ so as to acknowledge conversion at pericenter R_i^-. The solution of (6.6b) can be written as,

$$\rho_i^+(S) = \int_0^S \rho_i^-(R_i^-)\omega_i^-(R_i^-)P_S^+(R_i^-, S)dR_i^- \tag{6.7}$$

for S in the range $0 \leq S \leq R_0$ of Region I. The physics of this result is that the source of outgoing pairs are the incoming pairs which undergo conversion at each pericenter R_i^- between R = 0 and S. The outgoing pairs formed at R_i^- then survive to S with probability

$$P_S^+(R_i^-, S) = \exp\left(-2\int_{R_i^-}^S \frac{dR}{\lambda_i}\right). \tag{6.8}$$

The fractional weight of incoming pairs with pericenters R_i^- within the interval dR_i^- about R_i^- is,

$$\omega_i^-(R_i^-)dR_i^- = \frac{dL_i^2}{L_{max}^2} = \frac{d\left(R_i^{-2}p_i^{-2}\right)}{S^2p_S^2} \tag{6.9}$$

under L^2-equilibrium. Pairs with angular momentum $L_{max} = Sp_s$ have a relative orbit which just touches the S-sphere at S which in turn encloses all the pericenters R_i^- between 0 and S.
The probability of association,

$$P_i^A(E_i, R_0) = 1 - \frac{\rho_i^+(E_i, R_0)}{\rho_i^-(E_i, R_0)}, \tag{6.10}$$

within R_0, with (6.5) and (6.7), yields

$$P_i^A(E_i, R_0) = 1 - \frac{1}{R_0^2p_0^2}\int_0^{R_0} P_S^-(R_0, R_i^-)\omega_i^-(R_i^-)P_S^+(R_i^-, R_0)dR_i^-. \tag{6.11}$$

The physics of this result is that the incoming (−) pairs which arrive at the pericenter with probability $P_S^-(R_0, R_i^-)$ and weight $\omega_i^-(R_i^-)$ per unit dR_i^- are converted at each R_i^- to outgoing (+) pairs which survive to R_0 with a probability $P_S^+(R_i^-, R_0)$ With the above definitions of P_S^+ and ω_i^-, integration by parts then yields,

$$P_i^A(E_i, R_0) = \frac{1}{\pi\rho_0^2}\int_0^{R_0} 4\pi R^2\left(1 - \frac{V(R)}{E}\right)\exp\left[-\frac{4}{\lambda_i}(R_0 - R)\right]dR/\lambda_i, \tag{6.12}$$

where the maximum impact parameter ρ_0 which has its pericenter on R_0 is given by $\rho_0^2 = R_0^2[1 - V(R_0)/E_i]$ and where λ_i may depend on E_i. In the limit of low gas densities $R_0/\lambda_i \rightarrow 0$ and (6.12) reproduces the previous low-density limit (4.16).

For energy independent λ_i, the macroscopic probability (3.28) with (6.12) yields,

$$P^A(R_0) = \frac{1}{\pi\rho_{max}^2}\int_0^{R_0} 4\pi R^2\left[1 - \frac{V(R)}{kT}\right]e^{-4(R_0-R)/\lambda}\left[\frac{dR}{\lambda}\right] \tag{6.13}$$

Expressions (6.12) and (6.13) pertain to general interactions V(R) and are valid when the (E_i, L_i^2) pairs with $R \leq R_0$ are in L_i^2 equilibrium and in (E_i, L_i^2)-equilibrium, respectively. The corresponding distributions (6.5) and (6.7) at R_0 associated with P_i^A are not in R-equilibrium.

On recalling the original complexity entailed with the multidimensional integrations (3.23) and (3.24) involving the microscopic distributions (3.5) and (3.6) and the probabilities (3.25), both expressions (6.12) and (6.13) represent a significant algebraic reduction applicable to general V(R).

6.2 Apocenter Region II ($E < E_b = V(R) + \frac{1}{2}\frac{dV}{dR}; R \geq R_b$): Microscopic Distribution of Bound Pairs.

Equation (5.25) reduces in the absorption limit to,

$$\frac{\partial \rho_i^+}{\partial R} = -\frac{2}{\lambda}\rho_i^+ \tag{6.14}$$

for ρ_i^+ and to

$$\frac{\partial}{\partial R}\left[R^2 p^2 \rho_i^-(R)\exp(-2R/\lambda)\right] = -\left|\frac{\partial}{\partial R}\left(R^2p^2\right)\right|\rho_i^+(R)\exp\left(-2R/\lambda\right) \tag{6.15}$$

for ρ_i^-. The solution of (6.15) subject to pre-assigned $\rho_i^-(R_0)$ is,

$$\rho_i^-(S) = \frac{R_0^2 p_0^2}{S^2 p_S^2}\rho_i^-(R_0)P_S^-(R_0,S) + \int_S^{R_0}\rho_i^+(R_i^+)\omega_i^+(R_i^+)P_S^-(R_i^+,S)dR_i^+ \tag{6.16}$$

for S in the range $R_b \le S \le R_0$. The first term on the RHS is the direct contribution from incoming R_0-pairs which survive against collision to S with probability,

$$P_S^-(R_0,S) = \exp\left(-2\int_{R_0}^{S}\frac{dR}{S}\right) \tag{6.17}$$

and $R_0^2p_0^2/S^2p_S^2$ is the fractional number of L^2-states accessible under L^2-equilibrium. The second term is the contribution from apocenter $(+) \rightarrow (-)$ conversions at R_i^+ which survive against collision back to $S \le R_i^+$ with probability P_S^-. The fractional weight of apocenter pairs within interval dR_i^+ is,

$$\omega_i^+(R_i^+)dR_i^+ = \frac{d\left(R_i^{+2}p_i^{+2}\right)}{S^2p_S^2(S)}. \tag{6.18}$$

The solution of (6.14) subject to $\rho_i^+(R_b)$ at the boundary between Regions I and II is,

$$\rho_i^+(R_i^+) = \rho_i^+(R_b)P_S^+(R_b,R_i^+), \qquad RegionII \tag{6.19}$$

where (6.8) provides the probability for survival of outgoing pairs to R_i^+ in the range $R_b \le R_i^+ \le R_0$. The distribution ρ_i^+ at R_b is obtained from the pericenter Region I solution (6.7) which gives,

$$\rho_i^+(R_b) = \rho_i^-(R_b)\int_0^{R_b}P_S^-(R_b,R_i^-)\omega_i^-(R_i^-)P_S^+(R_i^-,R_b)dR_i^-, \tag{6.20}$$

which is by now self explanatory. On using (6.16) for $\rho_i^-(R_b)$ then in terms of the assigned $\rho_i^-(R_0)$,

$$\rho_i^+(R_i^+) = \left\{\frac{R_0^2p_0^2}{R_b^2p_b^2}\rho_i^-(R_0)P_S^-(R_0,R_b) + \int_{R_b}^{R_0}\rho_i^+(R_i^+)\omega_i^+(R_i^+)P_S^-(R_i^+,R_b)dR_i^+\right\}$$
$$\times\left\{\int_0^{R_b}P_S^-(R_b,R_i^-)\omega_i^-(R_i^-)P_S^+(R_i^-,R_b)dR_i^-\right\}P_S^+(R_b,R_i^+), RegionII \tag{6.21}$$

The notation adopted here facilitates the recognition of the various sequences involved in the generation of ρ_i^+ from ρ_i^- in Region II. It also illustrates quite dramatically that ρ_i^+ is the solution of an integral equation in R-space. The use of the absorption limit adopted in this section §6 essentially eliminates the integral equation in E-space involved with the original Master set of equations (5.24) and (5.25). The full solution of the Master equations involves integral equations in E and R space, which are difficult to solve numerically.

The distribution $\rho_i^-(R)$ in Region I which originates from $\rho_i^-(R_0)$ in Region II is,

$$\rho_i^-(R) = \rho_i^-(R_b)P_S^-(R_b,R); \qquad RegionI \tag{6.22}$$

6.3 Application: Coulomb Association Probabilities for Pericenter Region I.

Dissociated pairs with all R are all in Region I. For Coulombic attraction $V(R) = -e^2/R$, and constant free-path-length λ, (6.12) yields,

$$P_i^A(R_0, E) = 1 - \frac{1}{8\tilde{X}^2}\left[\left(1 - e^{-4X}\right)\left(\frac{2}{X}\left[\tilde{X}^2 - X^2\right] - 1\right) + 4X\right] \tag{6.23}$$

where the parameters

$$X = R_0/\lambda; \quad \tilde{X}(\epsilon) = \rho_0(\epsilon)/R_0 \tag{6.24}$$

are related by

$$\tilde{X}^2(R_0, \epsilon, X) = \left[1 + \frac{R_e}{R_0\epsilon}\right] X^2 \tag{6.25}$$

in terms of the natural units $R_e = e^2/kT$ and $\epsilon = E/kT$ of length and energy.

The low-energy parabolic ($E \to 0$) limit to (6.12) yields

$$P^A(R_0, E \to 0) = 1 - \frac{1}{4X}\left(1 - e^{-4X}\right) \to \begin{cases} 2R_0/\lambda, & X \to 0 \\ 1, & X \to \infty \end{cases} \tag{6.26}$$

and the high-energy rectilinear ($E \to \infty$) limit is,

$$P^A(R_0, E \to \infty) = 1 - \frac{1}{8X^2}\left[4X - 1 - e^{-4X}\right] \to \begin{cases} \frac{4}{3}R_0/\lambda, & X \to 0 \\ 1, & X \to \infty \end{cases} \tag{6.27}$$

The initial gradients of P^A are proportional to the enclosed parabolic and chord segments $2R_0$ and $\frac{4}{3}R_0$, respectively. The above limits (6.26) and (6.27) are the envelopes to the family of plots of (6.23) versus gas denisty for various energies ϵ. The E-integrated probability (6.13) is,

$$P_i^A(R_0) = P^A(R_0, kT) \tag{6.28}$$

and is identical with the probability (6.23) evaluated at $\epsilon = 1$. The above probabilities derived under the assumption of L^2-equilibrium will not in general agree with the corresponding results (3.27), (3.31) and (3.34) based on non-equilibrium distributions (3.5) and (3.6), except in the low density ($X \to 0$) limit when the gradients of all the envelopes are equal to $2X$ and $\frac{4}{3}X$, respectively. Figure 4 provides the X-variation of the E-averaged envelopes (6.26) and (6.27), and probabilities (6.23) for various ϵ. The probabilities are in general lower than the corresponding probabilities of fig. (1a) associated with L^2-nonequilibrium since not all collisions result in absorption (cf. fig. 5).

All collisions with (E_i, L_i^2)-pairs are not expected to result in stabilized recombination, eg. those involving only angular-momentum redistributions in $(E_i, L_i^2 \to E_i, L_f^2)$ transitions can be excluded. These collisions which involve only angular momentum changes are expected to promote equilibrium in L^2 rather than absorption. In this sense therefore the classical (absorption) solutions (6.12) and (6.13) associated with L^2-equilibrium represent a more natural outcome than those (3.5) and (3.6) associated with full absorption of all L_i^2 levels upon collision. The probabilities (6.12) or (6.23) and (6.13) or (6.28) are therefore expected to provide a representation more physically correct than (3.27) and (3.31) ie. the lower curve of fig. 5 is to be preferred.

7. Solution as a Function of Gas Density: Reaction and Transport Rates

The rate (2.14) is exactly,

$$\alpha \tilde{N}_A \tilde{N}_B = \lim_{R_0 \to \infty} \int_0^\infty dE_i \int_0^{R_0^2 p_0^2} dL_i^2 \left[4\pi R_0^2 \tilde{n}_i^-(R_0) v_R\right] \rho_i^-(R_0) P_i^A(R_0) \tag{7.1}$$

where the microscopic distributions $\rho_i^{\pm}$ implicit in $P_i^A \left(= 1 - \rho_i^+/\rho_i^-\right)$ are solutions of the transport-collisional Master Equations (2.20) for general non-equilibrium in (L_i^2, E_i, R) coordinates, or of (5.24) and (5.25) for non-equilibrium only in E_i and R. This procedure provides in principle the full variation of α with gas density N.

The pairs with large R are generally in (E_i, L_i^2) equilibrium but not in R equilibrium. Further insight and development may however be achieved by address to the macroscopic continuity equation. The net microscopic current $J(R, E, L_i^2)$ and the net L_i^2-integrated current $J(R, E_i)$ satisfy microscopic equations of continuity (2.15b) and (5.8), respectively. On integrating (5.8) which holds quite generally for non-equilibrium in R, E_i and L_i^2, over all E_i accessible at a given R and use of Leibnitz's rule,

$$\int_{V(R)}^{\infty} \frac{1}{R^2}\frac{\partial}{\partial R}\left[R^2 J(R,E_i)\right]_{E_i} dE_i = \frac{1}{R^2}\frac{\partial}{\partial R}\left\{R^2 \int_{V(R)}^{\infty} J(R,E_i)dE_i\right\} + \frac{1}{R^2}\frac{\partial V}{\partial R}\left[R_i^2 J(R_i, E_i = V(R))\right] = 0 \tag{7.2}$$

is zero due to the null effect of all the collisional redistribution terms,

$$\int_{V(R)}^{\infty} dE_i \int_{V(R)}^{\infty} dE_f \left[\rho_f(R) - \rho_i(R)\right] C_{if}(R) = 0. \tag{7.3}$$

Since the net current $J(R_i, E_i = V(R)) = \frac{1}{2}(n_i^+ - n_i^-)v_i$ vanishes at the outermost turning point R_i given by $E_i = V(R)$, (7.2) provides the macroscopic continuity equation,

$$\nabla \cdot \mathbf{J}(\mathbf{R}) = 0 \tag{7.4}$$

which is always valid for the net macroscopic radial current

$$J(R) = \int_{V(R)}^{\infty} J_i(R) dE_i = \int_{V(R)}^{\infty} dE_i \left[n^+(R,E_i) - n^-(R,E_i)\right]\frac{v_i}{2}, \tag{7.5}$$

$$= \int_{V(R)}^{\infty} dE_i \int_0^{L_{m_i}^2} dL_i^2 \left[n^+(R,E_i,L_i^2) - n^-(R,E_i,L_i^2)\right] v_R, \tag{7.6}$$

$$= \int_{V(R)}^{\infty} dE_i \int_0^{L_{m_i}^2} dL_i^2 \left[\rho_i^+(R) - \rho_i^-(R)\right] (\tilde{n}_i^{\pm} v_R). \tag{7.7}$$

Assumption: For large $R \geq R_0$, the pairs are in (E_i, L_i^2)-equilibrium ie. $\rho_i^{\pm}(R) = \rho^{\pm}(R)$ irrespective of i. Hence (7.7) yields,

$$J_1(R) = j^+(R) - j^-(R) = \frac{1}{4}\tilde{N}_A \tilde{N}_B \exp\left(-V(R)/kT\right)\overline{v}\left[\rho^+(R) - \rho^-(R)\right],\ R \geq R_0 \tag{7.8}$$

when the bound levels in the range $[0 - V(R)]$ are included in the integration, or

$$J_2(R) = \frac{1}{4}\tilde{N}_A \tilde{N}_B \left[1 - \frac{V(R)}{kT}\right]\overline{v}\left[\rho^+(R) - \rho^-(R)\right] \tag{7.9}$$

when they are excluded. For $V \ll kT$, then $J_1 \rightarrow J_2$. Under steady-state conditions

$$4\pi R^2 J(R \geq R_0)/\tilde{N}_A \tilde{N}_B = \alpha\rho(R \rightarrow \infty) = \pi R_0^2 \left(1 - \frac{V(R_0)}{kT}\right)\overline{v} P^A(R_0)\rho^-(R_0) \tag{7.10}$$

where $\rho(R)$ is the non-equilibrium normalized distribution $n(R)/\tilde{n}(R)$ of expanding and contracting pairs and is related to $\rho^-(R)$ by

$$\rho(R) = \frac{\left[\rho^+(R) + \rho^-(R)\right]}{2} = \left[1 - \frac{1}{2}P^A(R)\right]\rho^-(R) \tag{7.11}$$

when $P^A(R_0)$ is the macroscopic probability for association within R. Since the incoming pairs are generated at infinity with a Boltzmann distribution $\rho^-(R \to \infty) \to 1$ and $\rho(R \to \infty) \to 1 - \frac{1}{2}P^A(\infty)$. The summed distribution $\rho(\infty)$ is therefore not in R-equilibrium. Also $\rho^-(\infty) > \rho^+(\infty)$ and a net inward current (7.8) exists at infinity.

7.1 Non-Equilibrium $\rho(R)$: The Transport Rate

The basic Master Equations (2.20) followed from (1.2) which was originally derived from a Boltzmann equation in (**R**, **p**) phase space. In the absence of a sink at R, it was also shown[6] from the same Boltzmann equation that (7.5) the macroscopic current **J** can be represented by the standard diffusion-drift expression,

$$\mathbf{J}(R) = -D\nabla n(R) - \left[\frac{K}{e}\nabla V(R)\right] n(R), \;\; R \geq R_0 \tag{7.12}$$

where n(R) is the non-equilibrium (A-B) pair distribution which is affected by the strength of sinks within $R \leq R_0$. The macroscopic collisional coefficients D and K for relative diffusion and drift of A towards B through a gas M are given respectively by $D = D_A + D_B$ and $K = K_A + K_B$ where $D_{A,B}$ and $K_{A,B}$ are the diffusion coefficients and mobilities for the individual species A and B in M. These coefficients at low field strengths (as Coulombic at large R) are related by $KkT = De$ or by $Ke = DR_e$ where R_e is the natural unit e^2/kT so that

$$\frac{J(R)}{\tilde{N}_A\tilde{N}_B} = -D\exp\left[-V(R)/kT\right]\frac{\partial\rho}{\partial R} = \frac{\alpha}{4\pi R^2} \tag{7.13}$$

The solution of (7.13) between R_0 and ∞ yields,

$$\rho(R_0) = \rho(\infty)\left(1 - \alpha/\alpha_{TR}(R_0)\right) \tag{7.14}$$

where the transport rate,

$$\alpha_{TR}(R_0) = 4\pi D\left[\int_{R_0}^{\infty}\exp(V(R)/kT)R^{-2}dR\right]^{-1} \tag{7.15}$$

is the rate of production by diffusional-drift of R_0-pairs from pairs originally with infinite separation. Once $\rho(R_0)$ can be furnished from (7.1) in terms of α, then (7.14) can be solved for α.

7.2 The Reaction Rate

We now choose R_0 in (7.1) to be finite, yet sufficiently large that no sinks exists outside R_0 (eg. $R_0 \geq 5(e^2/kT)$ for a Coulomb interaction[4] at low gas densities). Both (7.4) and (7.13) are then valid. The effect of non-reactive collisions outside R_0 will now be acknowledged via appropriate choice of $\rho_i^-(R_0)$ in (7.1). The component species A and B are assumed to be in collisional equilibrium with their mutual field $V(R)$ at these large $R \geq R_0$. The kinetic energy gained from V(R) by the contracting pairs as R is decreased is lost upon collision with the gas species M. Following each collision, the kinetic energy T at each $R \geq R_0$ is therefore reduced to the original kinetic energy $E_i = T_\infty$ of generation of pairs with infinite R. Assuming that the last collision suffered by the R_i-pair occurs at $(R_i + \lambda)$, where λ is the macroscopic *mean* free path, then the pre-collision kinetic energy of the R-pairs is,

$$T'(R) = T_\infty + [V(R+\lambda) - V(R)] \tag{7.16}$$

which represents an increase of $\delta V(R) = [V(R+\lambda) - V(R)]$ over its original thermal value T_∞ resulting from the previous collision. Prior to the next collision at R the internal energy is then,

$$E_i'(R) = T'(R) + V(R) = T_\infty + V(R+\lambda). \tag{7.17}$$

At low gas densities $\lambda \to \infty$, and E_i of course remains conserved for all $R \geq R_0$ while T_i increases from $T_\infty = E_i$ at infinity to $[E_i - V(R)]$ at R. The internal energy of pairs contracting at R_0 is

$E_i' = T_\infty - \mid V(R_0+\lambda) \mid$ rather than $E_i = T_\infty$ as it would be in the absence of diffusional-drift collisions outside R_0.

The degradation of E_i from its value at infinity therefore causes E_i in (7.1) to be replaced by E_i'. Hence (7.1) yields,

$$\alpha = \alpha_{RN}(R_0)\,[\rho(R_0)/\rho(\infty)] \tag{7.18}$$

$$= \left(\tilde{N}_A \tilde{N}_B\right)^{-1} \int_{V(R_0+\lambda)}^{\infty} dE_i \int_0^{R_0^2 P_0^2} dL_i^2 \left[4\pi R_0^2 \tilde{n}_i^-(R_0) v_R\right] P_i^A(R_0) \tag{7.19}$$

This defines the rate of reaction $\alpha_{RN}(R_0)$ within R_0 which equals α if full equilibrium, $\rho(R_0) = 1$, were to exist. On inserting (7.18) into (7.13) then the overall rate is,

$$\alpha = \frac{\alpha_{RN}(R_0)\alpha_{TR}(R_0)}{\alpha_{RN}(R_0) + \alpha_{TR}(R_0)}. \tag{7.20}$$

This decomposition (7.20) of α into reaction and transport rates was known in recombination since the macroscopic result of Natanson[15] was recast[20] in that form (which also can be deduced directly from Debye-Smoluchowski theory[21]). What is new here is the following expression to be used in (7.20) for the reaction rate,

$$\alpha_{RN}(R_0) = \frac{\rho(\infty)}{\rho(R_0)} \left[\alpha'_{RN}(R_0)\rho^-(R_0)\right] \tag{7.21}$$

where the macroscopic equivalent (3.20) of the integral in (7.19) is,

$$\alpha'_{RN}(R_0) = \pi \rho_{max}^2 \overline{v} \exp(-V(R_0+\lambda)/kT) P^A(R_0) \tag{7.22}$$

where,

$$\rho_{max}^2 = R_0^2 \left[1 - \frac{V(R_0)}{kT} + \frac{V(R_0+\lambda)}{kT}\right]. \tag{7.23}$$

With the use of (7.11) in (7.21) then,

$$\alpha_{RN}(R_0) = \left(\frac{1 - \frac{1}{2}P^A(\infty)}{1 - \frac{1}{2}P^A(R_0)}\right) \alpha'_{RN}(R_0) \tag{7.24}$$

since $\rho^-(\infty) \rightarrow 1$. Previous treatments had tacitly assumed that α_{RN} in (7.20) was given by α'_{RN} the microscopic rate (7.22). The factor in (7.24) which essentially arises from the differences between the values $\rho^-(R_0)/\rho^-(\infty)$ and $\rho(R_0)/\rho(\infty)$, tends to unity in the limits of low and high gas densities when $P^A \rightarrow 0$ and 1, respectively.

8. Summary

Basic sets of Coupled Collisional-Transport Master Equations have therefore been developed in this paper for the microscopic distributions $n^{\pm}(\mathbf{R}, E, L^2)$ of expanding (+) and contracting (−) pairs (A-B) in a gas M of variable density with respect to their (A-B) internal separation $\mathbf{R}$, internal (orbital) energy E and orbital angular momentum L, as well as for the corresponding L^2-averaged distributions $n^{\pm}(\mathbf{R}, E)$. Expressions have been introduced for the microscopic probability $P_i^A(R)$ for association of (E_i, L_i^2)-pairs with separations $\leq R$ and for the probability $P_f^S(R)$ of multicollisional stabilization of (E_f, L_f^2)-pairs with separation R formed collisionally from (E_i, L_i^2)-pairs. The recombination rate has then been expressed in the collisional form and the transport form which is more amenable to physical insight and to algebraic development.

Each set has been solved exactly in closed analytical form in the (classical) limit of collisional absorption where backward collisional couplings ν_{fi} are neglected. The corresponding probabilities $P_i^A(R)$

for association have also been determined. In particular the multidimensional integrations inherent in P_*^A for orbits under general $V(R)$, including Coulombic attraction, have been reduced to new and simple analytical results for association (a) at low gas density, and (b) at all gas densities for pairs which are maintained in L^2-equilibrium by collision.

A classical Variational treatment for which the highly excited bound pairs need not be in E-equilibrium has also been introduced, in order to provide assignment to the reaction radius R_0 adopted in the above classical treatments.

Expression for the rate α as a function of gas density in terms of the reaction and transport rates α_{RN} and α_{TR}, respectively , has been proposed. It differs from previous well known formula in the form of the macroscopic reaction rate α_{RN}. Finally, useful expressions for the microscopic path length in E, L^2-Coulombic Orbit enclosed by a sphere of radius R and simple analytical expressions for the L^2-averaged enclosed length over all trajectories under a general $V(R)$ have been derived in Appendix B.

Acknowledgments

This research is supported by the U. S. Air Force Office of Scientific Research under Grant no. AFOSR-89-0426.

Appendix A: One-Way Equilibrium Microscopic Flux and Distributions

These distributions can be calculated directly[21] from the relevant statistical formula[23] or from the simple differentiation of action integrals[24]. It is convenient here to summarize the key results. M is now the reduced mass of the (A-B) pair, and with internal separation, energy and orbital angular momentum R, E and L, respectively. $E = \epsilon kT$ and $L^2 = 2ME\rho^2$; where ρ is the impact parameter for dissociated A-B pairs with energy E, with radial speed $v_R = dR/dt$ and mean speed $\overline{v} = (8kT/\pi M_{AB})^{1/2}$.

1. (E, L)-Microscopic Current and Flux:

$$\tilde{j}^{\pm}(R, E, L^2) = \tilde{n}^{\pm}(\mathbf{R}, E, L^2) v_R$$

$$4\pi R^2 \tilde{j}^{\pm}(R, E, L^2) dE dL^2 = \frac{4\pi^2}{(2\pi M_{AB} kT)^{3/2}} \exp(-E/kT) dE dL^2$$
$$= \overline{v}\epsilon\, e^{-\epsilon}\; d\epsilon\; d(\pi\rho^2)$$

2. E-Microscopic Current and Flux:

$$\tilde{j}^{\pm}(R, E) = \int_0^{R^2 p^2} \tilde{j}^{\pm}(R, E, L^2) dL^2 = \frac{1}{2} v \tilde{n}^{\pm}(R, E)$$

$$4\pi R^2 \tilde{j}^{\pm}(R, E) dE = \overline{v}\epsilon\, e^{-\epsilon}\; d\epsilon \pi R^2 \left(1 - \frac{V(R)}{E}\right)$$
$$\equiv \pi\rho^2(R) \overline{v}\epsilon\, e^{-\epsilon}\; d\epsilon$$

3. Macroscopic Current and Flux:
The current is

$$\tilde{j}^{\pm}(R) = \int_{V(R)}^{\infty} \tilde{j}^{\pm}(R, E) dE = \frac{1}{4} \overline{v} e^{-V(R)/kT}$$

for all bound and dissociated pairs, and is

$$\tilde{j}_d^{\pm}(R) = \int_0^{\infty} \tilde{j}^{\pm}(R, E) dE = \frac{1}{4} \overline{v} \left[1 - \frac{V(R)}{kT}\right]$$

for dissociated pairs. Respective fluxes are,

$$4\pi R^2 \tilde{j}^{\pm}(R) = \pi R^2 \bar{v} \exp(-V(R)/kT)$$
$$4\pi R^2 \tilde{j}_d^{\pm}(R) = \pi \rho_{max}^2 \bar{v}; \qquad \rho_{max}^2 = R^2\left[1 - \frac{V(R)}{kT}\right]$$

4. (E, L)-Microscopic Distribution:

$$4\pi R^2 \tilde{n}^{\pm}(\mathbf{R}, E, L^2) dR dE dL^2 = \frac{(4\pi^2/v_R)}{(2\pi M_{AB} kT)^{3/2}} \exp(-E/kT) dR dE dL^2$$

5. E-Microscopic Distribution:

$$\begin{aligned} 4\pi R^2 \tilde{n}^{\pm}(R, E) dR dE &= \frac{2\bar{v}}{v} \epsilon\, e^{-\epsilon}\; d\epsilon \left(1 - \frac{V(R)}{E}\right) dR \\ &= 4\pi R^2 dR \left[\frac{1}{\sqrt{\pi}} \exp(-\epsilon)\; \sqrt{\frac{E-V}{kT}}\right] d\epsilon \\ &= (4\pi R^2 dR)\;\; [G_{MB}^{\pm}(\epsilon, R)\, d\epsilon] \end{aligned}$$

where $G_{MB}^{\pm}$ is the one-way Maxwell-Boltzmann velocity distribution in above [ ].

6. Macroscopic Distribution:

$$\tilde{n}^{\pm}(R) = \int_{V(R)}^{\infty} \tilde{n}^{\pm}(R, E) dE = \frac{1}{2} \exp(-V(R)/kT)$$

for available bound and dissociated pairs and,

$$\begin{aligned} \tilde{n}_d^{\pm}(R) &= \int_0^{\infty} \tilde{n}^{\pm}(R, E) dE \\ &= \frac{1}{2} \exp(-V(R)/kT) \left\{1 - \left[\Phi(\sqrt{X}) - \frac{2}{\sqrt{\pi}} X^{1/2} \exp(-V/kT)\right]\right\} \end{aligned}$$

for dissociated pairs, where the error or probability integral is,

$$\Phi(\sqrt{X}) = \frac{1}{\sqrt{\pi}} \int_0^X t^{-1/2} e^{-t} dt = \frac{2}{\sqrt{\pi}} X^{1/2} e^{-X} \sum_{k=0}^{\infty} \frac{(2X)^k}{(2k+1)!!}$$

in terms of $X = V(R)/kT$.

Appendix B: Microscopic Path Length $\mathcal{L}(E, \rho; R_0)$ of (E, ρ)-Coulombic Orbit Enclosed by Sphere of Radius R_0 and ρ-averaged Path Length for General $V(R)$.

The enclosed length may be determined either from

$$\mathcal{L} = \oint_{R_t}^{R_0} ds_t = 2 \int_{R_t}^{R_0} \left[1 + R^2 \left(\frac{d\theta}{dR}\right)^2\right]^{1/2} dR \qquad (B1)$$

which implies knowledge of the relevant orbit $\theta(R)$, or from

$$\mathcal{L}(E, L; R_0) = 2 \int_{R_t}^{R_0} \frac{v_t}{v_R} dR = 2 \int_{R_t}^{R_0} \frac{\sqrt{E - V(R)} dR}{\sqrt{E - V(R) - L^2/2MR^2}}, \qquad (B2)$$

where the pericenter R_t is the root of the denominator. For a hyperbolic orbit under Coulomb attraction $V(R) = -e^2/R$, (B.2) reduces to,

$$\mathcal{L} = 2 \int_{a(\epsilon-1)}^{R_0} \frac{\sqrt{(R+a)^2 - a^2}}{\sqrt{(R+a)^2 - a^2\epsilon^2}} dR = 2 \int_{a\epsilon}^{R_0+a} \frac{\sqrt{x^2 - a^2}}{\sqrt{x^2 - a^2\epsilon^2}} dx, \qquad (B3)$$

where the eccentricity ε and semi-major axis a are given by,

$$\varepsilon^2 = 1 + \frac{L^2}{(2mEa^2)} = 1 + \rho^2/a^2; \qquad a = e^2/2E. \tag{B4}$$

The maximum impact parameter for the enclosed family of trajectories is given by,

$$\rho_0^2(E) = R_0^2\left(1 - \frac{V(R_0)}{E}\right) \tag{B5}$$

Integral (B3), with a singularity at the lower limit, may be evaluated numerically by standard integration techniques or from the analytical expression,

$$\mathcal{L}(E, L; R_0) = \frac{a^2(\varepsilon^2 - 1)}{a\varepsilon} F(\phi, k) - a\varepsilon E(\phi, k) + (R_0 + a)\sin(\phi) \tag{B6}$$

in terms of the incomplete elliptic integrals F and E of the first and second kinds respectively, with angle ϕ and modulus k given by,

$$\sin^2\phi = \frac{(R_0 + a)^2 - a^2\epsilon^2}{(R_0 + a)^2 - a^2} = \frac{(R_0 + a)^2 - (R_t^- + a)^2}{(R_0 + a)^2 - a^2} = 1 - \rho^2/\rho_0^2 \tag{B7}$$

and

$$k = \sin\alpha = \frac{1}{\varepsilon} = \frac{a}{(\rho^2 + a^2)^{1/2}} \tag{B8}$$

respectively. The deflection angle ψ is $(\pi - 2\alpha)$. On eliminating ε via (B4) then (B6) is,

$$\mathcal{L}(E, \rho; R_0) = 2(\rho^2 + a^2)^{1/2}[k'^2 F(\phi, k) - E(\phi, k)] + 2(\rho_0^2 + a^2)^{1/2}\sin\phi \tag{B9}$$

where,

$$k'^2 = 1 - k^2 = \rho^2/(\rho^2 + a^2). \tag{B10}$$

Since the pericenter $R_t = a(\varepsilon - 1)$ satisfies

$$(R_t + a)^2 = \rho^2 + a^2 \tag{B11}$$

from (B4), then (B9) is alternatively recast in terms of energy E and R_t regarded as new independent variables, as

$$\mathcal{L}(E, R_t; R_0) = 2(R_t + a)[k'^2 F(\phi, k) - E(\phi, k)] + 2(R_0 + a)\sin\phi \tag{B12}$$

where

$$k'^2 = \frac{[(R_t + a)^2 - a^2]}{(R_t + a)^2}. \tag{B13}$$

For the limiting case of parabolic motion $\varepsilon \to 1 (k \to 1, k' \to 0), E \to 0$ $(a \to \infty)$ direct use of the orbit,

$$R(\theta) = 2R_t/(1 + \cos\theta), \qquad R_t(L) = L^2/me^2 \tag{B14}$$

in (B1) or on setting E = 0 in (B2) yields,

$$\mathcal{L}(E \to 0, R_t; R_0) = 2\int_{R_t}^{R_0} [R/(R - R_t)]^{1/2}\, dR, \tag{B15a}$$

$$= 2R_t \ln\tan\frac{1}{4}(\pi + \theta_0) + 2R_0\sin\frac{1}{2}\theta_0, \tag{B15b}$$

where $\theta_0 = \theta(R_0)$. This is also the corresponding limit of (B12) where $E(\phi, k)$ must be expanded to first order in k'^2, where $F(\phi, 1) = \ln \tan \frac{1}{4}(\pi + \theta_0)$ and where,

$$\sin^2 \phi \rightarrow \sin^2 \phi_0 = 1 - R_i/R_0, \tag{B16}$$

such that $\theta_0 = 2\phi_0$. For computational purposes the probability (3.11) with (B9) for $\mathcal{L}$ is recast in the dimensionless units,

$$\rho' = \rho/\rho_0; \quad \epsilon' = \frac{E}{kT}\frac{R_e}{R_0} \equiv \epsilon r_0; \quad X = R_0/\lambda; \quad R_e = e^2/kT \tag{B17}$$

as,

$$P^A(X, \epsilon') = \int_0^1 [1 - \exp(-\mathcal{L}(X, \epsilon'; \rho')/\lambda)]\, d\rho'^2; \tag{B18}$$

with,

$$\frac{\mathcal{L}(X, \epsilon'; \rho')}{\lambda} = 2X\left(1 + \frac{1}{\epsilon'}\right)^{1/2}\left[\frac{\rho'^2}{\sqrt{\rho'^2 + a'^2}}F(\phi, k) - (\rho'^2 + a'^2)^{1/2}E(\phi, k) + (1 + a'^2)^{1/2}\sin\phi\right], \tag{B19}$$

where,

$$a'^2 = [4\epsilon'(\epsilon' + 1)]^{-1}; \quad \sin^2\phi = 1 - \rho'^2; \quad k^2 = a'^2(\rho'^2 + a'^2)^{-1}. \tag{B20}$$

The variation of this probability (B18) with the density parameter X ($\sim$ gas density) and reduced energy parameter ϵ' or r_0 is displayed in Fig. 1. Expression (B19) is univerisal in that it simultaneously provides variation with gas density X and R_0 (see Fig. 2).

Averaged Enclosed Length $\mathcal{L}(E; R_0)$ Over All Accessible Trajectories.

At low gas densities the ρ-averaged collision probability (3.27) for constant λ is $\langle\mathcal{L}\rangle_\rho/\lambda$ where the average enclosed length of all possible trajectory segments,

$$\mathcal{L}(E; R_0) = \langle\mathcal{L}(E, \rho; R_0)\rangle_\rho = \frac{1}{\rho_0^2}\int_0^{\rho_0^2}\mathcal{L}(E, \rho; R_0)d\rho^2 \tag{B21}$$

enters into expression (4.7) for the low-density rate of ion-ion recombination. Direct use of (B9) in (B21) appears cumbersome, except for the limiting case ($E \rightarrow 0, a \rightarrow \infty, \epsilon \rightarrow 1$) of parabolic motion. Then use of the parabolic segment (B15b) in (B21) with,

$$\frac{d\rho^2}{\rho_0^2(E)} = \frac{2(R_i + a)dR_i}{(R_0 + a)^2 - a^2} \quad \longrightarrow \frac{dR_i}{R_0} \tag{B22}$$

in this parabolic limit. The ρ_0^2-averaged value (B21) after elementary integration of each term of (B15b) yields

$$\mathcal{L}(E \rightarrow 0; R_0) = \left(\frac{2}{3} + \frac{4}{3}\right)R_0 = 2R_0 \tag{B23a}$$

which also follows from (B15a) by noting that,

$$\mathcal{L}(E \rightarrow 0, R_0) = \frac{2}{R_0}\int_0^{R_0} dR_i \int_{R_i}^{R_0}\sqrt{\frac{R}{R - R_i}}\, dR = \frac{2}{R_0}\int_0^{R_0} dR \int_0^{R}\sqrt{\frac{R}{R - R_i}}\, dR_i = 2R_0 \tag{B23b}$$

At high energies $E \gg V(R)$, $\rho_0 \to R_0$ and the ρ^2-average (B21) of $\mathcal{L} = (R_0 - \rho_0^2)^{1/2}$ is $\frac{4}{3}R_0$. The enclosed length (B21) (and hence (3.27)) will therefore decrease from $2R_0$ to $\frac{4}{3}R_0$ as E increases for all gas densities (cf. gradient slopes of inset figure 1a).

For the case of electron-ion recombination the infinite limit to the energy E in (4.7) is replaced[16] by $E_m = (2m/M)(e^2/R)$ so that the low density rate (4.7) is,

$$\alpha_L = \frac{\overline{v}}{\lambda} R_0 \int_0^{R_0} dR_t \oint_{R_t}^{R_0} ds_t \int_0^{\epsilon_m} \epsilon\, e^{-\epsilon}\; d\epsilon (1 + R_e/\epsilon R_0), \tag{B24}$$

where here $\epsilon = E/kT$. This reduces to first order in (m/M) to,

$$\alpha_L = \frac{\overline{v}}{\lambda} \frac{2m}{M} \left[\frac{e^2}{kT}\right]^2 \int_0^{R_0} dR_t \int_{R_t}^{R_0} \frac{ds}{R} \tag{B25}$$

which, for the low-energy parabolic motion involves,

$$\oint_{R_t}^{R_0} \frac{ds}{R} = 4 \ln \tan \frac{1}{4}(\pi + \theta_0), \tag{B26}$$

the average of $\frac{1}{R}$ over each trajectory rather than the path length (B15). Hence (B25) reduces to

$$\alpha_L = 8\pi \frac{m}{M} \frac{\overline{v}}{\lambda} \left(\frac{e^2}{kT}\right)^2 R_0 \tag{B27}$$

for collisional electron-ion recombination, in exact agreement with the energy-diffusion result of Pitaevskii[17] when $R_0 = \frac{2}{3}R_e$ the Thomson radius.

For the general case of ion-ion recombination the averaged path length (B21) is required but direct use of (B9) appears prohibitive. On using (B11) however, for the transformation $\rho \to R_t^-$ at constant E, then

$$\mathcal{L}(E; R_0) = \frac{1}{\rho_0^2} \int_0^{\rho_0^2} d\rho^2 \oint_{R_t}^{R_0} ds_t = \frac{4}{\rho_0^2} \int_0^{R_0} (R_t + a) dR_t \int_{R_t}^{R_0} f(R, R_t) dR \tag{B28}$$

where for a Coulomb interaction $V_c(R)$,

$$f(R, R_t) = \frac{(R+a)^2 - a^2}{(R+a)^2 - (R_t + a)^2} \tag{B29}$$

is the integrand of (B3) expressed in terms of R_t rather than ϵ. On interchanging the order of integrations, then (B28) reduces to,

$$\mathcal{L}(E; R_0) = \frac{4}{\rho_0^2} \int_0^{R_0} dR \int_0^{R} (R_t + a) f(R, R_t) dR_t, \tag{B30}$$

which is in a form amenable to elementary integration. Thus,

$$\mathcal{L}(E; R_0) = \frac{4}{3} R_0 \left(1 - \frac{3}{2} \frac{V_c(R_0)}{E}\right) \Big/ \left(1 - \frac{V_c(R_0)}{E}\right) \tag{B31}$$

General $V(R)$: The result (B31) above is but a particular case of the following result for general V(R). On interchanging the order of integrations in (B21) with (B1) then

$$\mathcal{L}(E; R_0) = \frac{1}{\rho_0^2} \int_0^{\rho_0^2} d\rho^2 \oint_{R_t}^{R_0} ds_t = \frac{2}{\rho_0^2} \int_0^{R_0} dR \int_0^{\rho_m^2(R)} \left[\frac{ds_t}{dR}\right] d\rho^2, \tag{B32}$$

The trajectories which access R have impact parameters ρ in the range $0 \le \rho \le \rho_m(R)$ where,

$$\rho_m^2(R) = R^2\left(1 - \frac{V(R)}{E}\right). \qquad (B33)$$

Since

$$\left[\frac{ds_i}{dR}\right] = \frac{\rho_m(R)}{\sqrt{\rho_m^2(R) - \rho^2}} \qquad (B34)$$

from (B2), the inner integral of (B32) is simply $2\rho_m^2$ so that,

$$\mathcal{L}(E; R_0) = \frac{4}{\rho_0^2}\int_0^{R_0} \rho_m^2(R)dR, \qquad (B35)$$

to give

$$\mathcal{L}(E; R_0) = \left[\frac{4}{R_0^2(1 - V(R_0)/E)}\right]\int_0^{R_0} R^2\left(1 - \frac{V(R)}{E}\right)dR \qquad (B36)$$

as the ρ-averaged path length for general V(R). This valuable expression yields (B31) for Coulombic attraction is applicable to all V(R) and agrees with equation (4.9) of text.

References

1. M. R. Flannery and E. J. Mansky, J. Chem. Phys. **88** 4228 (1988).
2. M. R. Flannery, J. Chem. Phys. **89** 214 (1988).
3. M. R. Flannery, J. Chem. Phys. **87** 6847 (1987).
4. M. R. Flannery and E. J. Mansky, J. Chem. Phys. **89** 4086 (1988).
5. D. R. Bates and C. S. McKibbin, Proc. Roy. Soc. (Lond.) A **339** 13 (1974).
6. M. R. Flannery, Phil. Trans. Roy. Soc. (Lond.) A **304** 447 (1982).
7. W. Naumann, Physica A **150** 627 (1988).
8. M. R. Flannery, J. Phys. B: At. Mol. Phys. **20** 4929 (1987).
9. M. R. Flannery, J. Phys. B: At. Mol. Phys. **18** L839 (1985).
10. D. R. Bates and W. L. Morgan, Phys. Rev. Lett. **64** 2258 (1990).
11. S. P. Mezyk, R. Cooper and J. Sherwell, J. Phys. Chem. **93** 8187 (1989).
12. R. J. DiPerna and P. L. Lions, Annals of Math. **130** 321 (1989).
13. J. J. Thomson, Phil. Mag. **47** 337 (1924).
14. L. B. Loeb, *Basic Processes of Gaseous Electronics*, The Univ. Cal. Press (Berkeley) 1955, Chap. 5
15. G. L. Natanson, Sov. Phys.- Tech. Phys. **4** 1263 (1959).
16. D. R. Bates, J. Phys. B: At. Mol. Phys. **13** 2587 (1980).
17. L. P. Pitaevskii, Sov. Phys. - JETP **15** 919 (1962).
18. S. B. Byron, R. C. Stabler and P. I. Bortz, Phys. Rev. Lett. **8** 376 (1962).
19. D. R. Bates and I. Mendaš, Proc. Roy. Soc. (Lond.) A **359** 275 (1978).
20. D. R. Bates and M. R. Flannery, J. Phys. B: At. Mol. Phys. **2** 184 (1969).
21. M. R. Flannery and E. J. Mansky, Chem. Phys. **132** 115 (1989).
22. D. R. Bates and C. S. McKibbin, J. Phys. B: At. Mol. Phys. **6** 2485 (1973).
23. L. D. Landau and E. M. Lifshitz, *Statistical Physics*, Pergamon Press , 3^{rd} Edition, New York 1980, Chap. 3
24. M. R. Flannery, *in preparation*

Figure Captions

Figure 1a-b. (a) Probability $P^A(R_0, E; \lambda)$, equation (3.27), for collision of an ion in a hyperbolic (Coulomb) trajectory with the gas within a sphere of radius $R_0 = 0.4R_e$ as a function of reduced gas density $X = R_0/\lambda$ at various reduced Coulomb-orbit energies $\epsilon = E/kT$; (b) Dotted curve: E-averaged probability $P^A(R_0; \lambda)$, equation (3.28), and $P^A(R_0, kT; \lambda)$. Solid lines are parabolic ($\varepsilon = 0$) and rectilinear ($\varepsilon \to \infty$) envelopes to the collision probabilities, equations (3.34) and (3.31), respectively. Inset figure: E-variation between envelopes at low gas density. The ion-pairs here are *not* in L^2-equilibrium.

Figure 2. Collision Probability $P^A(R_0, E = kT; \lambda)$ as a function of radius R_0 for: (a) a *fixed* gas density with $\lambda = R_e$, and (b) for various gas densities proportional to f. Inset figure: P initially increases linearly with R_0 along parabolic envelope and with further increase of R_0 tends ultimately to the straight-line envelope.

Figure 3. The recombination rate $\alpha_V/(\frac{4}{3}\pi R_e^3 \frac{\overline{v}}{\lambda'})$ versus: (a) transition-state energy $\epsilon_0 = E/kT$, or (b) reaction radius $r_0 = R_0/R_e = 1/\epsilon_0$.

Figure 4. Analytic Probabilities $P^A(R_0, E)$, equation (6.23) for Coulomb Association within a sphere of radius $R_0 = 0.4R_e$ as a function of reduced gas density $X = R_0/\lambda$. Parabolic (equation (6.26)) and rectilinear (equation (6.27)) limits $\varepsilon = 0$ and $\varepsilon = \infty$, respectively. Note that L^2-equilibrium is assumed.

Figure 5. Comparison of E-averaged association probabilities as a function of reduced gas density $X = R_0/\lambda$ for ions with (lower curve) and without (upper curve) L^2-equilibrium.

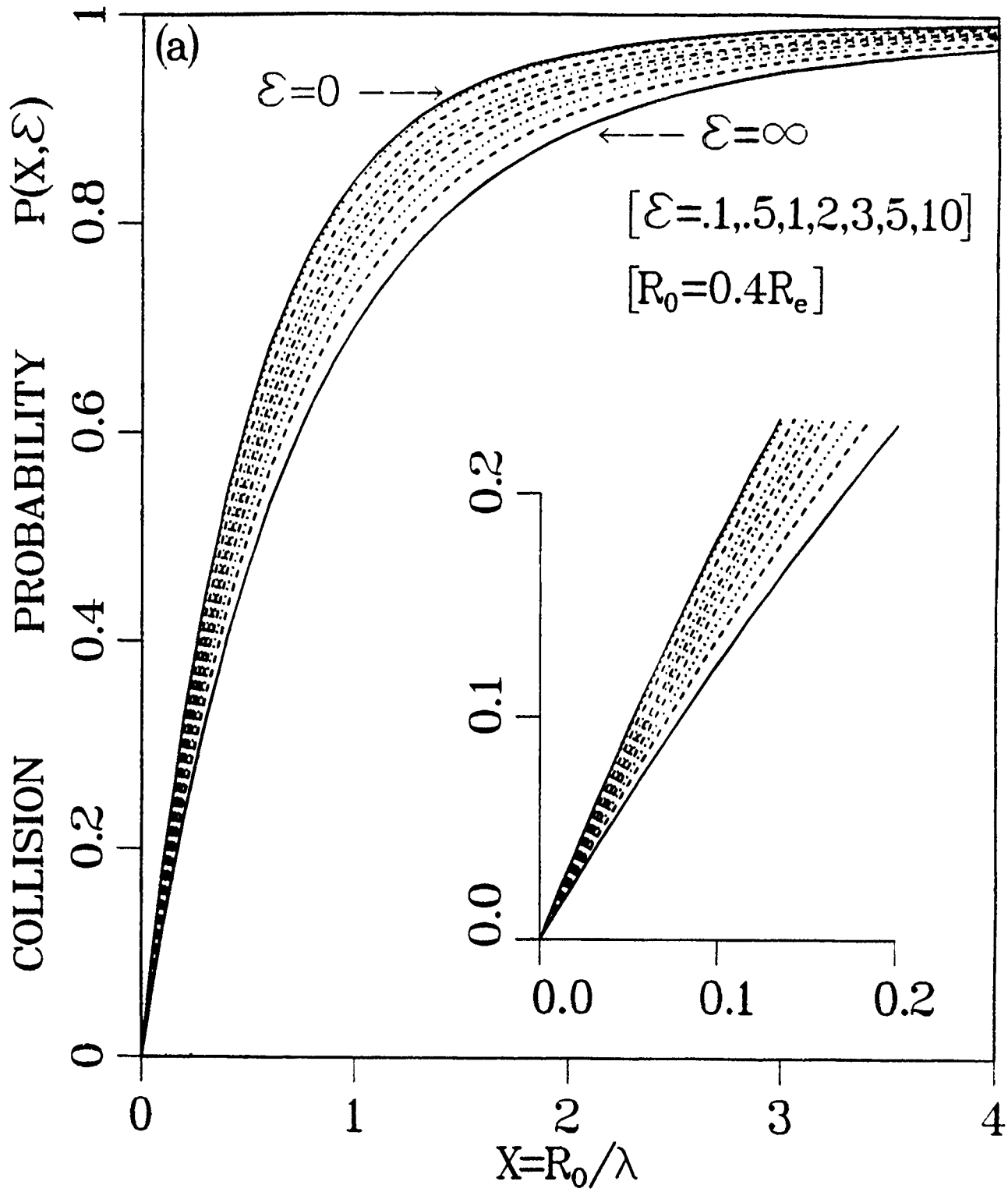

Figure 1a-b. (a) Probability $P^A(R_0, E; \lambda)$, equation (3.27), for collision of an ion in a hyperbolic (Coulomb) trajectory with the gas within a sphere of radius $R_0 = 0.4R_e$ as a function of reduced gas density $X = R_0/\lambda$ at various reduced Coulomb-orbit energies $\epsilon = E/kT$; (b) Dotted curve: E-averaged probability $P^A(R_0; \lambda)$, equation (3.28), and $P^A(R_0, kT; \lambda)$. Solid lines are parabolic ($\varepsilon = 0$) and rectilinear ($\varepsilon \to \infty$) envelopes to the collision probabilities, equations (3.34) and (3.31), respectively. Inset figure: E-variation between envelopes at low gas density. The ion-pairs here are *not* in L^2-equilibrium.

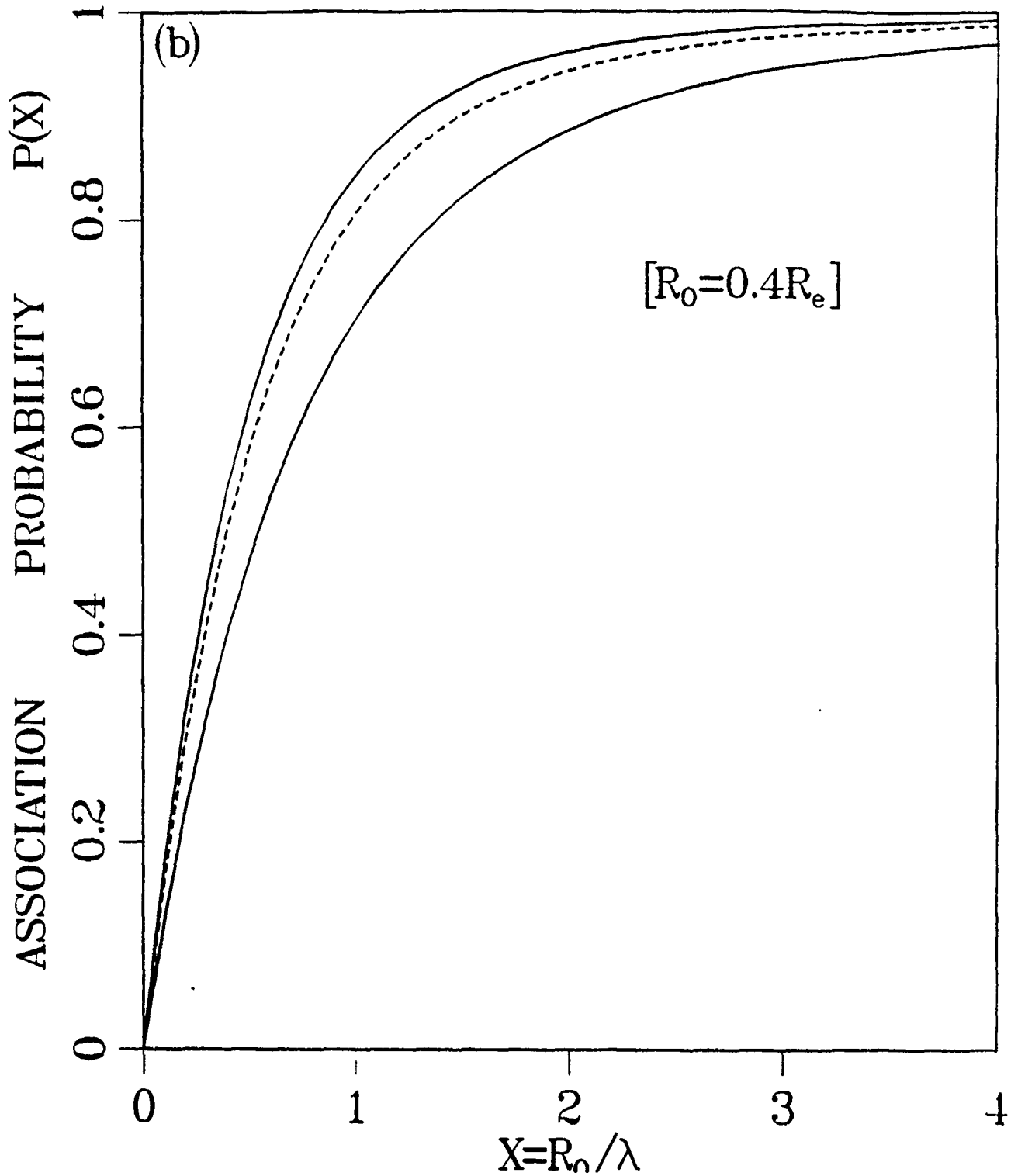

Figure 1a-b. (a) Probability $P^A(R_0, E; \lambda)$, equation (3.27), for collision of an ion in a hyperbolic (Coulomb) trajectory with the gas within a sphere of radius $R_0 = 0.4R_e$ as a function of reduced gas density $X = R_0/\lambda$ at various reduced Coulomb-orbit energies $\epsilon = E/kT$; (b) Dotted curve: E-averaged probability $P^A(R_0; \lambda)$, equation (3.28), and $P^A(R_0, kT; \lambda)$. Solid lines are parabolic ($\varepsilon = 0$) and rectilinear ($\varepsilon \to \infty$) envelopes to the collision probabilities, equations (3.34) and (3.31), respectively. Inset figure: E-variation between envelopes at low gas density. The ion-pairs here are *not* in L^2-equilibrium

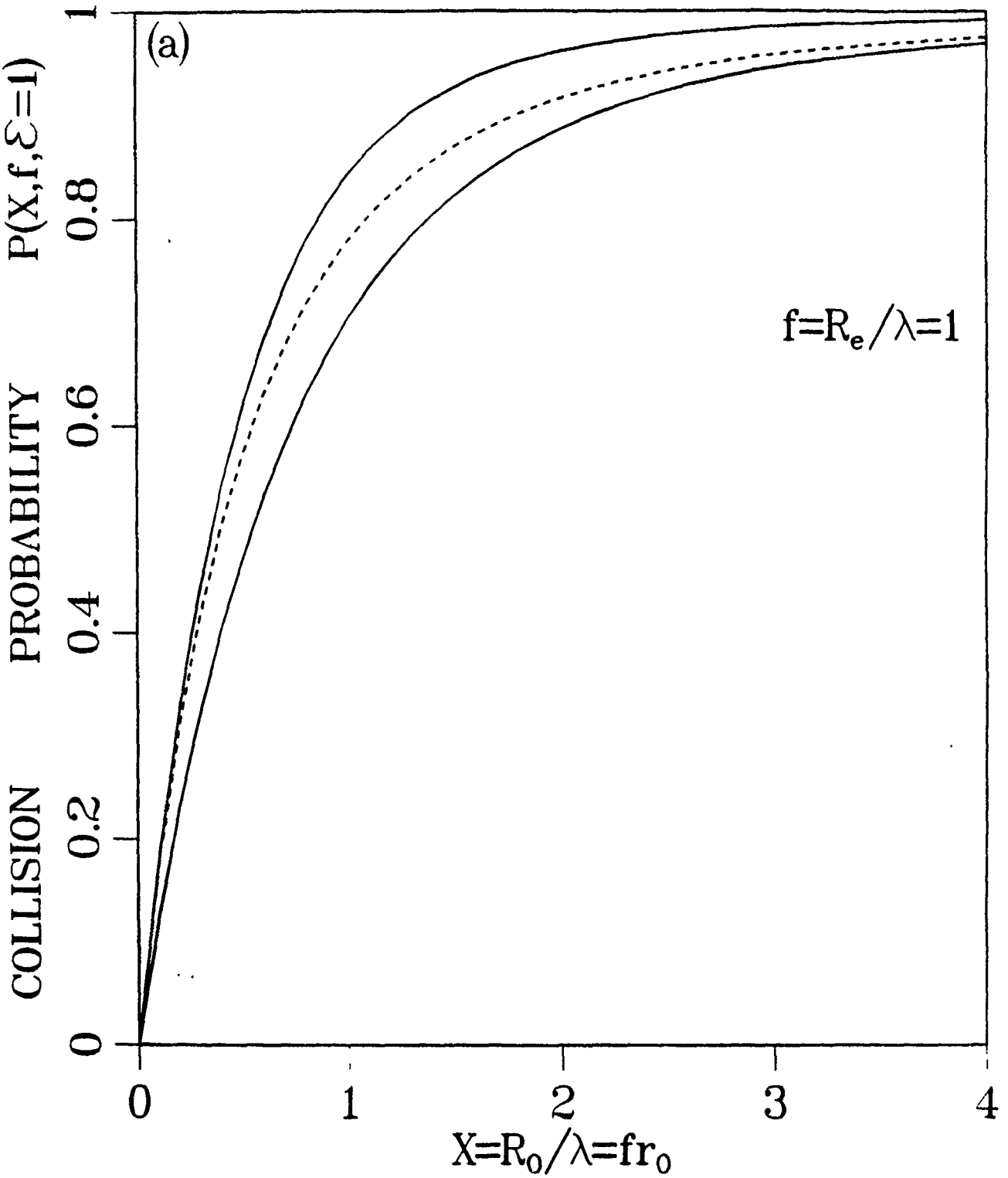

Figure 2. Collision Probability $P^A(R_0, E = kT; \lambda)$ as a function of radius R_0 for: (a) a *fixed* gas density with $\lambda = R_e$, and (b) for various gas densities proportional to f. Inset figure: P initially increases linearly with R_0 along parabolic envelope and with further increase of R_0 tends ultimately to the straight-line envelope.

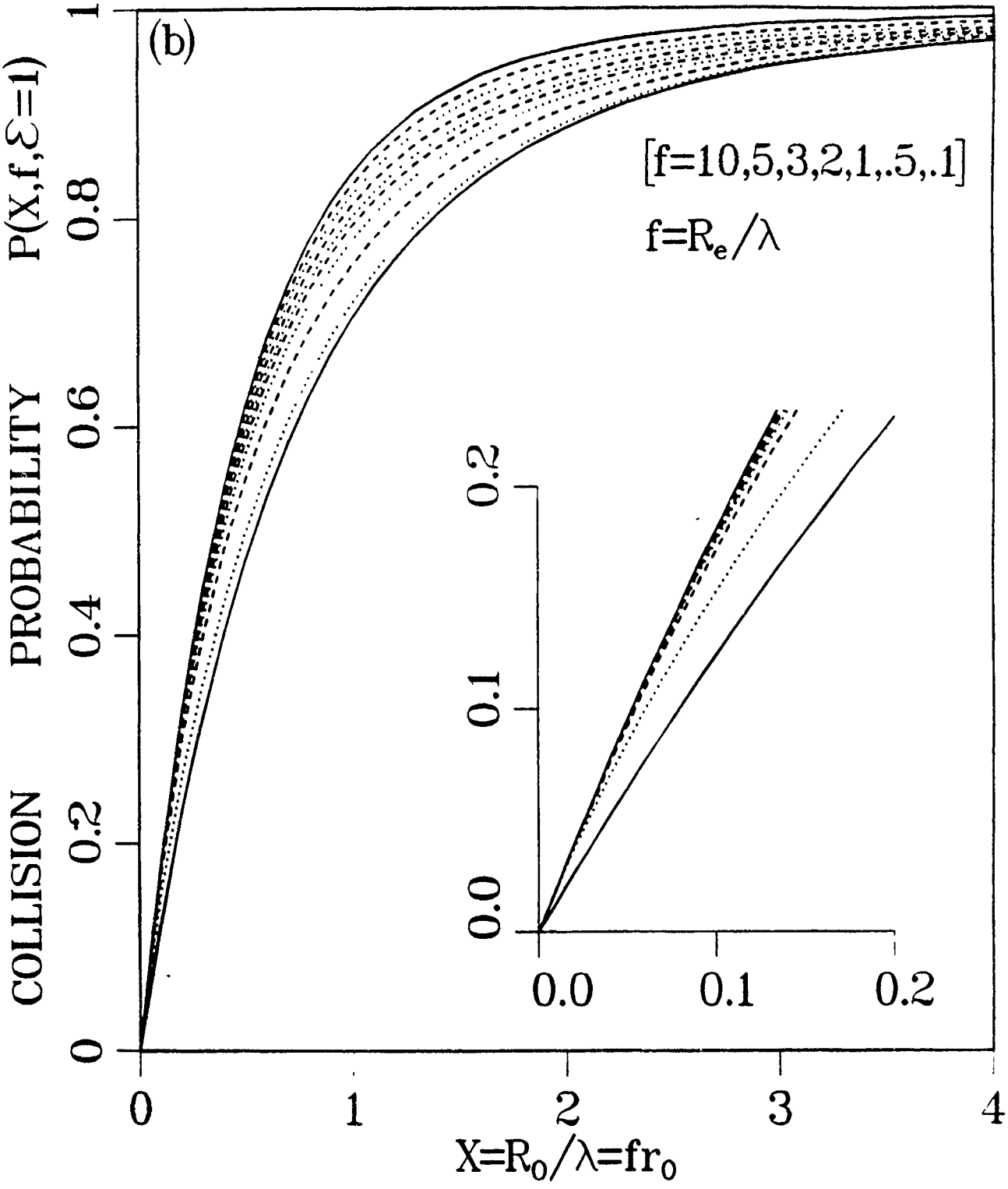

Figure 2. Collision Probability $P^A(R_0, E = kT; \lambda)$ as a function of radius R_0 for: (a) a *fixed* gas density with $\lambda = R_e$, and (b) for various gas densities proportional to f. Inset figure: P initially increases linearly with R_0 along parabolic envelope and with further increase of R_0 tends ultimately to the straight-line envelope.

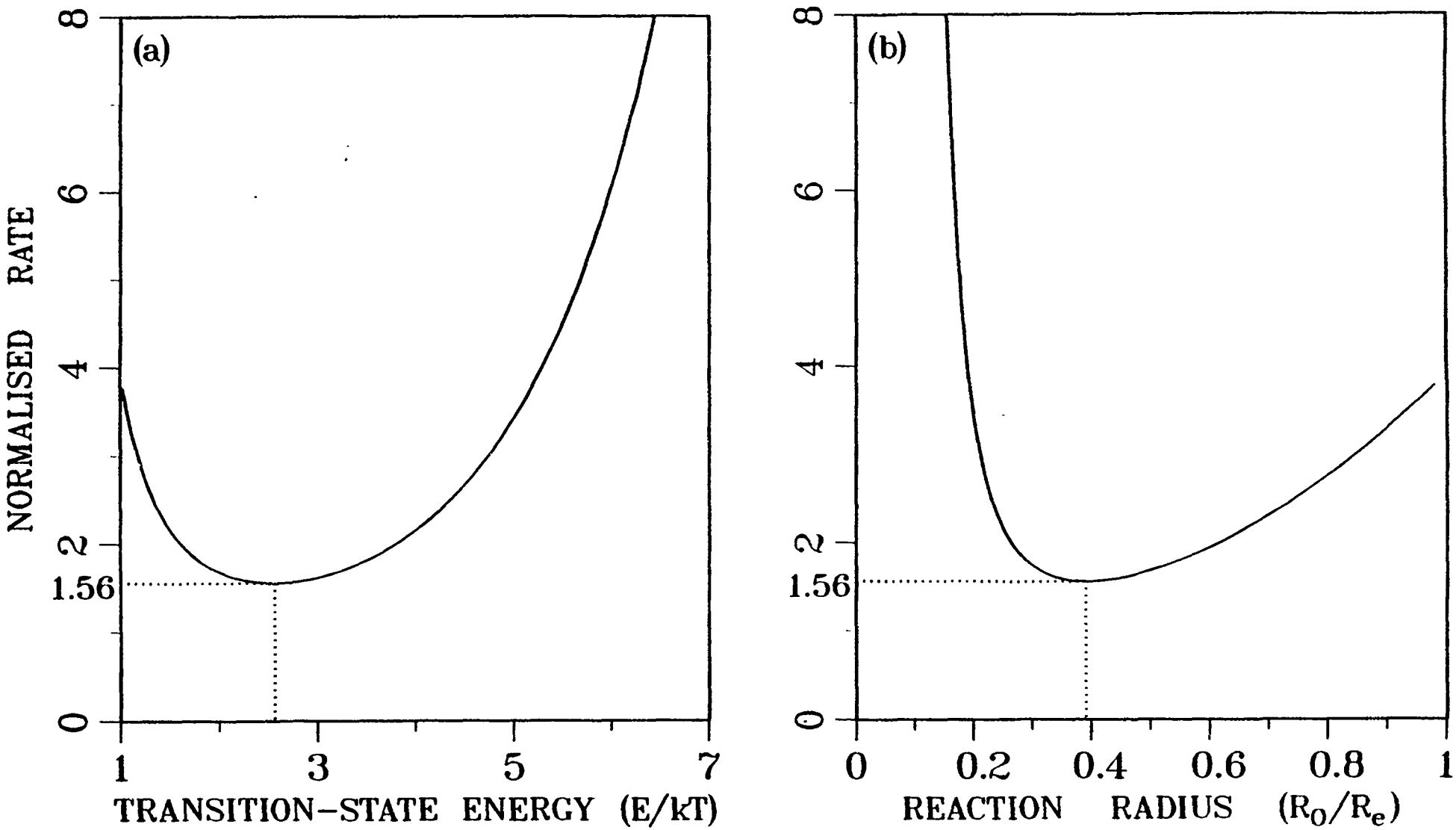

Figure 3. The recombination rate $\alpha_V/(\frac{4}{3}\pi R_c^3 \frac{F}{\lambda^2})$ versus: (a) transition-state energy $\epsilon_0 = E/kT$, or (b) reaction radius $r_0 = R_0/R_e = 1/\epsilon_0$.

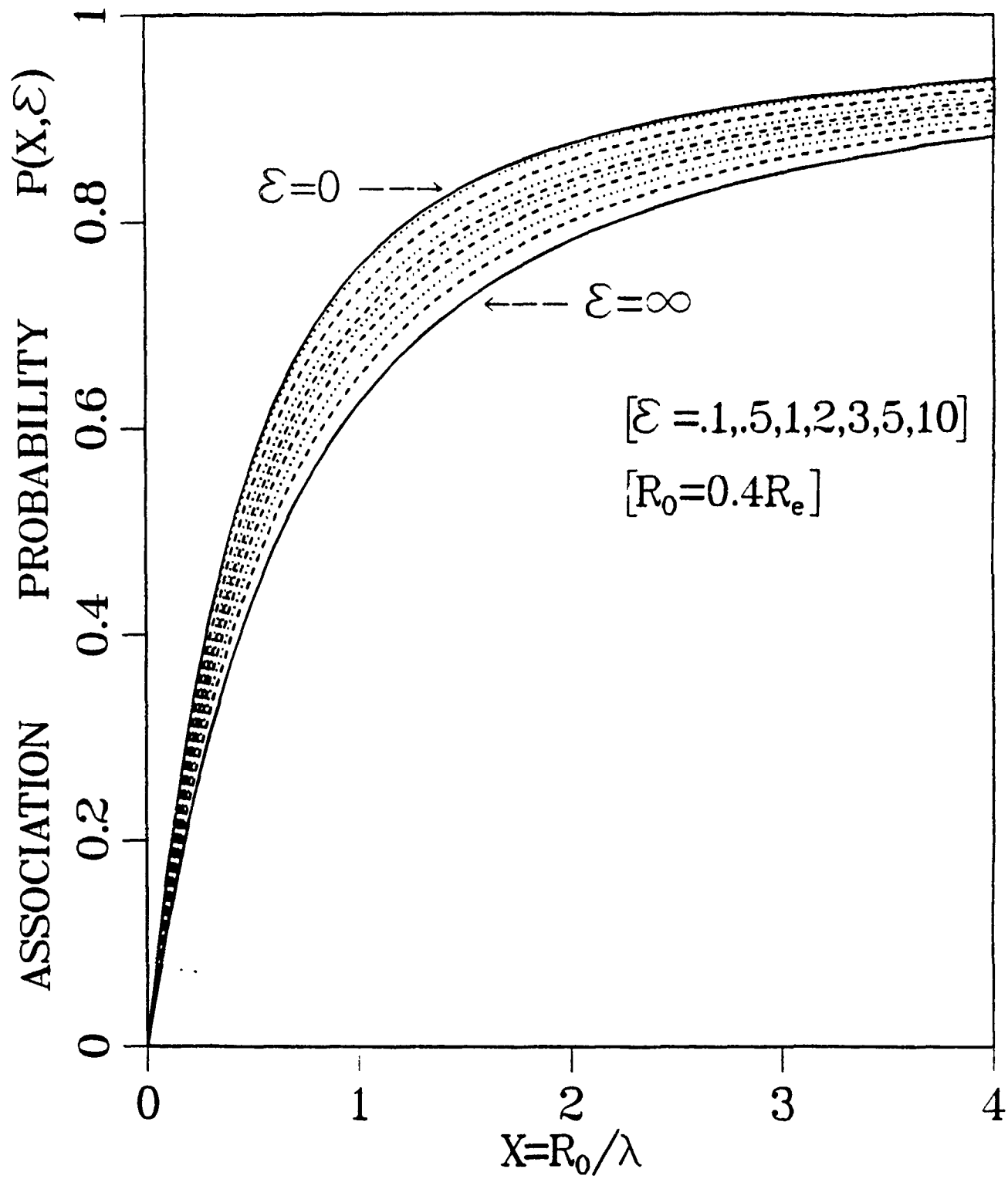

Figure 4. Analytical Probabilities $P^A(R_0, E)$, equation (6.23) for Coulomb Association within a sphere of radius $R_0 = 0.4R_e$ as a function of reduced gas density $X = R_0/\lambda$ for various ε. Parabolic (equation (6.26)) and rectilinear (equation (6.27)) limits $\varepsilon = 0$ and $\varepsilon = \infty$, respectively. Note that L^2-equilibrium is assumed.

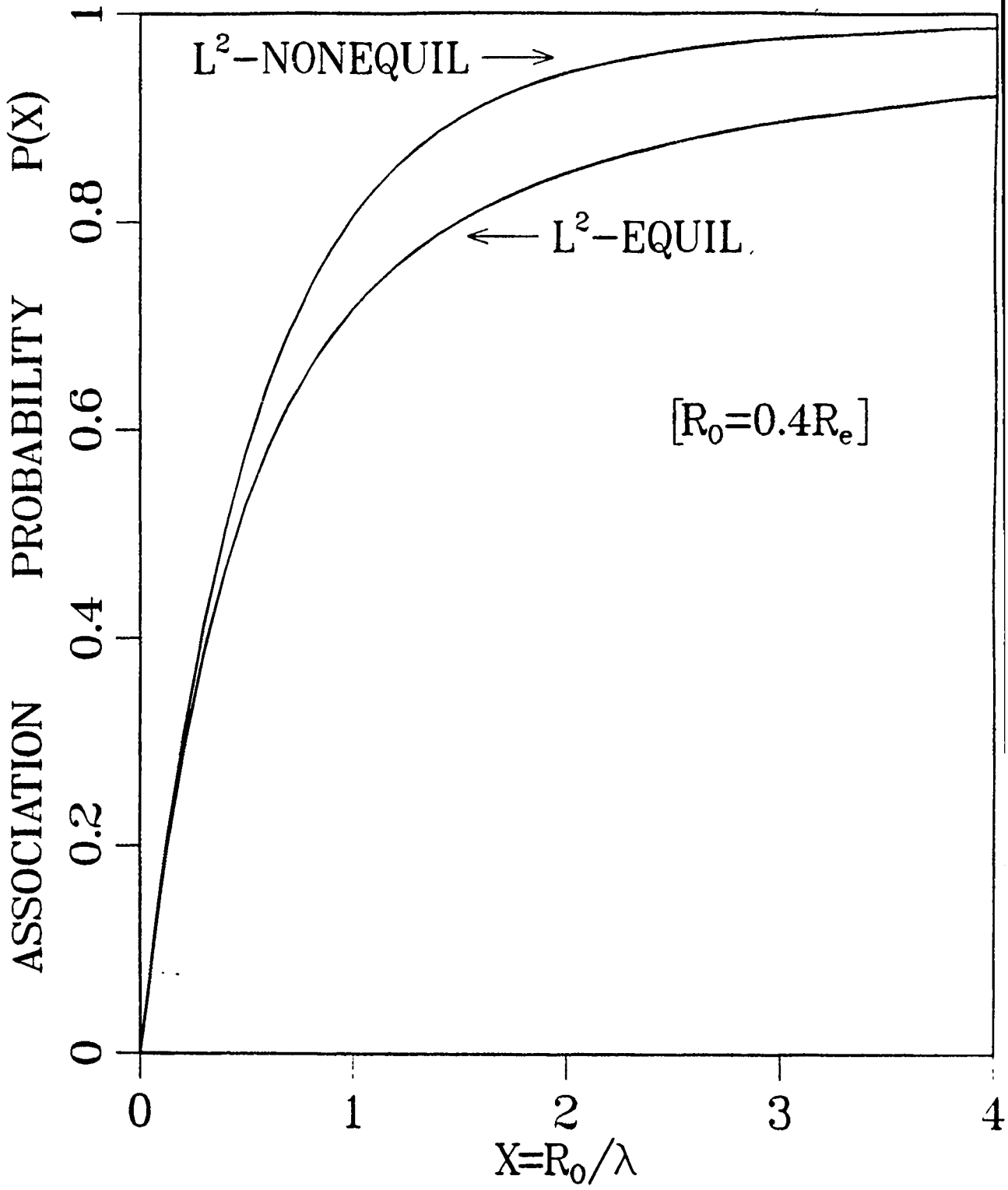

Figure 5. Comparison of E-averaged association probabilities as a function of reduced gas density $X = R_0/\lambda$ for ions with (lower curve) and without (upper curve) L^2-equilibrium.